

AD 730348

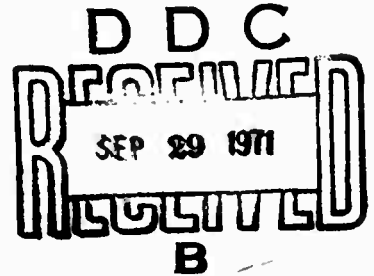
THE EARLY DETECTION OF FATIGUE DAMAGE

John F. Moore
Schillings Tsang
George Martin

Los Angeles Division of
North American Rockwell Corporation

TECHNICAL REPORT AFML-TR-71-185
AF CONTRACT NO. F33615-68-C-1706

September 1971



Approved for public release; distribution is unlimited

Air Force Materials Laboratory
Air Force Systems Command
Wright-Patterson Air Force Base, Ohio

Reproduced by
NATIONAL TECHNICAL
INFORMATION SERVICE
Springfield, Va 22151

**BEST
AVAILABLE COPY**

NOTICES

When Government drawings, specifications, or other data are used for any purpose other than in connection with a definitely related Government procurement operation, the United States Government thereby incurs no responsibility nor any obligation whatsoever; and the fact that the government may have formulated, furnished, or in any way supplied the said drawings, specifications, or other data, is not to be regarded by implication or otherwise as in any manner licensing the holder or any other person or corporation, or conveying any rights or permission to manufacture, use, or sell any patented invention that may in any way be related thereto.

ACCESSION NO.		
CPSTI	WHITE SECTION	<input checked="" type="checkbox"/>
DDC	BUFF SECTION	<input type="checkbox"/>
UNANNOUNCED		<input type="checkbox"/>
JUSTIFICATION		
.....		
DISTRIBUTION/AVAILABILITY CODES		
DIST.	AVAIL.	SPECIAL
A		

Copies of this report should not be returned unless return is required by security considerations, contractual obligations, or notice on a specific document.

13. ABSTRACT (Cont)

relation to the spent fatigue life. A marked change of acoustic emission intensity could also be related to the percentage of fatigue life. A correlation existed between the attenuation of ultrasonic surface wave and the length of fatigue time early in the process. Characterization of fatigue-damaged surface was studied by measurements of surface potential difference and ellipsometric parameters. There is a relationship between surface potential difference and the length of fatigue time. Values of ellipsometric parameters also undergo a change in fatigue process. Based on the promising potential of the exoelectron emission and ultrasonic surface wave test methods, further development is recommended using actual air vehicle components and service test conditions.

DOCUMENT CONTROL DATA - R & D

(Security classification of title, body of abstract and indexing annotation must be entered when the overall report is classified)

1. ORIGINATING ACTIVITY (Corporate author) North American Rockwell Corporation International Airport Los Angeles, California 90009		2a. REPORT SECURITY CLASSIFICATION Unclassified	
		2b. GROUP NA	
3. REPORT TITLE The Early Detection of Fatigue Damage			
4. DESCRIPTIVE NOTES (Type of report and inclusive dates) Final Technical Report, 1 July 1968 to 30 June 1971			
5. AUTHOR(S) (First name, middle initial, last name) John F. Moore Schillings Tsang George Martin			
6. REPORT DATE September 1971	7a. TOTAL NO. OF PAGES 174	7b. NO. OF REFS 68	
8a. CONTRACT OR GRANT NO. F33615-68-C-1706	8b. ORIGINATOR'S REPORT NUMBER(S) NA-71-590		
b. PROJECT NO. ARPA Order No. 1244			
c. Program Code No. 8D10	8c. OTHER REPORT NO(S) (Any other numbers that may be assigned this report)		
9. DISTRIBUTION STATEMENT Unlimited distribution			
11. SUPPLEMENTARY NOTES NA The report		12. SPONSORING MILITARY ACTIVITY Advanced Research Projects Agency monitored by Air Force Materials Laboratory, LLN, Wright-Patterson Air Force Base, Ohio	
13. ABSTRACT This is the final technical report for a program directed at the development of nondestructive test (NDT) methods for the detection of early fatigue and fracture damage in metals and alloys. The program is based on an interdisciplinary approach designed to interrelate the factors of early fatigue damage with measurable physical phenomena. The program initially concentrated on a comprehensive study of the existing knowledge of fatigue phenomena in metals, and the results of the study are described in terms of fatigue and fatigue-associated phenomena, metallurgical structure, effect of interrelating fatigue phenomena on physical properties, and the availability of appropriate measurement techniques and equipment. Next, the program developed a series of controlled fatigue experiments to quantitatively measure the fatigue effects in selected metal specimens. These tests also included a systematic metallographic evaluation to determine the actual depth and character of the surface layer affected by progressive fatigue, particularly in the early stages of fatigue. Finally, NDT methods were evaluated in terms of their potential detection and measurement capability of the observed fatigue-related effects and damage as determined by the study and fatigue evaluation tests. Based on this analysis, the following NDT methods were selected for detailed evaluation for static and in-process measurement of fatigue damage: exoelectron emission, acoustic emission, and ultrasonic surface wave attenuation and velocity. The change of exoelectron emission current was found to have a			

KEY WORDS

LINK A

LINK B

LINK C

ROLE

WT

ROLE

WT

ROLE

WT

1100-0 Aluminum
Acoustic Emission
Ellipsometry
Exoelectron Emission
Fatigue Damage
Fatigue Process
Material Characterization
Nondestructive Test
Surface Potential Difference
Ultrasonic Surface Wave

THE EARLY DETECTION OF FATIGUE DAMAGE

John F. Moore
Schillings Tsang
George Martin

Los Angeles Division of
North American Rockwell Corporation

FOREWORD

This is the final technical report on a study for the development of methods for the early detection of fatigue damage, carried out by the Los Angeles Division of North American Rockwell Corporation. This research was supported by the Advanced Research Projects Agency of the Department of Defense and was monitored by the Air Force Materials Laboratory, LLN, under contract F33615-68-C-1706, initiated under ARPA Order 1244, Program Code 8D10. Mr. R. R. Rowand, LLN, and Capt. J.W. Bohlen, LLN, were the responsible Air Force Project Engineers. This report covers the period from 1 July 1968 to 30 June 1971.

The program was conducted by the Materials and Processes Department, Mr. N. Klimmek, Manager, under the direction of Dr. G. Martin for the initial 2-year period, and Mr. J. F. Moore for the final 1-year period. The work described in this report was carried out by Mr. J. F. Moore, Dr. S. Tsang, Mr. F. Coate, Mr. D. Weinstein, Mr. H. Harvey, and Mr. R. Sapp of the Los Angeles Division; Dr. L. Hanson of Atomics International, a division of North American Rockwell; and Dr. B. Thompson and Dr. T. Smith of the Science Center of North American Rockwell Corp. Professor S. A. Hoenig of the University of Arizona served as consultant during the final 1-year period.

This technical report was submitted by the authors on 30 June 1971. This technical report has been reviewed and is approved.

THOMAS D. COOPER
Chief, Processing and
Nondestructive Testing Branch
Metals and Ceramics Division

ABSTRACT

This is the final technical report for a program directed at the development of nondestructive test (NDT) methods for the detection of early fatigue and fracture damage in metals and alloys. The program is based on an interdisciplinary approach designed to interrelate the factors of early fatigue damage with measurable physical phenomena. The program initially concentrated on a comprehensive study of the existing knowledge of fatigue phenomena in metals, and the results of the study are described in terms of fatigue and fatigue-associated phenomena, metallurgical structure, effect of interrelating fatigue phenomena on physical properties, and the availability of appropriate measurement techniques and equipment. Next, the program developed a series of controlled fatigue experiments to measure quantitatively the fatigue effects in selected metal specimens. These tests also included a systematic metallographic evaluation to determine the actual depth and character of the surface layer affected by progressive fatigue, particularly in the early stages of fatigue. Finally, NDT methods were evaluated in terms of their potential detection and measurement capability of the observed fatigue-related effects and damage as determined by the study and fatigue evaluation tests. Based on this analysis, the following NDT methods were selected for detailed evaluation for static and in-process measurement of fatigue damage: exoelectron emission, acoustic emission, and ultrasonic surface wave attenuation and velocity. The change of exoelectron emission current was found to have a relation to the spent fatigue life. A marked change of acoustic emission intensity could also be related to the percentage of fatigue life. A correlation existed between the attenuation of ultrasonic surface wave and the length of fatigue time early in the process. Characterization of fatigue-damaged surface was studied by measurements of surface potential difference and ellipsometric parameters. There is a relationship between surface potential difference and the length of fatigue time. Values of ellipsometric parameters also undergo a change in fatigue process. Based on the promising potential of the exoelectron emission and ultrasonic surface wave test methods, further development is recommended using actual air vehicle components and service test conditions.

BLANK PAGE

TABLE OF CONTENTS

Section		Page
I	INTRODUCTION	1
II	SUMMARY	3
III	LITERATURE SURVEY	7
	The Fatigue Process	7
	General Phenomena in the Fatigue Process	7
	Fatigue Damage	8
	Physical Properties Related to Fatigue Damage	10
	Magnetic Hysteresis and Eddy Current Losses	10
	Electric Impedance	11
	Optical Phenomena	12
	Internal Friction	13
	Propagation of Ultrasonic Waves	13
	Acoustic Emission	15
	Exoelectron Emission	15
	Other Phenomena	18
	Conclusions	19
IV	SPECIMEN DESIGN AND FATIGUE TEST SYSTEM	20
	Materials	20
	Specimens	21
	Fatigue Test Unit	22
	Fatigue Characteristics for 1100-0 Aluminum	26
V	EXO-ELECTRON EMISSION MEASUREMENTS	28
	Test System	28
	Exoelectron Detection by Luminescence	35
	Exoelectron Emission in Vacuum	35
	Exoelectron Emission in Air	42
	Exoelectron Emission in Fatigue Process	42
	Exoelectron Emission of Unstressed Material	50
	Discussion	56

TABLE OF CONTENTS (Continued)

Section		Page
VI	ACOUSTIC EMISSION MEASUREMENTS	66
	Test System	66
	Test Method and Results	66
	Discussion	68
VII	ULTRASONIC SURFACE WAVE MEASUREMENTS	76
	Test Systems	76
	Test Results and Discussion	79
VIII	MATERIAL CHARACTERIZATION	91
	Metallography	91
	Surface Analysis	96
	Surface Potential Difference	98
	Ellipsometry	105
IX	CONCLUSIONS AND RECOMMENDATIONS	109
APPENDIX I	BIBLIOGRAPHY RELATING TO EXOELECTRON EMISSION	113
APPENDIX II	ELECTRON ENERGY SPECTROSCOPY	151
REFERENCES		159
BIBLIOGRAPHY		160

LIST OF ILLUSTRATIONS

Figure	Title	Page
1	Hydraulic System.	24
2	Photograph of Specimen and Loading Frame.	25
3	Fatigue Curve for 1100-0 Aluminum	27
4	Block Diagram for Measuring Exoelectron Emission in Vacuum.	29
5	Channeltron Electron Multiplier and Loading Frame	30
6	Schematic Diagram of the System for Measuring Exoelectron Emission in Air	32
7	Photograph of the System for Measuring Exoelectron Emission in Air	33
8	Photograph of Specimen with Exoelectron Emission and Acoustic Emission Transducers	34
9	Exoelectron Emission of 1100-0 Aluminum in Vacuum at Tensile Stress 10,650 lb/in ²	37
10	Exoelectron Emission of 1100-0 Aluminum in Fatigue Test in Vacuum at 12,600 lb/in ²	39
11	Exoelectron Emission of 1100-0 Aluminum in Fatigue Test in Vacuum at 11,450 lb/in ²	40
12	Exoelectron Emission of 1100-0 Aluminum in Fatigue Test in Vacuum at 11,000 lb/in ²	41
13	Exoelectron Emission of 1100-0 Aluminum in Fatigue Test in Vacuum at 10,540 lb/in ²	43
14	Exoelectron Emission of 1100-0 Aluminum in Fatigue Test in Vacuum at 11,450 lb/in ² and under Various Light Conditions.	44
15	Exoelectron Emission of 1100-0 Aluminum in Fatigue Test in Air at 11,000 lb/in ²	47
16	Exoelectron Emission of 1100-0 Aluminum in Fatigue Test in Air at 11,400 lb/in ²	48
17	Exoelectron Emission of 1100-0 Aluminum in Fatigue Test Conducted in two Environments at 11,450 lb/in ²	49
18	Exoelectron Emission of 1100-0 Aluminum in Fatigue Test in Air at 11,650 lb/in ²	51
19	Equipment for Measuring Exoelectron Emission of Unstressed Material in Air.	53
20	Photograph of Electron - Collecting Electrode	54
21	Exoelectron Emission Scanning System and Record	57
22	Relation of the Strongest Exoelectron Emission Intensity in Vacuum to Fatigue Stress for 1100-0 Aluminum.	59
23	Relation of the Time at which the Strongest Exoelectron Emission Intensity in Vacuum Occurs to Fatigue Stress for 1100-0 Aluminum	60

Figure	Title	Page
24	Relation of Percentage Decrease of Exoelectron Current to Percentage of Fatigue Life for 1100-0 Aluminum of Source B	62
25	Relation of Percentage Decrease of Exoelectron Current to Percentage of Fatigue Life for 1100-0 Aluminum of Source A.	64
26	Block Diagram of Acoustic Emission Measurement System . . .	67
27	Acoustic Emission of 1100-0 Aluminum in Fatigue Test in Air at 11,650 lb/in ²	70
28	Acoustic Emission of 1100-0 Aluminum in Fatigue Test in Air at 11,450 lb/in ²	71
29	Relationship Between Acoustic Emission and Fatigue Life of 1100-0 Aluminum at Two Stress Levels.	73
30	Relationship Between Acoustic Emission and Fatigue Life of 1100-0 Aluminum at 11,000 lb/in ²	75
31	Block Diagram of the Precision Ultrasonic Wave Velocity Diagram	77
32	Schematic Diagram of Ultrasonic Surface Wave Measuring System.	78
33	Relationship Between Surface Wave Velocity and Fatigue Life of 1100-0 Aluminum at 11,500 lb/in ²	80
34	Relationship Between Surface Wave Attenuation and Fatigue Life of 1100-0 Aluminum at 11,500 lb/in ²	81
35	Amplitude as a Function of Specimen Position Showing Interference Effects at 3.4 MHz Frequency in Fatigue-Stressed 7075-T6 Aluminum Alloy	84
36	Attenuation of Surface Wave in Fatigue-Stressed 7075-T6 Aluminum Alloy.	86
37	Surface Wave Attenuation at 10 MHz Frequency in a Thick Aluminum Block.	90
38	Optical Micrographs of Fatigue-Stressed 1100-0 Aluminum at 11,500 lb/in ² (250X)	92
39	Electron Micrographs of Fatigue-Stressed 1100-0 Aluminum at 11,500 lb/in ² (2,500X).	93
40	Secondary Electron Emission Micrographs at 550X of Fatigue-Stressed 1100-0 Aluminum at 11,450 psi for 800 Cycles.	94
41	Secondary Electron Emission Micrographs at 550X of Fatigue-Stressed 1100-0 Aluminum at 11,450 psi for 3 x 10 ⁴ Cycles.	95
42	Photograph of Instrument for Measurement of Surface Potential Difference.	99
43	Surface Potential Difference of Fatigue-Stressed 7075-T6 Aluminum Alloy.	100

Figure	Title	Page
44	Variation of Surface Potential Difference Along Length of Fatigue-Stressed 7075-T6 Aluminum Alloy Specimen No. 6.	104
45	Variation of Surface Potential Difference Along Length of Fatigue-Stressed 7075-T6 Aluminum Alloy Specimen No. 13	106

LIST OF TABLES

Table	Title	Page
I	Summary of the Nondestructive Test Methods Evaluation. . . .	6
II	Summary of Exoelectron Emission Test on 1100-0 Aluminum in Vacuum	36
III	Results of Fatigue Test in Air for 1100-0 Aluminum	45
IV	Summary of Acoustic Emission Data for 1100-0 Aluminum of Source B in Fatigue Test in Air	69
V	Change in Slope of Acoustic Emission Curve for 1100-0 Aluminum of Source A in Fatigue Test in Air	74
VI	Surface Wave Attenuation in Fatigue-Stressed 7075-T6 Aluminum Alloy	85
VII	Depth of Surface Layer Removed by Electropolish from Fatigue-Stressed 1100-0 Aluminum Specimens	97
VIII	Surface Potential Difference and Ellipsometry Data for Fatigue-Stressed 7075-T6 Aluminum Alloy	102
IX	Effects of Handling on Surface Potential Difference	103
X	Surface Potential Difference and Ellipsometry Data for Fatigue-Stressed Annealed D6AC Steel	107

SECTION I

INTRODUCTION

One of the most critical problems in the aerospace industry is the lack of reliable nondestructive testing (NDT) techniques to detect and quantitatively measure the effects of fatigue damage under diverse loading and environmental service conditions. Stress concentration sites caused by cracks or crack-like defects that are too small to be detected by conventional nondestructive inspection techniques are sometimes present in the raw material or are introduced in aircraft structural components during fabrication or assembly. Since these defects can grow by subcritical crack propagation during service, they can lead to structural failure by unstable propagation once they attain a critical size. The possibility of the early detection of fatigue damage could significantly improve the material utilization and system reliability.

The phenomena of fatigue of metals and alloys and particularly the early detection of material damage due to these phenomena have always been high on the list of material problems. Our present understanding of the problem is largely based on a large number of phenomenological observations of the metallurgical events in a great variety of materials during the fatigue progress. There is a very large collection of fatigue test data reported in the literature without specified ambient conditions; there are a few tentative theories based on phenomenological observations, and a number of empirical rules based on fatigue test data; and there are comparatively few studies relating fatigue phenomena to physical effects which could serve as indicators of the extent of fatigue damage.

A program plan was developed to systematically define the fatigue phenomena in terms suitable for establishing a fundamental basis for considering an NDT method. The program plan included the following phases:

<u>Phase</u>	<u>Study</u>	<u>Objective</u>
I	Theoretical study of early surface layer damage phenomena with special reference to associated physical phenomena.	Selection of most suitable NDT method for a specific surface layer depth effect.
II	Fatigue tests and metallographic studies on aluminum material.	Experimental determination of depth of fatigue-affected surface zone depth.

<u>Phase</u>	<u>Study</u>	<u>Objective</u>
III	Design and construction of NDT equipment as selected from phase I, and correlation with fatigue effects using the specimens from phase II.	Preliminary characterization of test methods.
IV	Fatigue tests and metallographic studies on other materials.	Final definition of fatigue surface layer damage concept.
V	Correlation of NDT results and fatigue damage in other materials.	Characterization of test methods and development of design concepts for NDT instrumentation.

SECTION II

SUMMARY

This program, initiated in 1968, was directed toward the development of nondestructive testing (NDT) methods suitable for early detection of fatigue damage in metals and alloys under the sponsorship of the Advanced Research Projects Agency, and under the supervision of the Air Force Materials Laboratory (reference 1). The initial effort was a study of the metallurgical phenomena associated with early fatigue damage, and a survey was made of the physical phenomena related to these changes. It was shown that a number of fatigue theories exist and that none of these theories can quantitatively predict the fatigue behavior of metals and alloys which lead to the conclusion that the processes occurring in fatigue are not only complex, but also that several mechanisms may be involved in the fatigue process. These processes vary from initial damage to rapid crack propagation. A significant conclusion resulting from these studies is that fatigue is essentially a surface layer phenomenon and, as such, is influenced by environment. It was concluded that the development of methods for assessing the extent of fatigue damage to a structure should be based on the correlation of actual fatigue life data with surface layer depth affected by the physical phenomena changes. The general approach taken in this study has been that of determining (1) the depth of fatigue-mechanism-affected layers as a function of fatigue life, (2) the depth sensitivity of various inspection methods, and (3) a correlation between the two. Investigations for determining the actual fatigue mechanisms operative at the affected layer can involve a fairly considerable investigation, and this program concentrated on limited surface analysis in terms of the depth of the affected area and basic metallographic observations.

Early fatigue damage appears to consist of the formulation of a thin layer of possible intense dislocation tangling as evidenced on the surface by a dense pattern of slip markings. In the case of the 1100-O aluminum, these surface markings appear after the first few hundred cycles. The depth of the affected layer is of the order of 10 to 50 microns and does not seem to increase with increasing fatigue stressing. These depth data are consistent with observations reported in the literature for copper and iron. It is also noted, in the case of aluminum, that cracks detectable by low-power microscopes apparently develop only at very late stages of the fatigue process.

Based on the physical phenomena associated with these observations, the following measurement methods were recommended as promising: ultrasonic surface wave interactions, and exoelectron and acoustic emission methods. During the present study, attention was centered on ultrasonic surface wave methods, exoelectron emission methods, and acoustic emission methods. Breadboard test measuring systems were developed and evaluated statically and dynamically on fatigued aerospace materials.

Exoelectron emission experiments were initially performed in vacuum and showed promising correlations with early fatigue damage. The exoelectron emission current was subsequently characterized in air using a technique formulated by Hoening (reference 2) in terms of the fatigue deformation of 1100-0 aluminum. The emission was characterized by an early rapid rise and fall in emission intensity followed by a final rise near the end of the test. The initial fall of emission from the intensity peak coincides with the appearance of slip bands on specimen surface; the final rise is attributed to the formation and propagation of fatigue cracks. Although the emission intensity in vacuum appears to depend upon the applied stress, this dependence is not apparent in air. The emission is strongly influenced by the incident light energies, and illumination with ultraviolet light is necessary for measuring the emission current in air. There appears to be a stress-independent relationship between the change of emission current in air, relative to the current after the elapse of a few hundred or a few thousand cycles, and the time in fatigue deformation. This relationship was judged to offer a promising means to assess the accrued damage as well as to predict the remaining safe life of the fatigued material. Fatigued specimens can be uniformly heated and scanned with an exoelectron emission detector to detect and measure fatigued areas by comparison with unfatigued areas. Crack growth has been monitored from inception, without heating, by exoelectron emission detection.

The velocity and attenuation of ultrasonic surface waves were measured in aluminum and its alloy specimens partially fatigued to various degrees. In the case of the low-frequency velocity measurement, a maximum was observed in specimens fatigued to about 50 percent of their total life, and an attenuation minimum occurred at the same point. Additional velocity and attenuation measurements of surface waves on fatigued specimens at higher frequencies employed a new laser detection technique. With appropriate signal processing and specular reflection at the aluminum surface, the technique has been shown to be accurate to at least 1 percent. A new method of extracting the acoustic information from the reflected laser beam was developed. This method is based on detecting the Doppler shift in the reflected light produced by the fact that the surface is vibrating at the acoustic wave frequency. The ultrasonic attenuation data showed a promising correlation with early fatigue damage up to approximately 5 percent of the total fatigue life; however, no further correlation was observed up to approximately 25 percent of the total fatigue life. An analysis of the experimental conditions showed severe wave interference effects which require control or transducer redesign for technique improvement.

The acoustic emission from fatigue-stressed aluminum, steel, and titanium specimens was measured concurrently with exoelectron emission tests. The intensity of the acoustic emission, expressed in number of counts in 1,000 cycles, appears to vary by several orders of magnitudes during the fatigue life of a material. The acoustic emission curve for 1100-0 aluminum experiences a significant change of slope in fatigue process. This change occurs

between 33 and 50 percent and 28 and 43 percent of fatigue life, respectively, at the stresses of 11,650 and 11,450 psi. At a lower stress of 11,000 psi, the change shifts to between 65 and 75 percent of the life. The tests on the other three materials indicate either lack of or very weak acoustic emission.

Finally, characterization studies of fatigue-damaged surfaces indicated several promising methods for evaluating the effect of surface conditions and preparations as well as for defining areas of localized or varying mechanical stresses in the material. Surface potential difference measurements proved promising for scanning a material and detecting variations in fatigued areas in aluminum alloy specimens. Ellipsometric measurements indicated that the surface film thickness and refractive index varied significantly between various specimens; however, no correlation was evident with the degree of fatigue damage. This experiment demonstrates the need for controlled surface conditions and test preparation procedures.

The program objectives were generally met in terms of the systematic development of an understanding of the fatigue process and the development and evaluation of potential test methods. The results of this evaluation are shown in table I. The further development of one or more of these methods is recommended following the same interdisciplinary approach, including a sound understanding of the mechanical-metallurgical characteristics of the fatigue process, the relating of fatigue process properties with appropriate measurement parameters, and the development of a prototype fatigue test system qualified for service-type inspections of aerospace materials and structures.

TABLE I. SUMMARY OF THE NONDESTRUCTIVE TEST METHODS EVALUATION

Non-destructive Test Method	MATERIAL						Result
	1100-0 Aluminum	7075-T6 Aluminum Alloy	Annealed D6AC Steel	Heat-treated D6AC Steel	Annealed 6Al-4V Titanium Alloy		
Exoelectron Emission	tested showing strong emission	tested showing no or weak emission	not tested	tested showing no or weak emission	tested showing no or weak emission	tested showing no or weak emission	good potential for detecting fatigue damage in 1100-0 aluminum
Acoustic Emission	tested showing strong emission	tested showing no or weak emission	not tested	tested showing no or weak emission	tested showing no or weak emission	tested showing no or weak emission	good potential for detecting fatigue damage in 1100-0 aluminum
Propagation of ultrasonic surface wave	not tested	tested showing change of attenuation	not tested	not tested	not tested	not tested	needs further development
Surface Potential Difference	not tested	tested showing change of surface potential	tested showing change of surface potential	not tested	not tested	not tested	needs further development
Ellipsometric Parameters	not tested	tested showing change of ellipsometric parameters	tested showing change of ellipsometric parameters	not tested	not tested	not tested	needs further development

SECTION III

LITERATURE REVIEW

THE FATIGUE PROCESS

GENERAL PHENOMENA IN THE FATIGUE PROCESS

It has been suggested that fatigue damage of face-centered cubic metals at high and low stress levels occurs by different mechanisms (Wood, 1959). The H mechanism at high stress level occupies the steeper portion of the S-N curve where fatigue life increases slowly with decreasing stress. The F mechanism at low stress level operates in the flatter portion of the S-N curve where fatigue life increases rapidly with decreasing stress. It has also been suggested that there is no very clear-cut distinction between the mechanisms at high and low stress levels (Laird and Smith, 1962; Forsyth, 1963). In addition, experiments on aluminum and copper having different texture and ductility reveal that, regardless of the stress level, the operating mechanisms may be influenced to a great extent by texture and ductility (Nair and May, 1968).

It is not the purpose here to make a critical review of the fatigue mechanisms. But it is a concern to know in a specimen the successive events that take place in the fatigue process, leading to permanent damage and ultimate failure of the specimen. The H and F mechanisms concerning the formation of microcracks are briefly described to aid in such understanding, since they shed some light on how fatigue damage in the form of cracks develops.

Cyclic-stressing of face-centered cubic metals at large plastic amplitudes, those corresponding mainly to the H part of the S-N curve, produces coarse slip. At the early stage, severe local strains develop within grain boundaries, resulting in the breakdown of each grain into regions of different lattice orientation separated by irregular subboundaries. As cycling continues, micropores develop on the subboundaries. In copper or brass, these micropores appear during about 1/200 of the specimen life. The micropores multiply and coalesce into cavities which, with continued stressing, multiply and link into microcracks. These microcracks remain smaller than the grains for the greater part of the remaining life. An increase in the number of cycles of amplitudes only starts more cracks in other parts of a grain. The stage of crack formation encompasses the appearance of micropores, cavities, and microcracks in each grain. This stage occupies most of the time of the fatigue process of an annealed metal.

The specimens become structurally unsound early in the formation of micropores. Tests show, however, that there is no loss of mechanical

strength, which remains constant, although microcracks develop and multiply. Microcracks can be considered centers of fatigue damage, but they are harmless as long as they are confined in grains and are not self-propagating.

Cyclic-stressing of face-centered cubic metals at small plastic amplitudes produces fine slip zones or bands corresponding to the F part of the S-N curve. They are readily shown as traces brought up by etching and begin to appear after approximately 1/1000 of the specimen life. Though the existing bands are intensified by adding fine slip movements, they are limited in length and are usually shorter than a grain. Such bands are zones of abnormal distortion resulting from the to-and-fro slip movements and show up clearly in grains undergoing cross-slip. Surface notches and peaks, often called intrusions and extrusions respectively, may also form at the end of a slip band where slip bands meet the surface. These surface disturbances, which are about 10^{-4} cm in depth, have been considered responsible for forming fatigue cracks. However, they do not seem to develop with continued cycling. Isolated micropores then form in the interior of slip zones (Wood et al, 1963); they multiply and coalesce to elongated cavities along the zones as cycling continues further. These pores, however, are recently believed to be spurious interpretations of normal extrusions (Dover and Jones, 1967); they are tubular holes extending into the metal from the surface. These holes which constitute the crack front grow and link up to complete the failure of a grain in a direction compatible with the applied stress.

The S-N curve for a body-centered cubic metal, such as iron, generally consists of an inclined portion, called the H part, and a horizontal portion, called the S part, giving rise to a sharp knee (Wood et al, 1964). The basic structural change in iron above the knee in the H part is a pronounced cell formation in the grains, which determines irregular microcracks. At amplitudes below the knee in the S part, slip produces in the surface the form of dense clouds of short, faint markings. The clouds are composed of short, fine slip. Pores form but they are dispersed widely and cannot readily link into microcracks. The fine dispersed slip and dispersed pore formation is therefore an example of fatigue damage in its least effective form.

FATIGUE DAMAGE

Fatigue damage is assessed in different ways. The residual static strength after cracks grow to a certain size is one criterion, while another is the prediction of accumulations of damage when a specimen or a structure is subjected to a number of cycles at one or several different amplitudes. Both criteria have important practical aspects in engineering applications, but neither is suitable for developing early fatigue damage detecting techniques by nondestructive means. The few prominent cracks which may influence the

residual static strength are not of primary concern. Of greater concern is the damage which may occur before a macrocrack develops, so that its detection will prevent formation and growth of additional macrocracks that could cause sudden or catastrophic failure of a structure in service.

The micropores that develop very early in fatigue deformation at sub-boundaries and the intrusion extension by means of tubular hole growth in a grain are the smallest centers of damage since they eventually multiply and link up to form microcracks. However, even the microcracks existing in the confines of a grain may still be harmless because tests at this stage show no loss of mechanical strength of the specimen. Microcrack damage becomes apparent when the cracks multiply and extend beyond the confines of a grain to link together forming macrocracks.

Since X-ray experiments have shown that nearly all of the small angle X-ray scattering is due to the double-Bragg reflection process, an evidence of the existence of disoriented subgrains (Grosskreutz and Rollins, 1959), the micropores are not actual cavities. Since they show up by etching, they might be regions of concentrated plastic deformation. Transmission electron micrographs indicate that the apparently microporous areas shown in optical micrographs correspond to abnormally dense regions of loops and debris left by oscillating screw dislocations along etched-up slip zones or along subgrain boundaries (Grosskreutz et al, 1966). The slip zones are dense regions of loops and unresolved debris. The subgrain boundaries are dislocation arrays. Thus, micropores are only regions of high internal strain.

It should be noted that micropores, tubular holes, and microcracks are harmless only when the test specimen is subjected to pure fatigue with zero mean plastic strain. They become centers of mechanical weakness that can be pulled apart by a static tensile load which is superimposed on the pure fatigue (Wood and Bendler, 1962). Since structures are often subjected to combined static and cyclic loading, microcracks must be considered potentially dangerous.

Ideally, the early fatigue damage zone is then a few grains deep with each grain containing microcracks within its confines. Since it is difficult to determine this depth, a method of measuring the damage depth is to estimate the amount of surface layer that must be removed by electropolishing or other means to cause the disappearance of persistent slip bands because extrusion and intrusion form at the end of a slip band where the band meets the surface. For example, the persistent slip bands of copper (Thompson et al, 1956) and iron (Klesnil and Lukas, 1965; Sullivan et al, 1961) are 10 to 30 μm and 6 to 10 μm deep respectively.

Transmission electron micrography technique using thin foils reveals that the dislocation structure in regions near the fatigued iron specimen surface (less than $25\ \mu\text{m}$) is characterized by bands of intense dislocation tangling, individual dislocations within the bands being unresolved, and arrays of parallel rows of dislocation loops, the arrays often extending for considerable distances across a given grain (Wei and Baker, 1965). On the other hand, micrographs of the interior show isolated clusters of dislocations and scattered dislocation loops and loop trails. Since the dislocation structure in the surface region is completely different from the dislocation structure in the interior and since thickness of the foil (less than $25\ \mu\text{m}$) taken from the fatigued iron specimen surface is of the same order of magnitude as the amount of surface layer ($6\text{-}10\ \mu\text{m}$ for iron and $10\text{-}30\ \mu\text{m}$ for copper) removed by electropolish to eliminate persistent slip bands, the observed dislocation structure must be correlated with the fatigue damage zone because the damage occurs only at the surface layer.

PHYSICAL PROPERTIES RELATED TO FATIGUE DAMAGE

It is known that most physical properties of metallic materials change with plastic deformation. Some of the properties would also be influenced by cyclic stressing. It is then possible to utilize such changes to indicate fatigue damage. Though fatigue cracks on a macroscale in metals can be detected by various nondestructive techniques, detection or evaluation of the early damage prior to the formation of macrocracks is not simple or easy. Some knowledge of the change in physical phenomena in the course of fatigue deformation is needed for the development of techniques to detect early fatigue damage. Such knowledge, together with some other characteristics which might be useful, is described in the following paragraphs.

MAGNETIC HYSTERESIS AND EDDY CURRENT LOSSES

In the majority of ferromagnetic materials, magnetic hysteresis is caused by a delay in the change of magnetization. Loss of energy to magnetic hysteresis depends on the average amplitude of internal stresses. Internal stresses also have influence on the resistance of the metal, both magnetic and nonmagnetic, to alternating current. Changes in resistance and disturbance of continuity result in eddy current losses. The region having high internal stresses could be a nucleation site of fatigue crack since transmission electron micrographs of foils prepared from specimens subject to cyclic stressing reveal that the region of abnormally high dislocation density corresponds to the fatigue zone in the specimen (Grosskreutz et al, 1966).

The variation of the total losses in steels in fatigue process has been investigated by Gushcha (1965). The change of the losses in the course of deformation above the fatigue limit can be divided into four stages. In the

first stage, the losses decrease with number of cycles while work-hardening revealed by microhardness measurement intensifies. Slip lines appear in some grains. In the second stage, there is an increase in the losses, but microhardness is lowered. These changes are attributed to relaxation or softening of the most stressed grains. As the number of cycles increases, further softening becomes intensified while work-hardening is slowed down. When the process of softening is more intensified, microhardness is lowered even more and more. The slip lines become wider and longer, and the number of slip lines increases. The rise of the losses continues but at a lower rate in the third stage. Microcracks form and some of them link together and develop to a fatigue macrocrack. Formation of a macrocrack is marked by a certain lowering of the losses at the end of the third stage. A steep climb of the losses in the fourth stage indicates a rapid growth of the fatigue crack. Duration of each of these stages differs and depends on the material and the level of the cyclic stresses. The duration of each stage relative to the total fatigue life for a given material, however, is about the same for all stress levels.

Below fatigue limit, microhardness increases while the losses decrease with the increasing number of cycles. Softening can occur in weak grains, but this process does not spread to other grains because of low cyclic stresses.

Since the maximum of the losses vs number of cycles curve indicates the formation of a macrocrack, detection of earlier fatigue damage must then rely on the determination of the onset of the third stage when the rate of the losses is lowered due to the formation of microcrack.

It should be noted that the magnetic hysteresis and eddy current losses are not entirely caused by internal stresses. Inclusions, voids, cracks, and chemical segregation can also influence these losses.

Magnetic tests measuring perturbation in the magnetic field have been employed to detect fatigue damage in the form of cracks (Kusenberger et al, 1964 and 1966). The perturbation is caused by the change of magnetic permeability by internal stresses or the other factors mentioned previously. The crack is indicated by a sudden increase in peak-to-peak signal amplitude in a record. The detection of cracks is primarily a function of signals caused by the stressed volume adjacent to the crack and not by the material separation. The minimum crack length that can be detected in 4340 steel is 0.006 to 0.008 inch.

ELECTRIC IMPEDANCE

The electric impedance at a fixed frequency of a metallic specimen whose dimensions remain unchanged during measurement depends on electric conductivity

and magnetic permeability. To make the use of the skin effect of high-frequency currents, it is possible to study the change of electric impedance during fatigue deformation. When Armco iron wire is subject to torsional fatigue, no change in impedance at 35 kHz is observed if the shear strain is below a critical value which is less than the fatigue limit (Shlyapin et al, 1967). The impedance hysteresis loop also does not change its form. If the cycling strain exceeds the critical value but is below the fatigue limit, the impedance decreases gradually with an increasing number of cycles. Though the hysteresis loop changes in the process, it tends to approach the stable form below the critical strain. The impedance decreases more rapidly with an increasing number of cycles when the cycling strain is above fatigue limit. Shortly before failure, some increase in the impedance is observed, probably due to the appearance of fatigue cracks. The rate of change in the hysteresis loop during test differs little from the change at the fatigue limit. However, the loop cannot become stabilized because of failure of the specimen. Early fatigue damage must then be detected by analyzing the change in the form of the hysteresis loop and the trend of the impedance vs number-of-cycles curve before the rise of impedance due to the formation of macrocracks.

Another approach is to make the specimen after fatigue deformation one end of a low-loss cylindrical cavity resonator (Benson et al, 1968). The transmission loss of the cavity is mainly due to the loss of the specimen. The system must be operated at the exact resonant frequency of the resonator in order to make the magnitude of the signal transmitted through the cavity meaningful. The loss curve for a 2024-T3511 aluminum alloy specimen shows little change until approximately 80 percent of the fatigue life is spent. It then rises rather sharply before failure of the specimen.

Cylindrical specimens have also been made in the form of a low-loss, half-wave linear resonator operated at frequencies near 1 GHz (Benson et al, 1968). The increase in electric resistivity at the surface layer due to the presence of microcracks results in an increase in bandwidth of the resonator when it is considered as a band-pass filter. When fatigue deformation in aluminum alloys is measured, the surface resistivity does not change in the first one-fourth of fatigue life. Afterwards, the measured resistivity can be either above or below the previous constant value. The scatter is so wide that it is difficult to correlate fatigue damage with surface resistivity.

OPTICAL PHENOMENA

An optical correlation technique has been used to detect changes in surface structure resulting from fatigue deformation (Chuang, 1968). The correlation function for a given surface area is measured before and after cyclic stressing in terms of light intensity output of a coherent optical system.

Change in surface structure produces a decrease in correlation intensity. The surface strain that can be detected is of the order of 1 micron.

The correlation intensity vs number-of-cycles curve can generally be divided into three stages. A sharp loss of the correlation intensity (as much as 80 percent) in the first few minutes constitutes the first stage. The loss then becomes relatively steady in the second stage. Finally, a sharp loss before a visible crack appears starts the third stage. Early fatigue damage must therefore occur in the first two stages.

INTERNAL FRICTION

Internal friction of solution-treated aluminum alloys containing magnesium subject to cyclic stressing below the fatigue limit is practically constant. Above the fatigue limit, internal friction decreases with an increasing number of cycles. The formation of a fatigue crack is indicated by an increase in internal friction (Hanstock, 1947). However, tests on solution-treated and aged aluminum alloys containing mainly copper reveal that above but near the fatigue limit, the internal friction increases almost imperceptibly during many millions of cycles, followed then by a rapid rise before specimen failure. The rise is mainly due to precipitation induced by cyclic stressing and not to the formation of cracks (Hanstock, 1954). In pure metals, such as aluminum, cadmium, and copper, above the fatigue limit the internal friction first increases and remains practically constant with continued cyclic stressing. Near the end, there is again a rise which is attributed to the appearance of a fatigue crack (Gorshkov and Postnikov, 1965).

Both internal friction and early fatigue damage are related to the movement of dislocations and their interaction with point defects. Their relationship, however, is complex because internal friction is associated with bulk-property-type measurement while fatigue damage occurs only at the surface layer.

PROPAGATION OF ULTRASONIC WAVES

In addition to detecting flaws, propagation of ultrasonic waves in metal parts has also been employed to investigate early fatigue damage by means of noting the changes in ultrasonic attenuation and velocity. Measurement of the ultrasonic attenuation in aluminum specimens subject to tension-tension or tension-compression cyclic loading reveals that the attenuation starts to decrease from the beginning, reaching a minimum value between 100 and 1000 cycles or approximately at 1/100 to 1/1000 fatigue life (Truell et al, 1959 and 1961). Subsequently, the attenuation rises again as deformation

continues. This variation in attenuation with time is attributed to a dislocation effect. A large increase in the dislocation density can be expected within a few cycles at the beginning. The dislocation density increases with continued cycling until dislocation damping, which contributes to attenuation, is reduced both from the shortening of loop lengths, due to increased intersection and defect pinning, and from direct interference or interaction of the dislocations among themselves.

Another phenomenon also causes a rise in attenuation as the dislocation density increases with continued cycling. Regions of dense dislocation form because of the shortening loop lengths and their mutual interference. High internal strains are present in these regions within each grain. These regions are therefore scattering centers, causing increased attenuation as their size and number increase with number of cycles. The minimum of the attenuation vs number of cycles curve is a result of competition between the decrease in dislocation damping loss and the increase in the scattering loss. The increase in attenuation by scattering eventually becomes large and dominant.

Under fatigue deformation, either in tension or in compression, the velocity of wave propagation starts to decrease at the beginning with respect to the initial value before deformation. This decrease is characteristic of dislocation damping behavior. The change in velocity becomes smaller as deformation continues until the range of cycling for the attenuation minimum is reached. The change then again begins to increase rather rapidly with an increasing number of cycles.

The regions of high internal strain in a grain, which serve as scattering centers to the propagation of ultrasound, could be identified with the regions of abnormally high dislocation density revealed by transmission electron micrographs. Such regions are therefore the potential nucleation sites of microcracks.

The wave modes employed by Truell and his associates were mainly longitudinal waves. A longitudinal wave is a volume-type wave, but fatigue damage develops only at or near the surface of a test specimen. Rayleigh waves or surface waves therefore seem more appropriate for studying the change in attenuation and velocity of propagation. Moreover, depth of wave penetration is controllable.

The change in attenuation as well as velocity of propagation of a Rayleigh wave in mild steel subject to fatigue deformation has been investigated by Herlescu and his coworkers (1967). Both attenuation and velocity tend to increase slightly at the early stage of fatigue (about 1/100 to 1/1000 life). They then drop considerably and become somewhat constant as cycling proceeds.

Finally, there is a pronounced increase of attenuation as a result of dispersion of ultrasound at the microcracks. Velocity in this interval changes relatively little.

Relaxation and work-hardening are thought to cause such changes in the propagation of ultrasound waves. Relaxation is assumed dominant in the beginning. Later, work-hardening intensifies, and relaxation ceases to play an important role. Search of fatigue damage should thus be concentrated in the period prior to the formation of microcracks when both attenuation and velocity first decrease and then become constant.

ACOUSTIC EMISSION

Acoustic emission is the propagation of a spontaneously generated elastic wave created by discrete movements within the volume of the material being stressed. The generation of elastic wave is associated with plastic deformation processes, such as twinning, slip and microcrack formation. This phenomenon also includes the propagation of released strain energy upon fracturing. Acoustic emissions has been used to study the fracture process (Dunegan et al, 1968) and to monitor crack growth in precracked specimen so that its fatigue life can be predicted by combined fracture mechanics and acoustic emission techniques (Harris et al, 1969). Since slip movement in plastically deformed metallic materials can cause acoustic emission, and slip bands invariably appear on a metal surface in the fatigue process, there should be a certain relationship between acoustic emission and metallurgical change by fatigue. It is thus possible to detect fatigue damage due to this structural change by determining the acoustic emission characteristics of originally unflawed materials.

EXOELECTRON EMISSION

The term exoelectron has been used to describe electrons emitted from both metals and nonmetals which have been subjected to various treatments, such as abrasion, mechanical deformation, irradiation with ultraviolet light, X-rays or ultrasonic waves, electron bombardment, electric gas discharge, chemical interaction between the material surface and the ambient gas, phase transformation upon heating or cooling, etc. The first comprehensive discussion of this subject took place in an exoelectron conference held in 1956 in Austria. A number of reviews (Grunberg, 1958; Mueller, 1961; Bohun, 1963; Bohun, 1965; Ramsey, 1965; Brotzen, 1967) have been published since then. Because exoelectron emission can be excited in a variety of ways, there is much confusion in the literature on the mechanism of emission. The present survey will therefore not be devoted either to examining the mechanisms or to

reviewing the present state of the art. Rather, the objective is to make a concise report on the exoelectron emission arising mainly from abrasion or plastic deformation of metallic materials. Such knowledge is essential to developing new testing techniques based upon exoelectron emission for assessing the damage of metals subjected to cyclic stressing. An annotated bibliography containing articles dealing mainly with exoelectron emission from abraded or plastically deformed metals and published after 1956 is presented in appendix I.

The emission of electrons from abraded or deformed metal surfaces has been interpreted in several ways: (1) The interaction of gas with the freshly worked surface resulting either in the release of energy due to chemisorption of oxygen (Haxel et al, 1952; Lohff, 1956) or the absorption of water vapor (Ramsey, 1967) or in the formation of a layer of defected structure containing trapping sites which produce a surface of lower work of function (Grunberg and Wright, 1955; Ramsey and Garlick, 1964), (2) the release of energy associated with the vacancies reaching the surface by diffusion (von Voss and Brotzen, 1959; Ku and Pimbley, 1961), and (3) the transfer of energy associated with the stress field around dislocation to electrons (Krogstad and Moss, 1965). The active emission centers are assumed to be chemisorbed atoms, vacancy clusters, points of emergency of dislocations on the surface, etc. Therefore, exoelectron emission can occur by the interaction between the metal surface and the ambient gas as well as by the deformation of the metal lattice. It is also found that the effect of the former can be weakened by localized and dynamic loading in vacuum (Mints and Kortov, 1967).

Emission caused by the deformation of the lattice must be associated with dislocations or point defects. This is demonstrated by the correspondence between the darkened spots on the emulsion applied to a statically strained zinc single crystal and dislocation etch pits along the slip lines (Meleka and Bari, 1960), and by the emission of electrons from aluminum after quenching from temperatures between 300° and 450° C (Claytor et al, 1966). The release of electrons can be facilitated by lowering the work function of the metal surface, since change in the contact potential with strain in molybdenum and tantalum indicates that the work function of these metals is reduced as a result of plastic deformation (Andreev and Paligé, 1962 and 1964). The work function changes are associated with surface structure modifications.

The kinetic characteristics of emission is influenced by the mobility of point defects. The time for ground aluminum to reach the maximum emission before decay sets in is shorter than the time for ground gold at a pressure about 10^{-4} torr (Mints and Kortov, 1967). Shorter time to peak emission is attributed to higher mobility of point defects because time is required for dislocations and point defects moving to the metal surface. By the same reasoning, decay of the emission from the metal surface having point defects of lower mobility should be slower. This phenomenon is observed in the experiment with ground silicon and germanium (Kryuk et al, 1966). The slower decay for silicon is due to lower mobility of vacancies, indicated by a greater activation energy for self-diffusion in silicon.

The mobility of point defects increases with temperature. The emission from abraded metal surfaces (Ku and Pimbley, 1961; Ramsey, 1965; Williams, 1966) or strained metal specimens (Hempel et al, 1964) has been found to increase with rising temperature. However, the relation between exoelectron emission and migration of the point defects to the surface is still not well understood because it is difficult to avoid the influence of ambient gas exerted on the surface. Freshly abraded aluminum specimens and those that were abraded and aged at room temperature for 8 days exhibited similar emission when their surfaces were etched (Mueller and Pontinen, 1964). Defects in the aged specimens had ample time to migrate to the surface and to internal sinks. The observed emission from abraded, aged, and etched specimens is probably due to interaction between the ambient gas and the new surface produced by etching.

In addition to surface conditions, structure of the metal surface can influence exoelectron emission. Local indentation on metallurgical phases of steels results in varying emission intensity (Kortov and Mints, 1965; Bogachev et al, 1966). The intensity of ferrite is greater than that of austenite which in turn has more intense emission than either martensite or epsilon carbide. Grains and grain boundary may also have different exoelectron emission.

Emission from most abraded or otherwise deformed metals is not observed in total darkness. Light is necessary, and the photoelectric threshold is shifted (Conrad and Levy, 1961). The explanation is that the energy of impinging photons is needed to add to the energy which is released by vacancies at the surface in order to exceed the work function of the surface (Pimbley and Francis, 1961). However, emission without photostimulation has been observed during plastic deformation of aluminum coated with a thick (over 50 μm) oxide layer (Gieroszynski and Sujak, 1965). Two emission peaks occur at a strain of 0.01-0.02 and 0.03-0.04. The emission is considered to originate from the oxide layer and is attributed to large electric fields (about 10^7 v/cm) when the cracks in the oxide layer are formed.

Deceleration methods have been used to determine the average kinetic energy of exoelectrons (Lohff, 1957; Bathow, 1958). The value for abraded metals in vacuum varies from 0.13 to 0.20 ev. The highest energy that can be determined depends on the emission intensity and the sensitivity of the measuring apparatus. The emission intensity prior to saturation relates to the grid potential by the equation:

$$N = N_0 \exp \left(\frac{U - U_k}{\bar{U}} \right)$$

where

N = number of emitting electrons per second

N_0 = saturated number of emitting electrons per second

U = grid potential

U_k = contact potential between grid and the specimen

\bar{U} = a constant

A design of a spectrometer to measure electron energy is shown in appendix II.

Since exoelectrons emit at the surface of a material, it is essential to know the thickness of the surface responding to emission. Experiments on emission excited by electron bombardment reveal that the estimated thickness varies from $2 \times 10^2 \text{ \AA}$ at 1 kv for tungsten and germanium (Seeger, 1955 and 1957) to $5 \times 10^3 \text{ \AA}$ at 5 kv for CaSO_4 containing manganese (Vogel, 1960). Successive removal by etching of surface layers from an abraded aluminum specimen shows that emission dies out at approximately a depth of 0.2 \mu m or $2 \times 10^3 \text{ \AA}$ (Mueller and Pontinen, 1964).

Since fatigue cracks usually start at or near the surface, both fatigue damage and exoelectron emission belong to surface phenomena. Furthermore, cyclic stressing can accumulate rather large amounts of plastic strain, and the emission intensity increases with increasing amount of deformation (von Voss and Brotzen, 1959). Therefore, exoelectron emission could be a measure of cumulative fatigue damage.

Exoelectron emission by fatigue deformation has been reported (Grosskreutz and Bensen, 1963; Hempel et al, 1964; Krogstad and Moss, 1965; Bogachev et al, 1966; Mints and Kortov, 1967; Mints et al, 1968). The intensity generally increases with the number of cycles. After it reaches a saturated value, it slowly decreases until specimen failure. A rapid rise of intensity shortly before failure has also been observed. This rise is attributed to the formation of fatigue cracks, but it cannot be used to assess fatigue damage because the damage occurs and grows at the early stage of fatigue deformation. Therefore, the progressively changing emission events during the test before the final rise should be analyzed.

OTHER PHENOMENA

Since fatigue damage is a surface phenomenon, the change of certain surface-sensitive properties may offer an indication of this damage. Besides

the optical properties described above, the surface potential difference between a fatigue-stressed material and a reference metal has also a potential toward developing nondestructive test technique for detecting fatigue damage.

The possibility of using nuclear phenomena can also be considered. The use of the Mössbauer effect for the measurement of residual stresses has been considered by Gonser and Martin (1963), and Gonser (1968) suggests that plastic deformation would affect nearest neighbor interactions. However, for practical purposes, the use of the Mossbauer effect is limited to ferrous alloys.

CONCLUSIONS

Fatigue damage can be correlated with the changes of a number of physical properties. The physical properties which have been investigated have their own merits as well as drawbacks. Magnetic hysteresis losses are limited to ferrous materials. Internal stresses are the principal factor that causes magnetic hysteresis and eddy current losses, but fatigue process is not mainly dependent upon internal stresses. The electric impedance method is better to indicate crack formation and propagation leading to specimen failure than to detect earlier fatigue damage. The changes of correlation intensity of a coherent system in a fatigue process might offer an indication to earlier fatigue damage. More information is needed. Internal friction is a bulk-type physical property, but early fatigue damage concentrates in the surface layer. Their correlation is therefore poor. Propagation of ultrasonic waves is a promising method to detect fatigue damage. Surface waves instead of longitudinal or shear waves should be utilized to interrogate only the surface layer. There is likely a relation of fatigue damage with exoelectron emission because both belong to surface phenomena. Acoustic emission also looks promising because of its relation to plastic deformation processes.

Five physical phenomena were therefore chosen for the study toward developing nondestructive methods to detect fatigue damage. They are exoelectron electron emission, acoustic emission, propagation of ultrasonic surface wave, surface potential difference and optical properties in terms of ellipsometric parameters.

SECTION IV

SPECIMEN DESIGN AND FATIGUE TEST SYSTEM

MATERIALS

The selection of test materials was based on consideration of the following factors: the material should represent current and planned engineering materials, available in production quantities, machineable and heat treatable, capable of definition in terms of metallographic and dislocation structure, and the material should have been previously evaluated in terms of metallurgical and fatigue test data to permit comparisons of results. Of these requirements, the definition of metallurgical properties was considered a paramount consideration. Dislocation motion is generally dependent on the lattice structure and the existence of dispersions, inclusions, etc., of a size which causes the maximum effect on dislocation motion and generation of secondary dislocations. The following material alloys were initially considered to represent the most promising candidate materials:

1. Pure aluminum, representative of a FCC metal with the minimum of pinning of dislocations.
2. 2024 aluminum alloy in the T6 condition representing a FCC alloy of engineering interest, providing maximum pinning of dislocations.
3. Titanium 6Al-4V alloy, annealed condition, representing a CPHex alloy with minimum dislocation pinning.
4. Titanium 6Al-4V alloy, STA condition, presenting a CPHex alloy of engineering interest with some dislocation pinning.
5. Mild steel, normalized, representing a ductile BCC alloy.
6. 4340 steel, quenched and tempered, representing a complex BCC alloy.

These candidate materials and others were discussed with other participating contractors and the final material selections are identified in the following section.

Initially, Armco iron was selected on the basis of wide industrial interest, ready availability, and as typical of body-centered cubic material. Preliminary fatigue tests indicated that specimens loaded to 95.7 and 98.2 percent of the ultimate strength failed after 9,000 and 15,000 cycles, respectively, with indications of considerable necking; whereas a specimen loaded to 88.5 percent of the ultimate strength did not fail after 3.6×10^6 cycles. These results indicated an extremely flat fatigue curve, which would have made

accurate control of life to failure very difficult. It was, therefore, decided to store the Armco iron for possible future use and, for initial studies, to use a grade 1100-0 aluminum alloy. The material gave the following mechanical properties:

	Supplier Data	Own Data
Ultimate tensile strength, ksi	13.5/13.8	12.76
Tensile yield strength, ksi	6.7/6.8	6.53
Elongation to failure, % in 2 inches	33/34	31.80

Other materials which are used in manufacturing components of air vehicles and structures were also used in this program. The materials were 7075-T6 aluminum alloy, D6AC steel and EI grade annealed 6Al-4V titanium alloy, and were furnished by Aerojet Solid Propulsion Company. The D6AC steel was in mill annealed condition. In addition to the three materials, Aerojet Solid Propulsion Company also supplied 1100-0 aluminum, which had already been selected for this program.

Tensile properties of the four materials are shown below.

<u>Material</u>	<u>Tensile yield strength, ksi</u>	<u>Tensile ultimate strength, ksi</u>
1100-0 aluminum	—	13
7075-T6 aluminum alloy	70	80
annealed 6Al-4V titanium alloy	130	140
annealed D6AC steel	70	100

Since the 1100-0 aluminum came from two sources, it was necessary to distinguish the one from the other so that the test results could be compared. Henceforth the aluminum purchased by North American Rockwell Corporation for the use in this program is referred to as the aluminum of source A, whereas that furnished by Aerojet Solid Propulsion Company is called the aluminum of source B.

SPECIMENS

Standard fatigue test specimens 7 inches long were cut from the 0.09-inch-thick 1100-0 aluminum sheet stock of source A. Each side of the test section has a 6-inch radius. The widths at the center and at the end of the test section are 1/2 inch and 1-1/8 inch, respectively. After machining they were

electropolished in a bath containing 25 percent nitric acid and 75 percent methanol. After electropolish, they were rinsed with water and then with isopropyl alcohol. In addition, several specimens were not electropolished but chemical polished with a solution similar to Keller's etch for aluminum but containing twice the usual amount of hydrofluoric acid. The surfaces of both electropolished and chemical polished specimens exhibit the same grain structure when examined under a microscope.

The specimens fabricated by Aerojet Solid Propulsion Company had a straight 2-inch test section with a 1/2 inch width. A fillet of 1-inch radius joined the test section to the specimen end which is 1 inch wide. The nominal thickness of the aluminum and its alloy specimens was 0.09 inch, whereas that of the titanium alloy and steel specimens was 0.10 inch. This specimen configuration was found unsatisfactory since fatigue fracture repeatedly occurred at either the end of the test section or the fillet. Each side of test section was then notched with a 6-inch radius cutter so that the smallest specimen width between the notch roots was about 0.41 inch. The fillet radius was increased to 3 inches. Fatigue fracture of the modified specimen then took place at the middle reduced section.

The thickness of one-half of the annealed D6AC steel specimens was further reduced by grinding to about 0.062 inch. They were heat treated by austenitization at 1,600°F for 1 hour followed by oil quench, snap temper in salt bath at 400°F for 4 hours and final temper at 1,000°F for 4 hours followed by air cool. Hardness of the heat-treated specimen was about 46 on Rockwell scale.

The 1100-0 aluminum specimens were either chem-milled or electropolished before test. Composition of the chem-milling solution on a one-gallon basis is 20 ounces sodium hydroxide, two percent by weight sodium gluconate and two percent by weight sodium sulfide. The temperature of the solution was kept at around 160°F. Electropolishing was carried out at a current density of 0.15 ampere per square centimeter in a bath containing 60 percent phosphoric acid and 40 percent sulfuric acid heated between 160 and 170°F. The 7075-T6 aluminum alloy specimens were chem-milled in the same solution used for preparing the 1100-0 aluminum specimens prior to test. The 6Al-4V titanium alloy specimens were chem-milled in Turcoform 200 Etchant at about 135°F. The annealed D6AC steel specimens were first chem-milled in an acid bath but the resulting surface was very rough. The bath was abandoned and both the annealed and the heat-treated specimens were hand polished with emery papers down to grade 600.

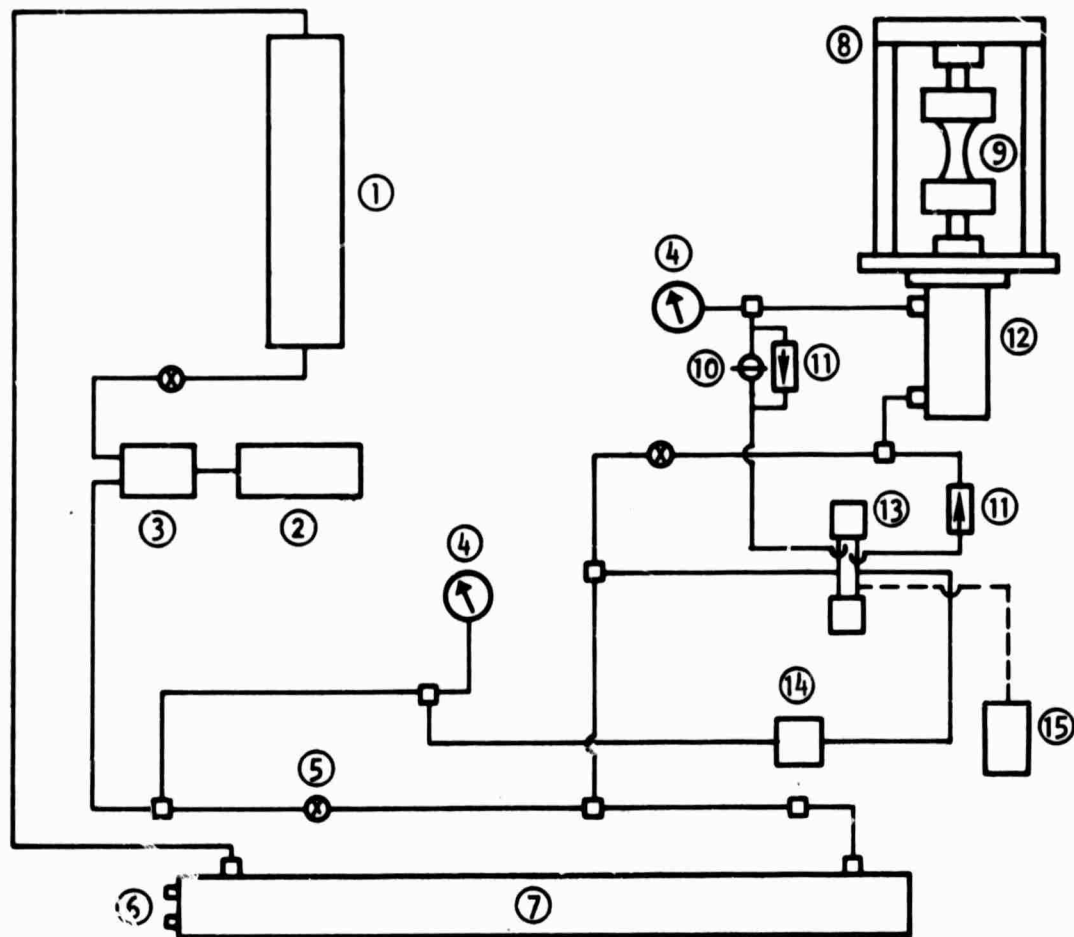
FATIGUE TEST UNIT

To investigate the various nondestructive test approaches under dynamic conditions and appropriate environmental control, it was necessary to con-

struct a small, portable fatigue test unit. This unit consists of a pumping, timing, and metering unit which feeds hydraulic fluid into a double-acting piston and cylinder arrangement connected directly to one end of the specimen (figure 1). The piston and cylinder unit is rigidly attached to a loading frame, which also supports the other end of the specimen. A microswitch attached to the loading frame stops all circuits on specimen failure. A plate inserted between the piston and cylinder unit and the specimen serves as a base for mounting a ring carrying a glass chamber, which can be evacuated and which contains necessary instrumentation. Figure 2 shows a specimen in the loading frame. The unit is designed for loads up to 5,000 pounds and for cycling rates varying from a steady pull to 120 cycles per minute. The rate for the tests planned is standardized at the upper limit. Actual loads are measured by four strain gages mounted on a link between the loading frame and the upper specimen grip. Connecting the lower specimen grip and the base plate is a metal bellows, which gives a flexible vacuum seal. The number of cycles is counted by a counter installed on and electrically connected to the control box of the hydraulic system. Variation of the load during test is displayed on a recorder connected to a carrier amplifier into which the output of the strain gages is fed. A calibration curve relates the load to hydraulic pressure.

Because of the use of the 4-way solenoid valve to apply hydraulic pressure to the loading cylinder, both the mechanical and electrical surges generated by the valve in cycling were high, so that the background noise in acoustic emission could not be lowered to the desired level. Furthermore, since this type of valve is designed for low number of cycles, its useful life is fairly short, when it is used in fatigue tests each lasting about a million cycles. Therefore, in the later part of this program the solenoid valve was replaced with an electro-hydraulic servo system. A sine-wave signal generator creates the forcing function and establishes the desired load pattern. The actual load is sensed at any instant during fatigue test by the strain gage load cell and is compared with the desired function. Any difference between the desired value and the actual value is amplified and applied as a correction voltage to the hydraulic servo valve to increase or decrease the pressure as required. The servo loop maintains a load which is analogous to the generator signal. This system runs much quieter and the test frequency can be increased from two to about twenty cycles per second. All the fatigue tests were henceforth conducted at ten cycles per second.

The vacuum system consists of a mechanical pump, an oil diffusion pump, two liquid nitrogen cold traps, gages necessary for measuring pressure, and a glass chamber in which the loading frame is housed. The use of a second cold trap is to prevent backstreaming of oil from the diffusion pump and contamination of the instruments in the glass chamber. The ring on which the glass chamber is mounted is pierced by a 2-inch-diameter vacuum suction tube, a 5/16-inch air inlet hole, and electric vacuum leadthroughs. Altogether, provision is made for a high-voltage leadthrough, an RF leadthrough, a



—— HYDRAULIC LINE - - - - ELECTRICAL LINE

- | | | | |
|---|--------------------------|----|-------------------------|
| 1 | RESERVOIR | 10 | NEEDLE VALVE |
| 2 | MOTOR | 11 | CHECK VALVE |
| 3 | PUMP | 12 | HYDRAULIC CYLINDER |
| 4 | HYDRAULIC PRESSURE GAUGE | 13 | FOUR-WAY SOLENOID VALVE |
| 5 | BY-PASS VALVE | 14 | PRESSURE RELIEF VALVE |
| 6 | WATER INLET AND OUTLET | 15 | CONTROL |
| 7 | HEAT EXCHANGER | | |
| 8 | LOADING FRAME | | |
| 9 | SPECIMEN | | |

Figure 1. Hydraulic System

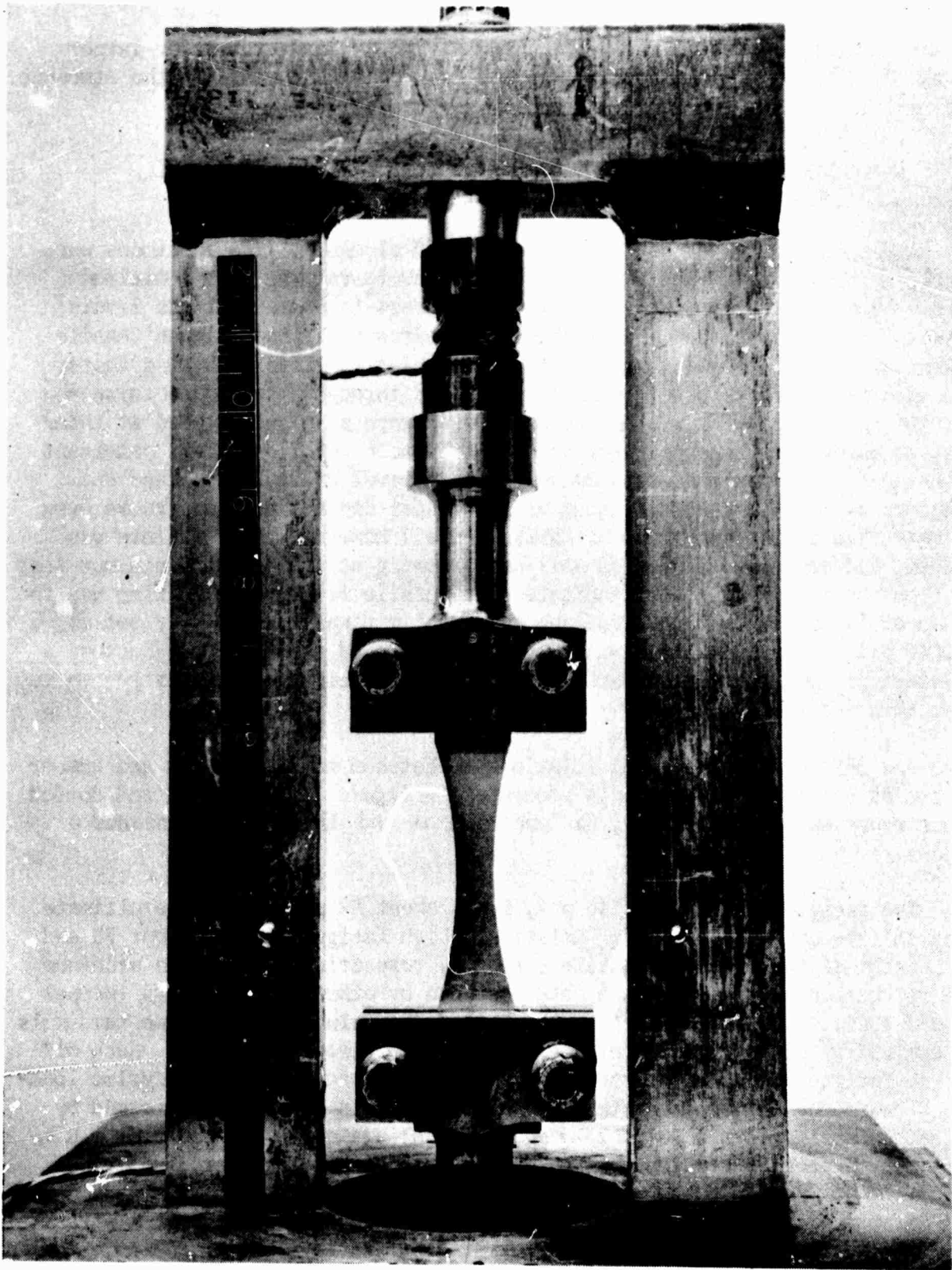


Figure 2. Photograph of Specimen and Loading Frame

seven-pin milliampere leadthrough, and an eight-pin leadthrough for larger currents. The load strain gage leads for load calibration are on the atmosphere side of the bellows.

FATIGUE CHARACTERISTICS FOR 1100-0 ALUMINUM

A fatigue curve was determined for 1100-0 aluminum. The specimens were tested in tension-tension loading at stress levels varying from a minimum stress equal to 2.5 percent of the maximum stress to maximum stress levels between 11,160 and 11,800 psi or about 92.5 percent of the ultimate tensile strength. Three specimens were tested at each stress level. During tests, the specimen surfaces were continually watched through a telescope to search for the appearance of a visible crack. Tests were also interrupted at intervals to check for the appearance of cracks by means of fluorescent penetrant technique. Two specimens at a maximum stress level of 11,800 psi and one specimen at a maximum stress level of 11,640 psi did not develop cracks even at more than their 94 percent of fatigue life. However, their failure was sudden, and ample stretching as well as narrowing at and near the minimum test section observed in the test indicate that tensile fracture by necking was the cause of failure. The upper fatigue loading limit was consequently set at 11,640 psi. The lower limit was roughly established at 10,540 psi because a specimen did not exhibit a crack at this stress level after being stressed to more than 5.3×10^6 cycles.

The S-N curve showing the relationship between maximum stress and number of cycles for 1100-0 aluminum is presented in figure 3. The solid and dotted lines represent, respectively, fatigue failure and the first appearance of cracks.

The fatigue limit is 10,540 psi, i.e., about 82 percent of the ultimate tensile strength (12,760 psi). Relatively high fatigue limits (about 70 and 75 percent of the ultimate tensile strength, respectively, for pure aluminum and low carbon steel) have been obtained also by other investigators (Hempel et al, 1964). These figures are higher than the values for the same materials determined by symmetrical alternate loading with zero mean stress. Such different fatigue behavior is probably due to the characteristics of cyclic loading because the dislocation structure and density in a specimen deformed by repeated tensile stresses (nonzero mean stress) are quite different from a specimen in reverse bending test with zero mean stress (Feltner, 1963).

From the fatigue curve, it appears that necking could occur at a stress level of 11,640 psi, but does not occur at a stress level of 11,500 psi. The corresponding average fatigue life is 400,000 cycles, which is convenient from a test-time point of view. A total of 15 specimens were therefore prepared as noted and cycled, in lots of three, at this stress level to fractions of the total estimated life of 30, 50, 70, 80, and 90 percent. These specimens were used for metallographic evaluation of the fatigue-affected zone and for ultrasonic surface wave tests.

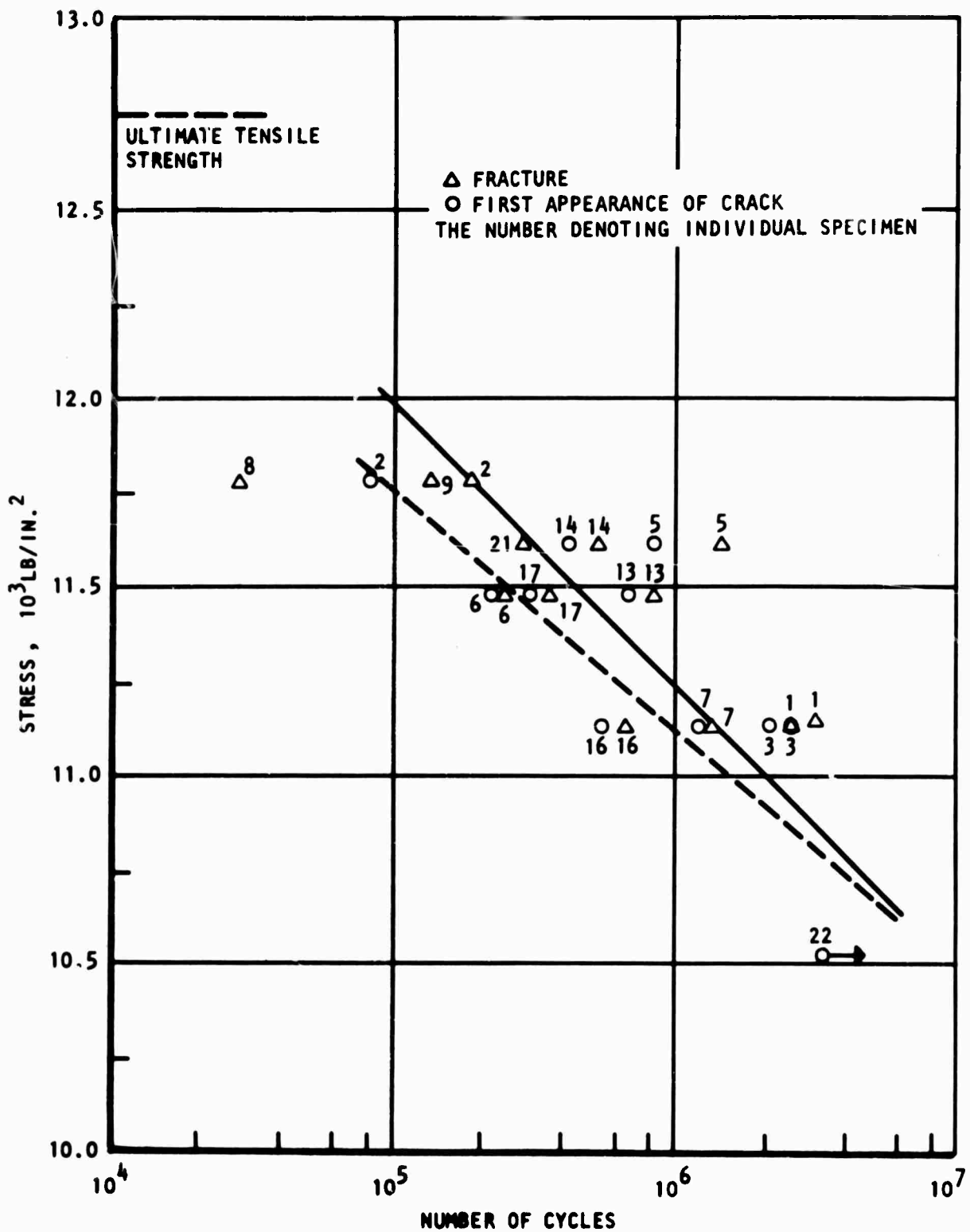


Figure 3. Fatigue Curve for 1100-0 Aluminum

SECTION V

EXOELECTRON EMISSION MEASUREMENTS

TEST SYSTEM

Two approaches to detect and measure exoelectron emission were evaluated. The first consisted of attempts to detect exoelectrons by means of phosphors. A number of cathode ray phosphors were available. Attempts at detection were both visual with the unaided eye and by means of an image intensifier. The instrument used was an Army Night Vision Sight AN/PVS-2 Starlight Scope with about 4X image magnification and approximately 40,000X intensity magnification. The use of this instrument required a completely blacked-out room in which the entire fatigue and vacuum equipment was placed.

The other approach was to measure the exoelectron emission intensity in both vacuum and air. A Bendix type 4039 Channeltron electron multiplier, connected as shown in figure 4, was utilized for the measurement in vacuum. The semiconductor-type multiplier is helical in shape and has a horn of 10 mm diameter at one end. The horn faces the middle portion of the specimen about 3/8 inch away through a hole at one side of a shield box. The shield box is charged at the same positive potential as the bias voltage to the electron multiplier so that only the electrons emitted from the specimen surface facing the horn enter the electron multiplier. The multiplier has a gain of about 10^8 with the application of 3,000 volts dc. The pulses from the electron multiplier are amplified and stretched before they are counted. The number of counts in either 1 or 10 seconds is finally printed on a tape by a digital printer. Figure 5 shows the Channeltron electron multiplier with the shield off and mounted on the loading frame.

After completion of several tests, the type 4039 Channeltron electron multiplier started to behave erratically. It was therefore replaced with a type 4013 electron multiplier which is circular shaped and has a horn with 3 mm diameter. Owing to this change of multiplier configuration as well as the space available in the glass chamber, the type 4013 Channeltron electron multiplier was placed about 2 inches away from the specimen. To compensate for the longer path for electron travel and the smaller horn, the shield box in which the electron multiplier was mounted was not at bias potential but was grounded to collect as many electrons as possible from the specimen surface.

The current of exoelectron emission for deformed metal is generally very small. It is necessary to stimulate the emission to enhance the current level so that it can be measured in air. A special current measuring system was

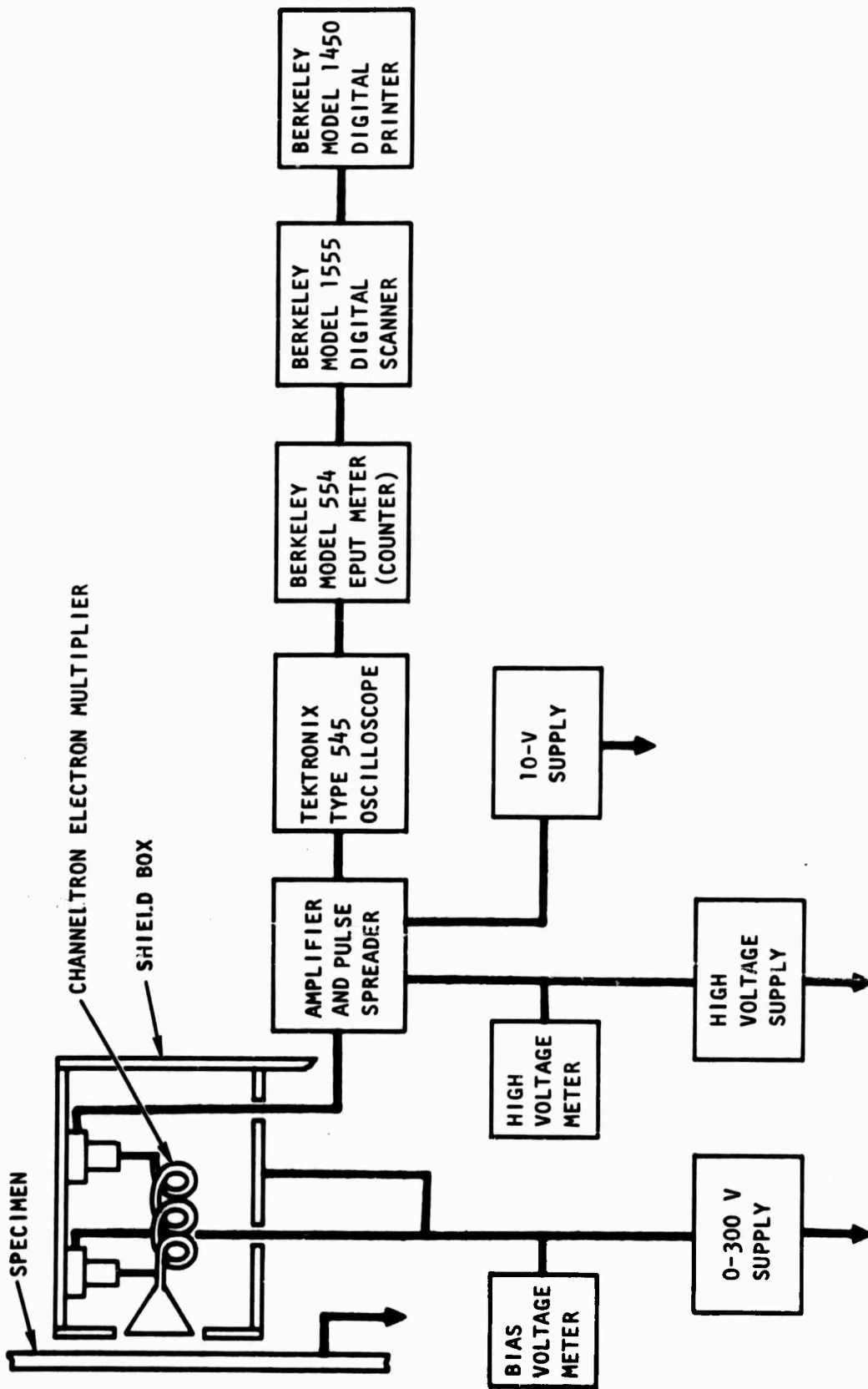


Figure 4. Block Diagram for Measuring Exoelectron Emission in Vacuum

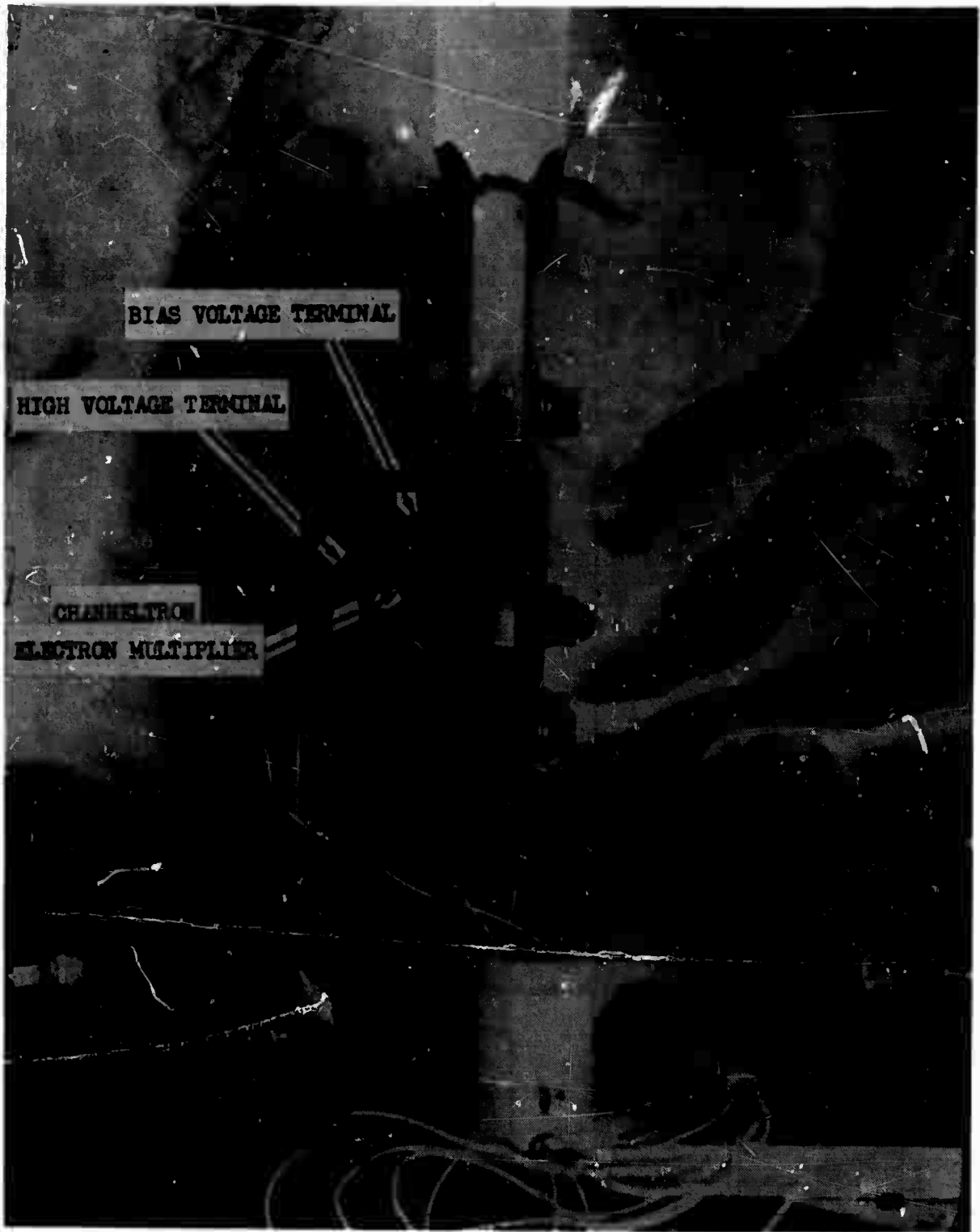


Figure 5. Channeltron Electron Multiplier and Loading Frame

devised (based on designs for a similar instrument developed by Professor S. Hoenig of the University of Arizona) to measure currents as small as 10^{-14} ampere. The system (figure 6) was an operational amplifier having field-effect transistors in the input stage. Current feedback through a very high precision resistor is used to null the input of the amplifier. The amplitude of the average voltage applied to the feedback resistor is a direct indicator of the current entering the collector plate from the specimen. The voltage is then converted to digital readings, using Electro Instruments electronic digital voltmeter (Model 8409), and is printed on tape with Hewlett-Packard digital recorder (Model 561A). The time interval between printing is controlled by the cycling of the hydraulic system of the fatigue test unit. A current reading is printed every 10^1 , 10^2 , 10^3 or 10^4 fatigue cycles. Measurements of exoelectron emission during a test requires three current ranges of 10^{-12} , 10^{-11} and 10^{-10} ampere per volt of output. The ranges are manually selected. Figure 7 shows this system enclosed in two boxes on top of the digital voltmeter and the recorder.

The exoelectron emission was stimulated with a short-wave ultraviolet lamp shielded in a metal box. The electron collector plate consists of a fine stainless steel screen mounted on a copper frame and having about 80 percent of open area. The ultraviolet light leaves the box through a 1/2-inch-diameter hole, passes through the screen and impinges upon the middle portion of the test specimen. The distance between the specimen and the screen is maintained at 1/4 inch; the ultraviolet lamp is 5/8 further away from the screen.

The electron-collecting system was later modified to improve the collection efficiency. The collector electrode in the form of a copper wire loop is surrounded by a copper casing. The collector is electrostatically shielded on one side by the specimen and on the other sides by a copper box. The three holes in the rear surface of the shield box give the effect of a screen to shield the collector from the electrostatic field around the ultraviolet lamp, which is housed in metal box described above. The ultraviolet light passes through these three holes and shines upon the specimen surface. Figure 8 shows the specimen installed in the loading frame with the collector electrode and the box housing the ultraviolet lamp.

The specimen and instrumentation for detecting exoelectron emission in air were enclosed in the glass chamber which was used for fatigue tests in vacuum, in order to lessen air movement around the specimen to preclude drift of the emission current. The acoustic background noise level was also greatly reduced for the acoustic emission measurements.

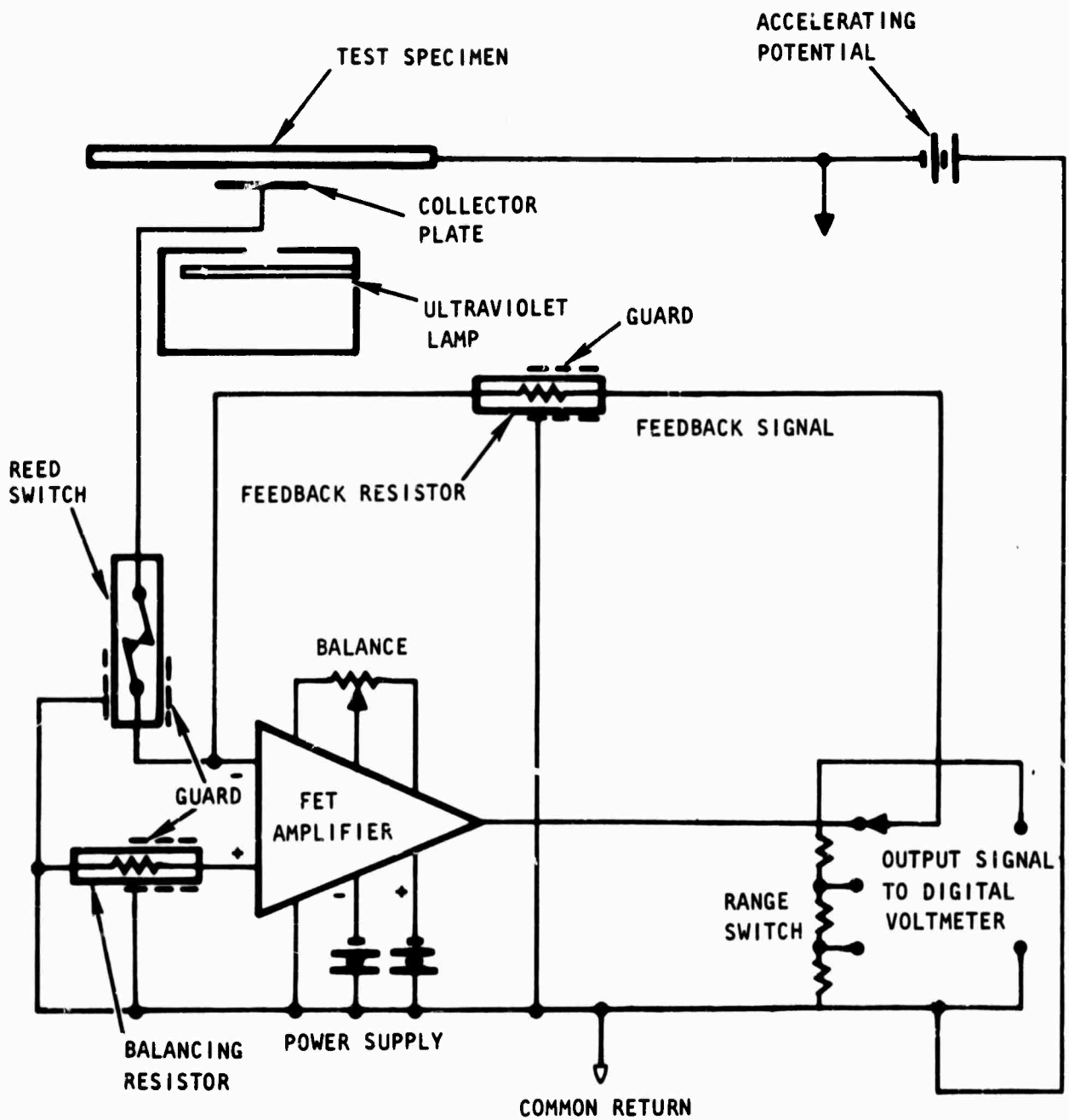


Figure 6. Schematic Diagram of the System for Measuring Exoelectron Emission in Air

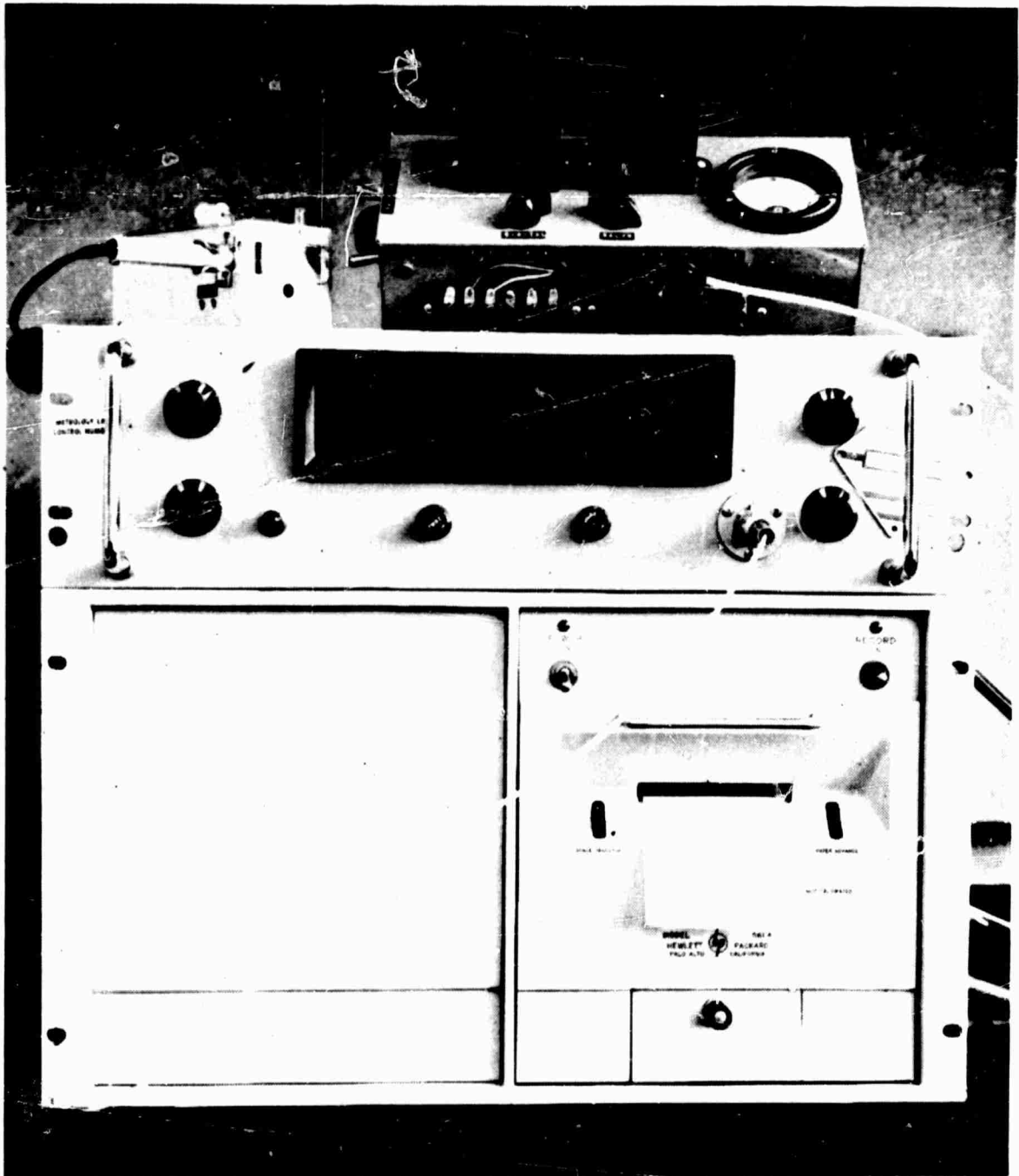


Figure 7. Photograph of the System for Measuring Exoelectron Emission in Air

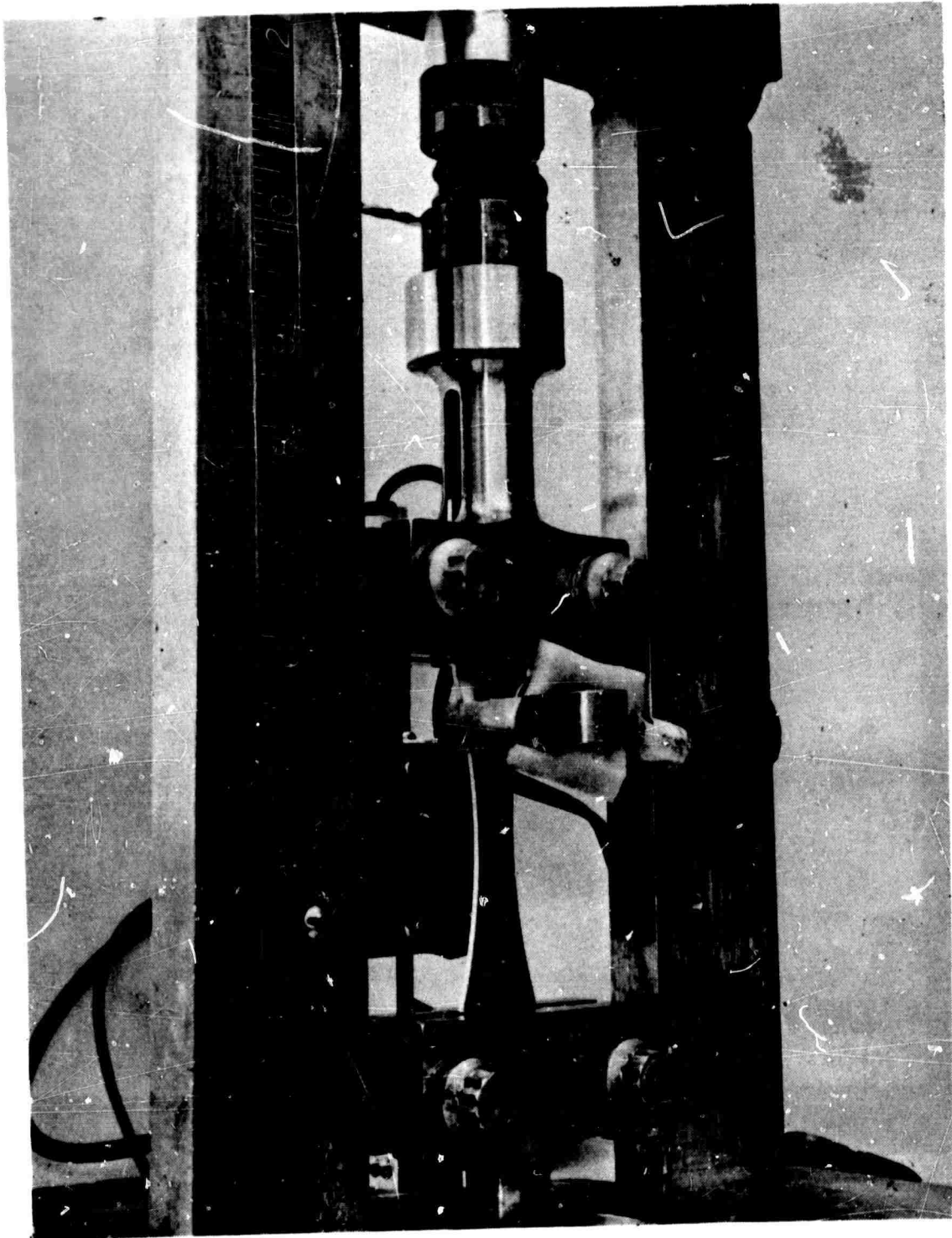


Figure 8. Photograph of Specimen With Exoelectron Emission and Acoustic Emission Transducers

EXOLECTRON DETECTION BY LUMINESCENCE

Several types of luminescent coating were tried. In one, a ZnO phosphor (lot T 962) developed specially for low-energy electron excitation and supplied by Dr. R. Schraeder of the RCA Laboratories was mixed with distilled water and air sprayed onto a silver film vapor-deposited on a glass substrate. This glass slide was connected to the positive terminal of an electric circuit and hung on the loading frame at an approximate 60-degree angle to the specimen. The Army Night Vision Sight AN/PVS-2 Starlight Scope was aimed at the phosphor-coated glass slide. The phosphor plate was charged with a potential of 5 volts relative to the specimen. Loading tests of the test specimens were carried out in complete darkness, with the specimen in air at atmospheric pressure and under a vacuum in the 10^{-5} torr range. In both tests, the stress was increased from 4,000 to 12,500 psi at an increment of 500 psi. Time at each increment was 2 minutes. No phosphorescence could be seen through the image intensifier at any time during either test.

To settle the problem of the usefulness of phosphor for direct observation of exoelectron emission, two thermal electron sources were used in a vacuum in the 10^{-5} torr range to simulate the emitter. The ZnO-coated glass slide and a cathode luminescent screen from an electron microscope acted as receivers. Circuiting was designed to allow charging of the receivers relatively to the emitters and measurement of the current between receivers and emitters. No electron-generated luminescence was observed with potentials up to 270 volts dc, though currents up to 10 microamperes were measured. Both luminescent receivers, however, responded readily to irradiation by ultraviolet light.

EXOLECTRON EMISSION IN VACUUM

Exoelectron emission in vacuum was measured by means of a Channeltron electron multiplier at room temperature. The bias voltage and high voltage at the electron multiplier were 10 and 3100 volts, respectively. The results for 1100-0 aluminum specimens of source A are summarized in table II.

For checkout of the electron multiplier, specimen 42 was subjected to static tensile loading at 10,650 psi under daylight for 20 seconds before the load was released. The intensity of emission, expressed in number of counts in 10 seconds, rose rapidly from a background level of 100 to more than 3,250 in about 50 seconds (figure 9). It then decreased to 1,450 counts in about 630 seconds. To prove that the emission phenomenon was indeed associated with deformation of the specimen, the same load was again applied for 15 seconds. The intensity responded by increasing the number of counts to about 4,300 in 34 seconds. Subsequent decay appeared to take place fairly slowly with the intensity still above 1,000 counts after the elapse of 22 minutes since the appearance of the second peak emission.

TABLE II. SUMMARY OF EXOELECTRON EMISSION TEST ON 1100-0 ALUMINUM IN VACUUM

Specimen No.	Maximum Stress (psi)	Number of Cycles		Strongest Emission (No. of Counts in 10 Sec)	Remarks
		Strongest Emission	End of Emission		
42	10,650	See figure 9	45,000	1,830	(1), (3), (4), (7)
45	12,600	See figure 10		3,430	(2), (3), (4), (7)
34	11,450	790		2,600	(2), (3), (4), (7)
46	11,450	740		1,090	(2), (3), (4), (6), (7)
66	11,450	630		0	(2), (3), (5), (7)
52	11,450	780			(2), (3), (5), (7)
43	11,450				(2), (4), (7), tested in darkness
44	11,450	See figure 14			(2), (4), (8), tested in ultraviolet light
35	11,000	650	10,500	600	(2), (3), (4), (7)
37	11,000	460	28,800	700	(2), (3), (4), (7)
65	11,000	940	32,500	570	(2), (3), (5), (7)
56	10,540	1,080	8,500	100	(2), (3), (5), (7)
57	10,540	830	6,100	110	(2), (3), (5), (7)
36	10,540			0	(2), (3), (4), (8)
61	10,000	950	3,200	70	(2), (3), (5), (7)

- NOTE:
- (1) The specimen was subject to tensile loading.
 - (2) The specimen was subject to fatigue loading.
 - (3) The specimen was tested under daylight.
 - (4) The specimen was electropolished prior to testing.
 - (5) The specimen was chemical polished prior to testing.
 - (6) The glass chamber was purged with argon prior to testing.
 - (7) Type 4039 Channeltron electron multiplier was used in the test.
 - (8) Type 4013 Channeltron electron multiplier was used in the test.

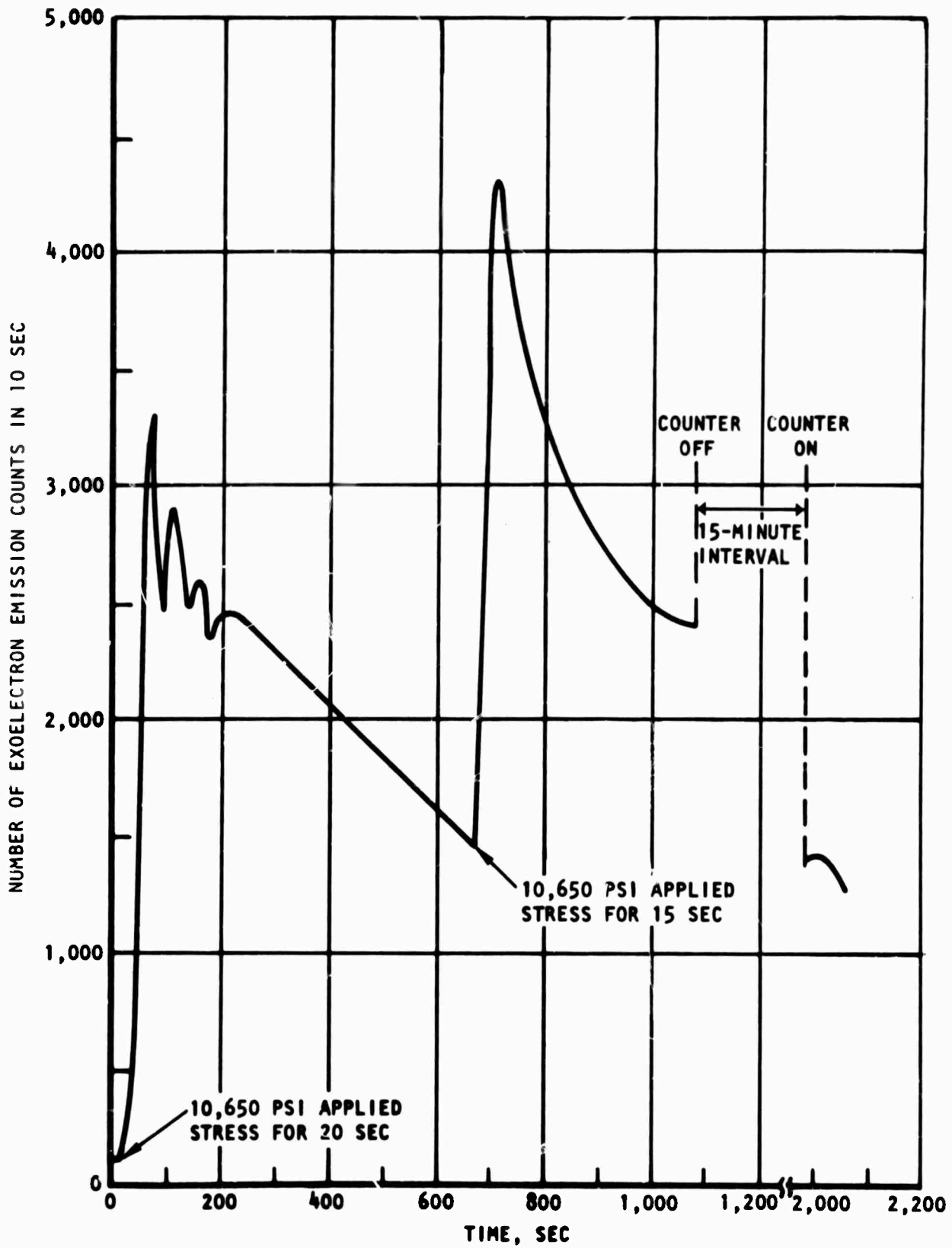


Figure 9. Exoelectron Emission of 1100-0 Aluminum in Vacuum at Tensile Stress 10,650 lb/in.²

With the assurance that the electron multiplier worked properly, a specimen (No. 45) was tested under daylight at a high fatigue load resulting a stress of 12,600 psi. The intensity of emission was measured by the number of counts in 1 second. The emission curve in figure 10 shows that a peak was reached in 3.5 seconds or 7 cycles. The emission then appeared to die out quickly, falling to the background level as cycling proceeded. At this point the midsection of the specimen started to fail by necking. The emission, however, rose again upon specimen fracture.

To avoid failure by necking, the stress applied to specimen 34 was reduced to 11,450 psi. Exoelectron emission started at about 100 cycles. Afterwards, the emission appeared to take place in bursts, as evidenced by a number of peaks in figure 11. The strongest intensity occurred at around 800 cycles. With further cycling, however, the emission intensity exhibited a decreasing trend despite the numerous peaks. The intensity fell to the background level after 4.5×10^4 cycles and it maintained at this level until about 6.69×10^5 cycles had elapsed. The emission intensity then rose again while a visible fatigue crack propagated during the continuation of fatigue loading. Finally the intensity experienced a rapid rise as the crack traversed the specimen at the point of final failure.

The same test condition was repeated on three more specimens. The emission of each specimen rose rapidly soon after start of the test and reached the highest peak in less than 1000 cycles. Thereafter it decreased gradually to the background level. Since the test on specimen 34 reveals that after falling to the background level, no further rise would take place until fatigue cracks developed near the end of the test and since this earlier emission period may offer some means to detecting early fatigue damage, testing of the three specimens was discontinued shortly after the emission intensity fell to the background.

Another specimen (No. 52) was also tested at 11,450 psi. Its emission behavior was slightly different from that of the other specimens described above. The fall of emission intensity of this specimen from the highest peak did not reach the background level before it rose again. Apparently this earlier rise was associated with formation and propagation of fatigue cracks. The premature failure of the specimen at 14,740 cycles (table II) substantiate this reasoning.

Three lower stress levels; namely 11,000, 10,540 and 10,000 psi, were applied to more 1100-0 aluminum specimens in order to investigate the effect of stress on exoelectron emission. All tests were conducted under daylight and discontinued shortly after the emission intensity reached the background level. A comparison of figure 12 with figure 11 reveals that the emission

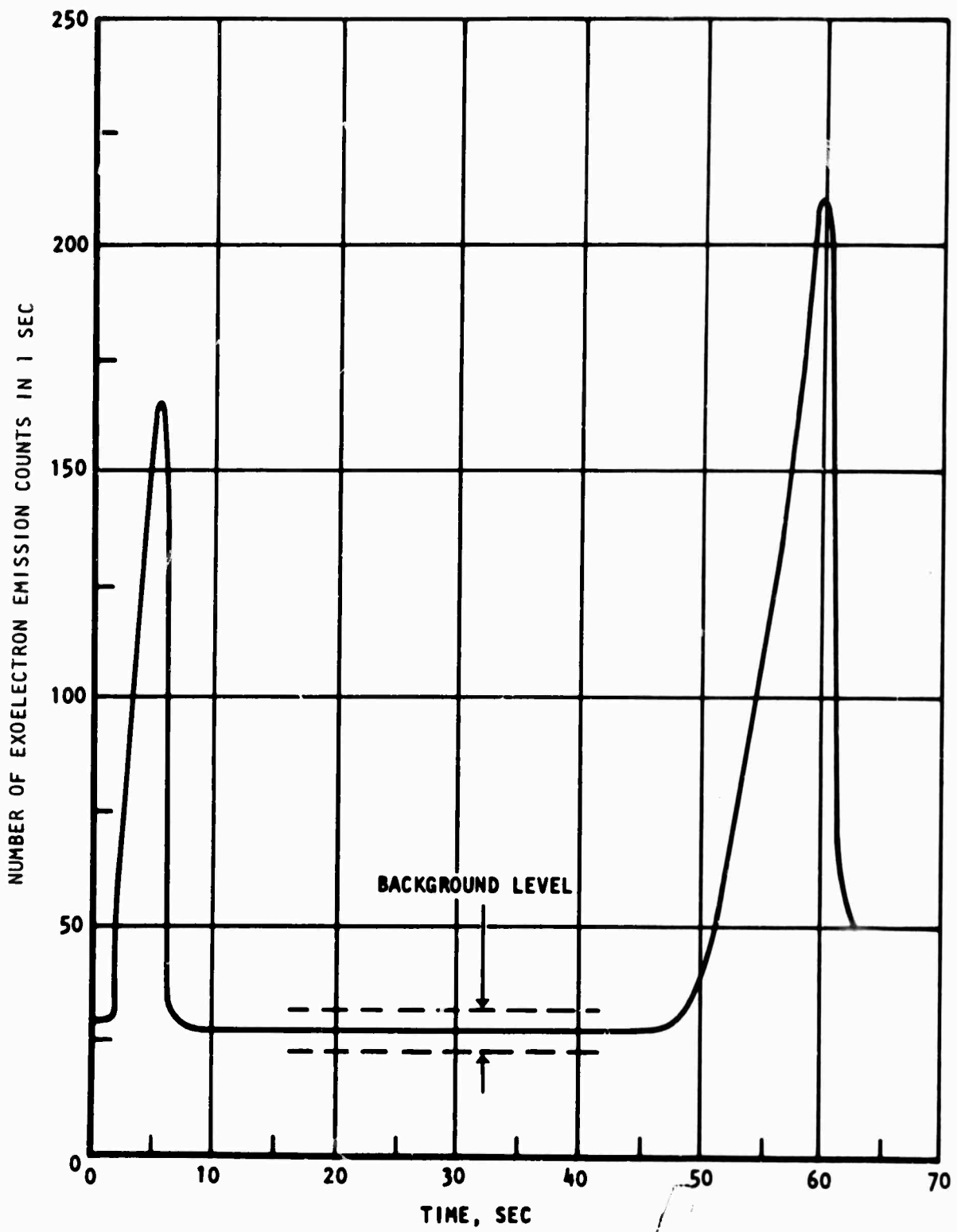


Figure 10. Exoelectron Emission of 1100-0 Aluminum in Fatigue Test in Vacuum at 12,600 lb/in.²

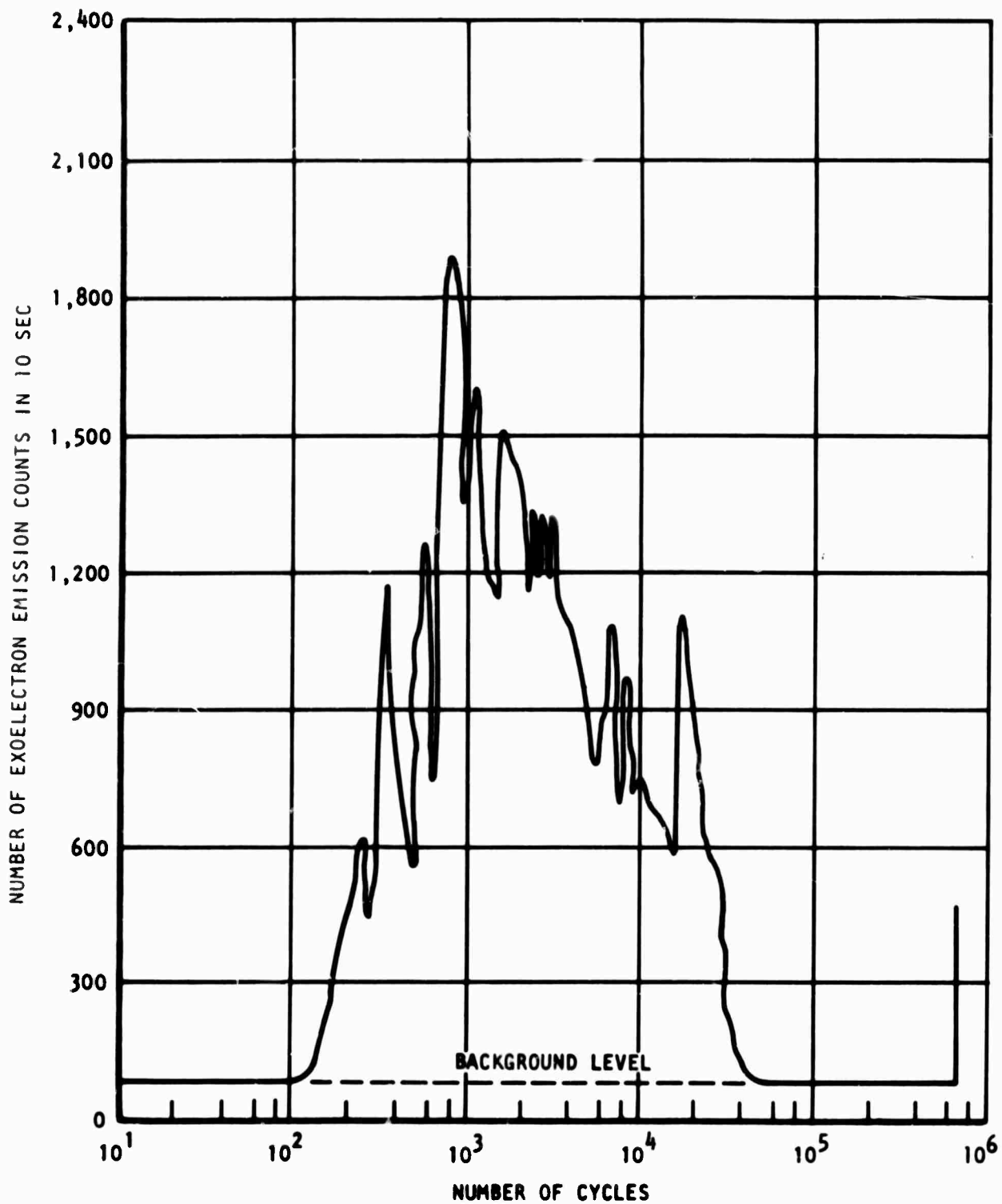


Figure 11. Exoelectron Emission of 1100-0 Aluminum in Fatigue Test in Vacuum at 11,450 lb/in.²

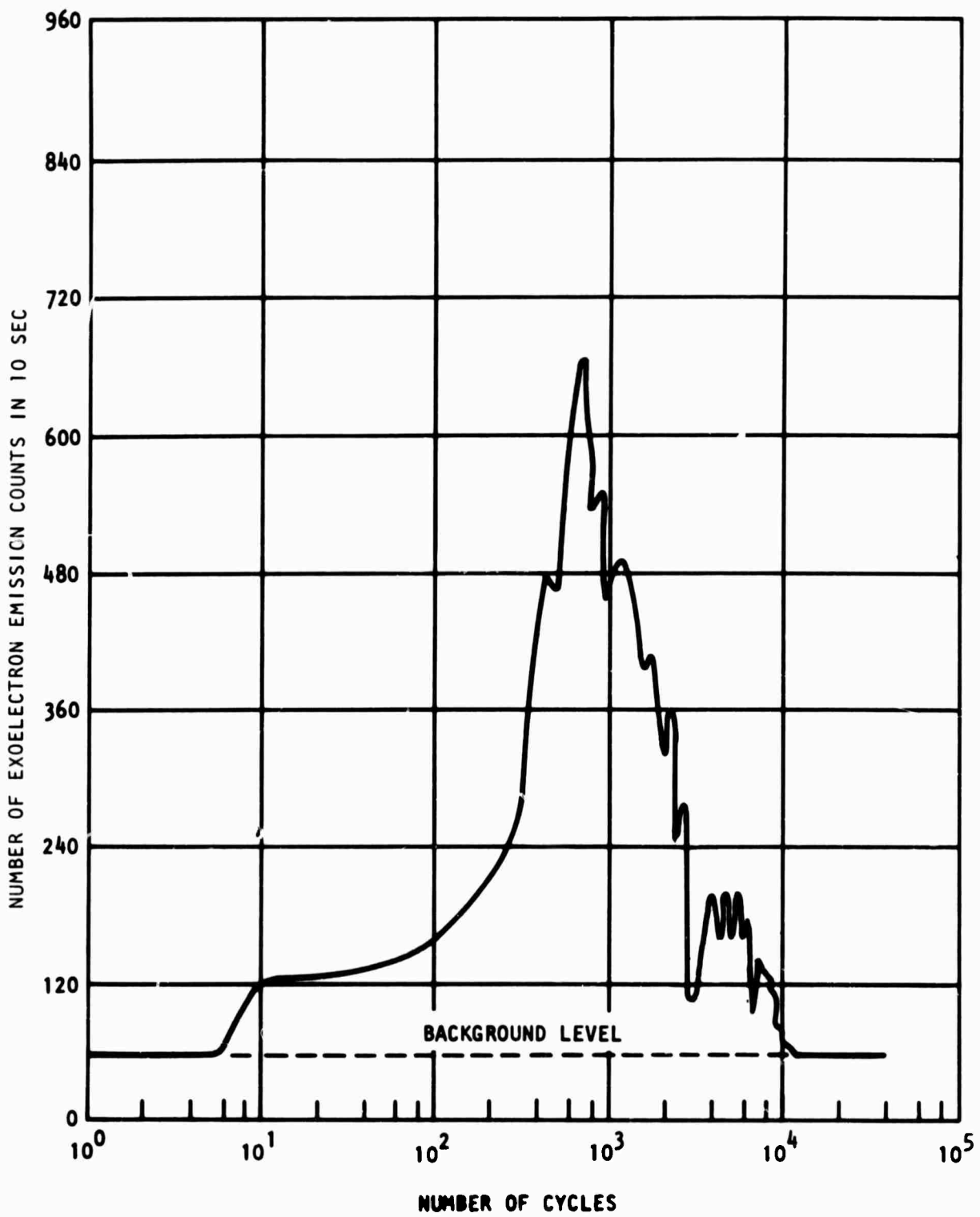


Figure 12. Exoelectron Emission of 1100-0 Aluminum in Fatigue Test in Vacuum at 11,000 lb/in.²

behavior of 1100-0 aluminum at 11,000 and 11,450 psi are quite similar except that the highest emission peak is lower and its occurrence is later in the fatigue process when the applied stress was lowered.

On the other hand, there is a change in emission behavior at even lower stress (10,540 or 10,000 psi). Though exoelectrons started to emit from the specimens after more than 100 cycles, the intensity was quite weak, being only two or two and half times the background level (figure 13). As cycling proceeded the intensity fluctuated a little above the background level and below the strongest emission.

Some sources in the literature cite that electrons do not emit from deformed aluminum in darkness. Some light must be provided as a stimulator. A specimen was therefore subjected to fatigue loading at a stress of 11,450 psi in complete darkness. The recorded intensity in number of counts in 10 seconds did not rise above the background level, indicating no exoelectron emission. The test was discontinued after 3.9×10^4 cycles.

To investigate further the effect of light on exoelectron emission of 1100-0 aluminum, a specimen under fatigue stressing at 11,450 psi was irradiated alternately in a 15-minute period with daylight and long-wave ultraviolet light. The source of the latter was a 15-watt ultraviolet tube housed in a metal tube, throwing a half-inch diameter beam directly to the middle portion of the specimen. The angle of incidence was approximately 45 degrees. Type 4013 Channeltron electron multiplier was used to measure emission in the test. A considerable increase in emission during ultraviolet illumination was observed (figure 14), though the actual levels of emission were much lower than recorded on other specimens using the type 4039 Channeltron electron multiplier. The emission could not be measured after about 6,000 cycles, but the test was continued to 5×10^4 cycles.

EXO-ELECTRON EMISSION IN AIR

Exoelectron Emission in Fatigue Process

Exoelectron emission from 1100-0 aluminum specimens of both Sources A and B under fatigue deformation at various stress levels were measured in air. Table III summarizes the fatigue test results.

Prior to test, the background level for the exoelectron emission was established after the specimen was irradiated with short-wave ultraviolet light for about 16 hours and the electron collector of the current measuring system was charged to a positive 45-volt potential. This procedure was followed to insure that spurious electron emission due to specimen preparation

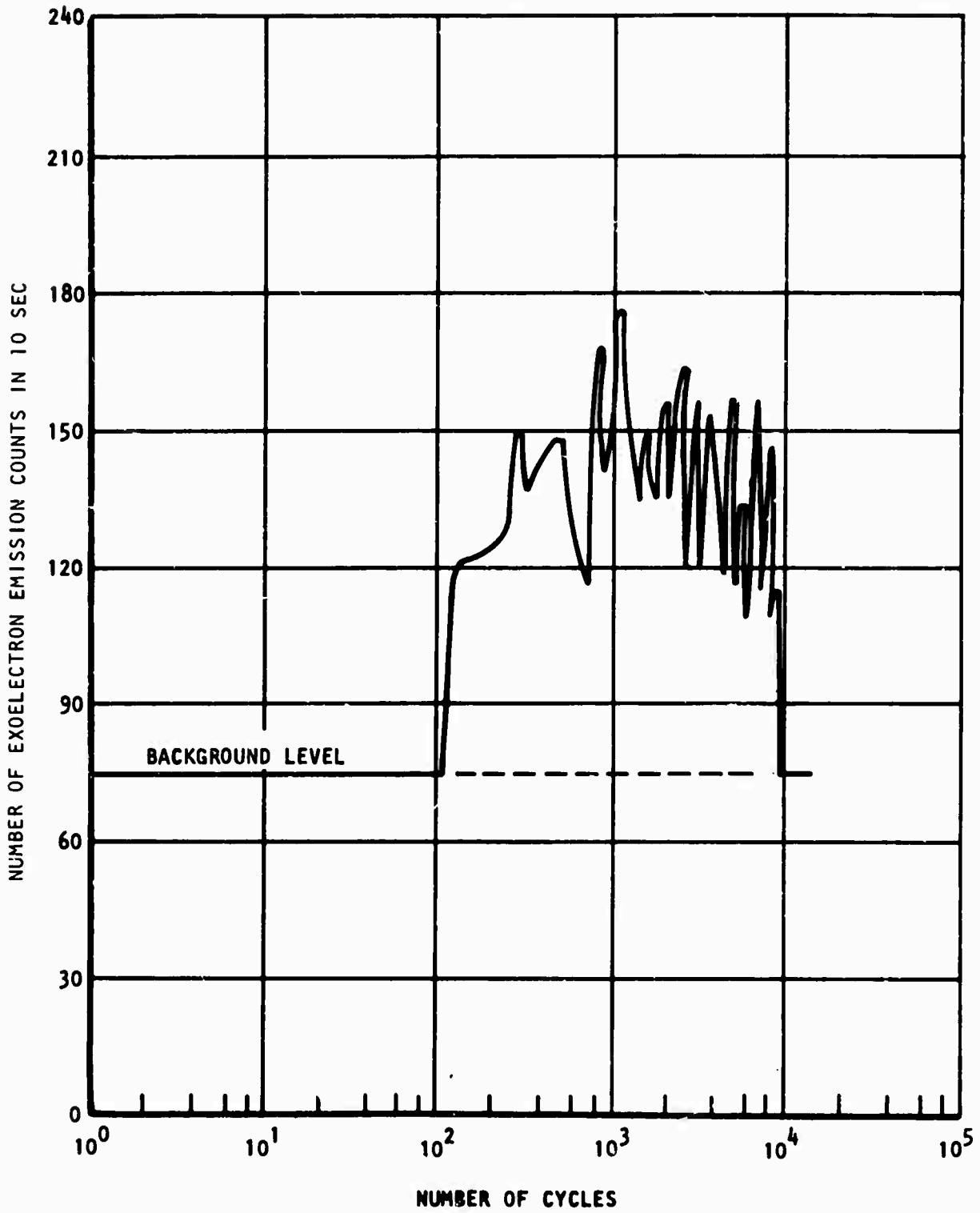


Figure 13. Exoelectron Emission of 1100-0 Aluminum in Fatigue
 Test in Vacuum at 10,540 lb/in.²

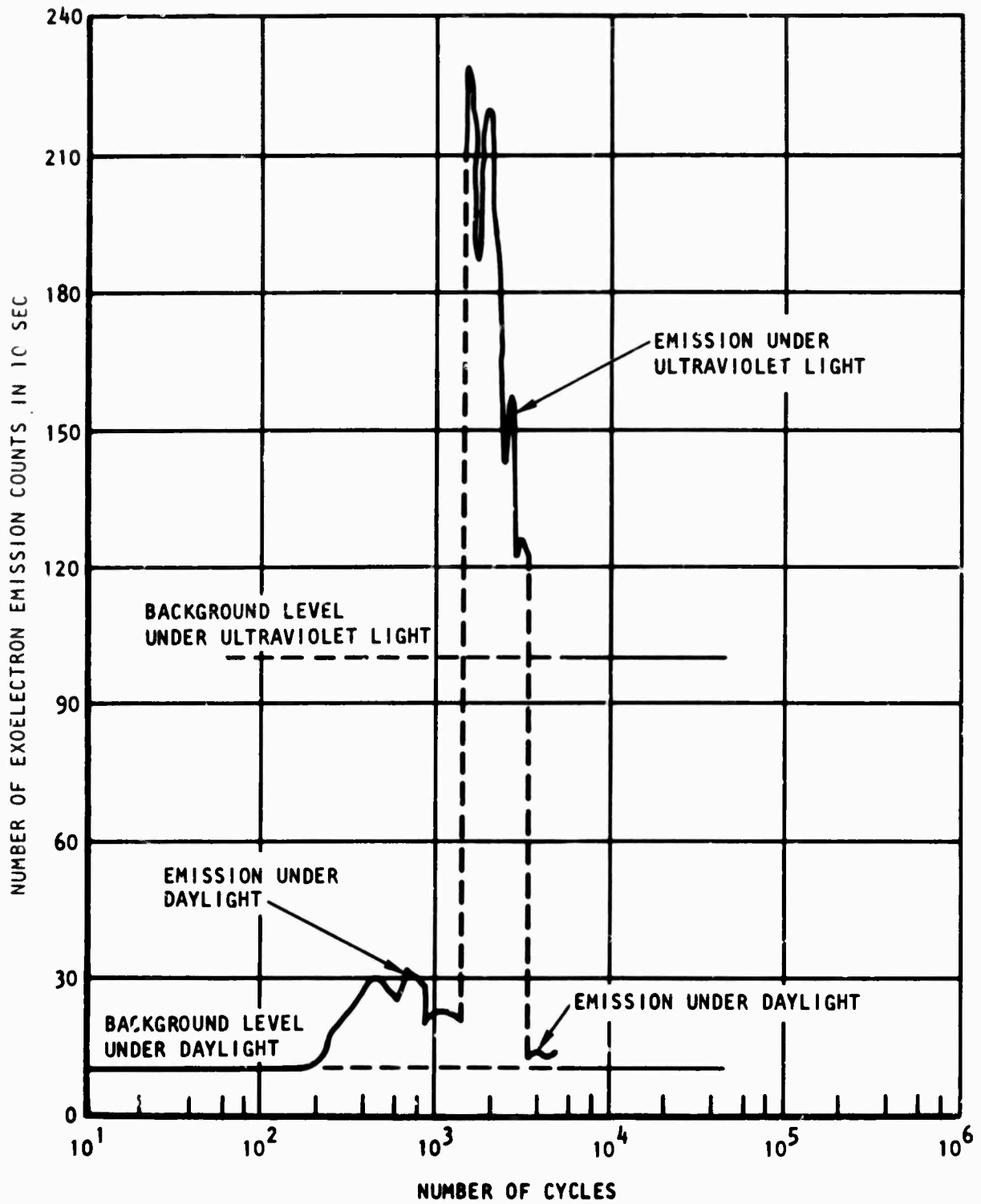


Figure 14. Exoelectron Emission of 1100-0 Aluminum in Fatigue Test in Vacuum at 11,450 lb/in.² and Under Various Light Conditions

TABLE III. RESULTS OF FATIGUE TEST IN AIR FOR 1100-0 ALUMINUM

Source	Specimen No.	Surface Preparation	Stress, psi	No. of Cycles at Failure
A	90	(1)	11,650	472,800
	101			521,960
	110			185,200
	115			684,130
	118			544,020
	93	(1)	11,450	1,003,740
	94*			573,630
	97			889,740
	98			1,273,350
	99			488,080
	100*			428,220
	102			681,090
	106			981,350
	107			1,316,500
	108*			997,880
	110	185,200		
	96	(1)	11,000	3,326,060
	103			2,017,600
109	1,914,620			
114	851,430			
B	71	(2)	11,400	53,370
	72			11,990
	74	(1)	11,000	345,430
	80	(2)		696,500
	82	(1)		802,000
	88	(1)		271,000
	85	(2)	10,540	761,100
	86	(2)		336,490

* Instead of testing in air, the specimen was tested in nitrogen.

(1) Specimen surface was chem-milled.

(2) Specimen surface was electropolished.

or mounting was quiescent. The specimens from Source B were first tested in the fatigue test unit which had a 4-way solenoid valve for applying hydraulic pressure to the loading cylinder. Test frequency was two cycles per second. Figure 15 shows the exoelectron emission curves for two specimens at a stress of 11,000 psi. The emission current rises rapidly soon after start of the test, reaching the peak between 40 and 100 cycles. Thereafter, the emission intensity decreases gradually as cycling proceeds. After the current reaches the initial background level, it continues to drop until fatigue cracks form. The current first rises slowly and then rapidly as the cracks propagate through the test section, leading to complete specimen failure.

Two specimens were then tested at a lower stress level of 10,540 psi. Both exoelectron emission curves exhibit characteristics similar to the curves for 11,000 psi, even though the magnitudes of the current for different specimens at a given number of cycles could differ widely.

At a higher stress level of 11,400 psi, the overall shape of the emission curves (figure 16) is repeated, but the emission current does not drop to the initial background level before it rises again due to the formation and propagation of fatigue cracks.

After completion of the exoelectron emission measurements on the 1100-0 aluminum specimens of source B, the 4-way solenoid valve of the hydraulic system was replaced with a servo-drive system so that the fatigue test frequency could be raised from two to ten cycles per second. The 1100-0 aluminum specimens of source A were then tested in fatigue at this higher rate.

Since the use of ultraviolet light to stimulate exoelectron emission in air could accelerate the oxidation process on specimen surface by the action of ozone, it is thought that some means to control the oxidation rate might lessen the influence of oxidation on the exoelectron emission process. Attempts to control the oxidation was made by conducting fatigue test in a nitrogen atmosphere, which was provided by introducing dry nitrogen at a rate about three cubic feet per hour into the glass chamber. The use of a nitrogen atmosphere also stabilized the variation in relative humidity in the atmosphere surrounding the test specimen.

Three specimens (nos. 94, 100 and 108) were tested in a nitrogen atmosphere at a stress of 11,450 psi. As a comparison, two additional specimens (Nos. 98 and 106) were tested in air at the same stress level. The results in table III indicate that the fatigue life of 1100-0 aluminum apparently is not significantly affected by the test environments. The exoelectron emission in the two environments, however, appears to be different (figure 17). The emission curves for specimen tested in air are similar to those previously determined on 1100-0 aluminum of source B (figures 15 and 16). They exhibit

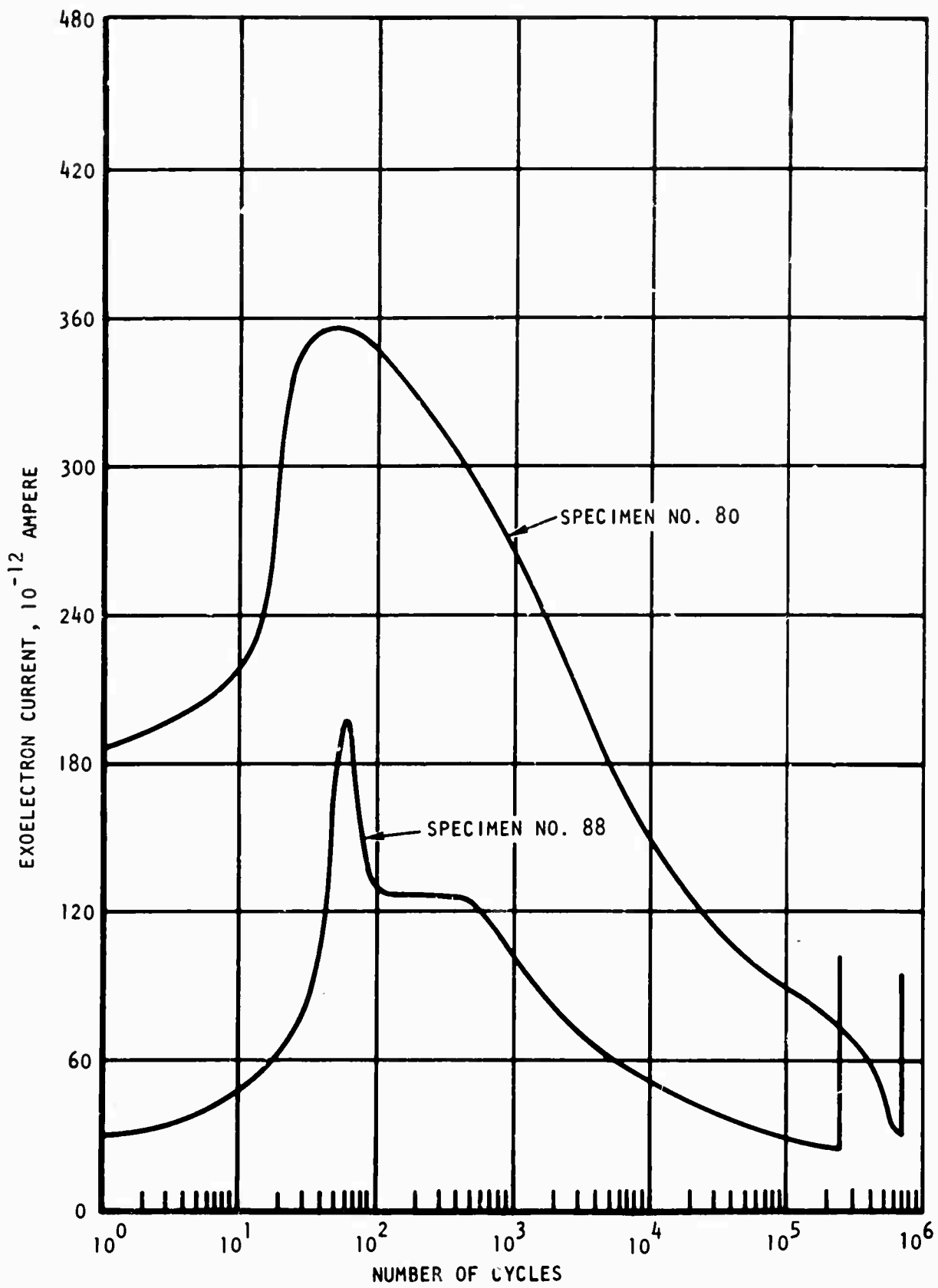


Figure 15. Exoelectron Emission of 1100-0 Aluminum in Fatigue Test in Air at 11,000 lb/in.²

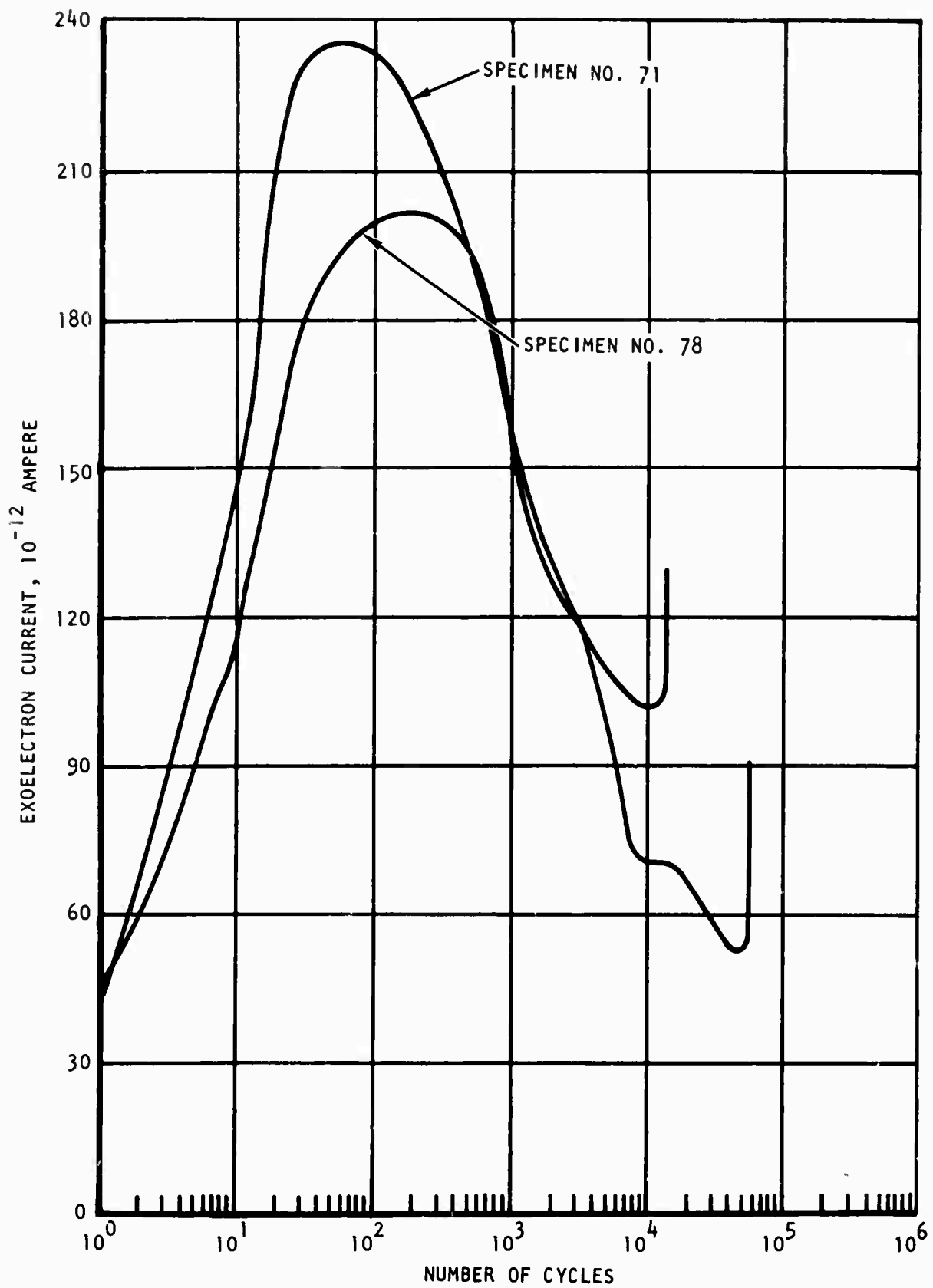


Figure 16. Exoelectron Emission of 1100-0 Aluminum in Fatigue Test in Air at 11,400 lb/in.²

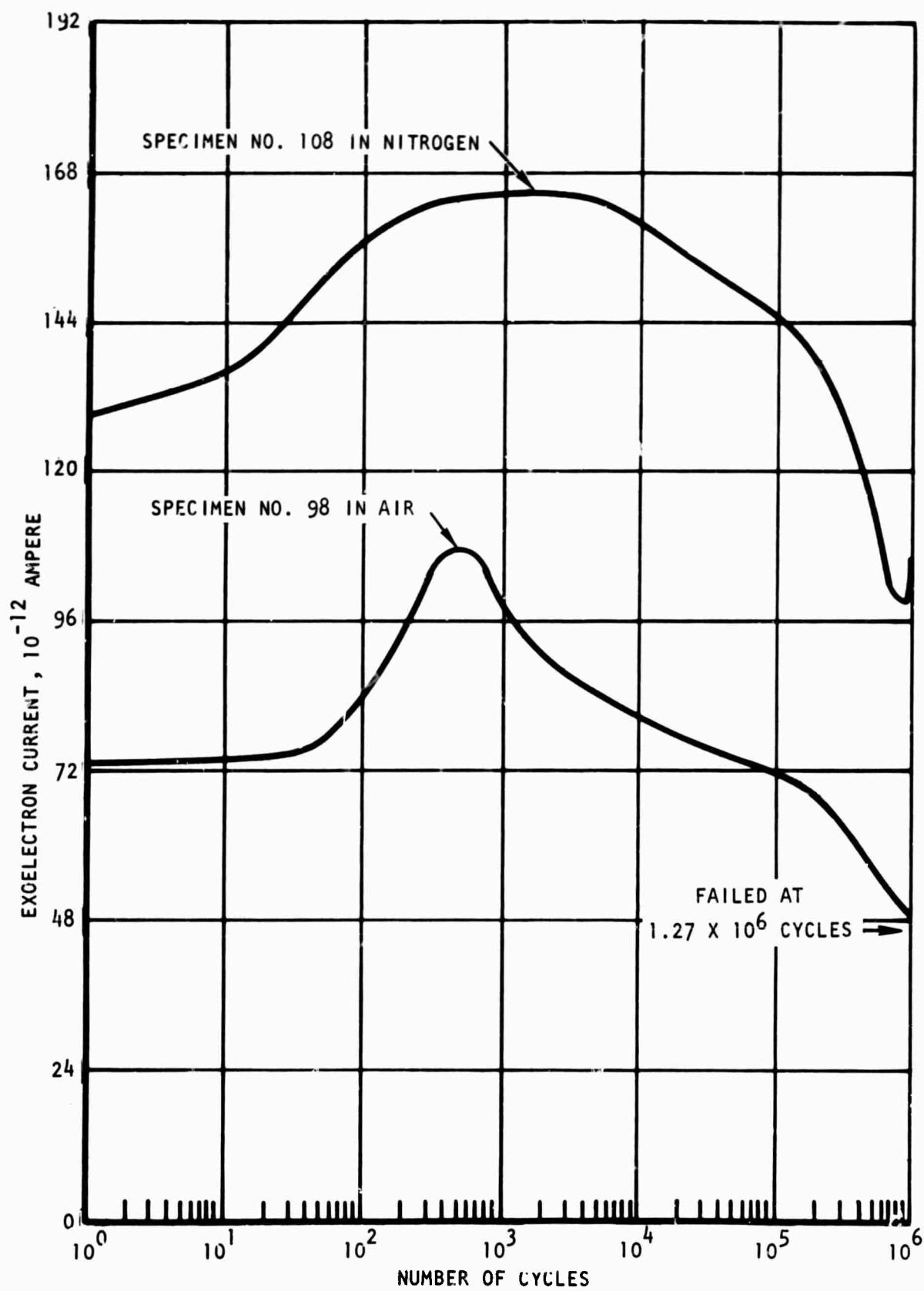


Figure 17. Exoelectron Emission of 1100-0 Aluminum in Fatigue Test Conducted in Two Environments at 11,450 lb/in.²

an early rapid rise followed by a rapid and then a gradual decline in emission. The emission curves for specimens tested in nitrogen, however, exhibit a slower initial rise which last for a longer time period; the subsequent emission decrease, especially in the later stage of fatigue, is faster. Moreover, the reproducibility of the shape of the emission curve in the nitrogen environment is poor. Therefore, all subsequent fatigue tests were again conducted in air.

Six more 1100-0 aluminum specimens were tested in fatigue at the stress of 11,450 psi. All exoelectron emission curves are similar to the one for test in air shown in figure 17. Table III indicates that at about the same stress level (11,400 to 11,450 psi) the fatigue life for the aluminum of source A is more than ten times longer than the life for the aluminum of source B. Five specimens of source A were then tested at a higher stress of 11,650 psi. Again, the emission curves (figure 18) are similar to the curves shown in figures 15 and 16. Finally, a lower stress of 11,000 psi was applied to four specimens. Three of the exoelectron emission curves obtained in the four fatigue tests are like those at higher stress levels. The emission curve for specimen 96 (table III) displays a slight difference in emission behavior. The rise of the emission current soon after the start of the tests on all other specimens persisted only in less than 1,000 cycles. In the case of specimen 96, however, the emission continued to rise beyond 1,000 cycles; it did not decrease until about 20,000 cycles had elapsed. Reason for this change of emission behavior is yet to be known.

Attempts were then made to measure exoelectron emission in other materials. Three and one 7075-T6 aluminum alloy specimens were fatigue stressed, respectively, at 60,000 and 40,000 psi. The rise of emission current during test, before the final rise due to failure by propagating fatigue cracks, was no greater than 0.6×10^{-12} ampere above the background level prior to test. Furthermore, the current fluctuated around the background level for the most part of the test before its final rise near the end. The similar behavior was also noted in two 6Al-4V titanium alloy specimens tested at 110,000 psi. When two heat-treated D6AC steel specimens were tested at 150,000 psi, no rise of the emission current above the initial background level prior to test was observed. The current fluctuated in the test but still displayed a downward trend as cycling proceeded. It rose only slightly at the end of the test. Since the rise of the emission current in 7075-T6 aluminum alloy and 6Al-4V titanium alloy falls within the region of fluctuation of the initial background level, it is not certain whether the emission was lacking or very weak, when the current was measured using the present measuring system.

Exoelectron Emission of Unstressed Material

It is noted in the exoelectron emission measurements in fatigue process that the initial background level for the specimens prior to test could vary

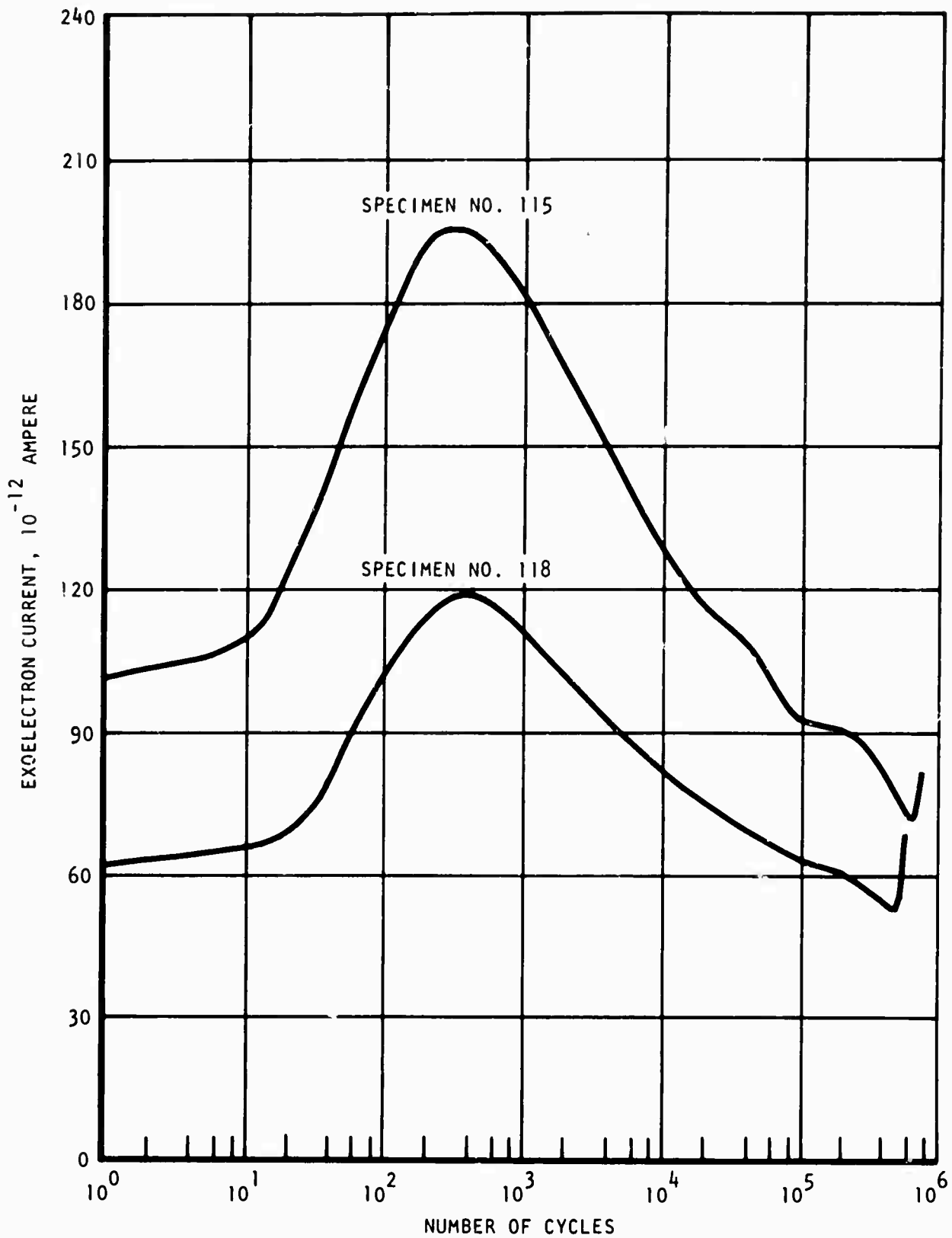


Figure 18. Exoelectron Emission of 1100-0 Aluminum in Fatigue Test in Air at 11,650 lb/in.²

widely. A test system separate from the fatigue test unit was constructed to identify and evaluate some of the factors that contribute to such variations. The test system in figure 19 consists of an electron collecting electrode mounted adjacent to the specimen holder and an ultraviolet source. This assembly is covered by a bell jar which acts as an environmental chamber. The electron current is measured by a picoammeter capable of detecting currents of 10^{-13} ampere or less. A strip chart recorder is used to monitor the current for long term tests. The internal construction of the collector head can be seen in figure 20. The ultraviolet lamp is at the back of the chamber and provides short-wave ultraviolet light. The light passes between the strands of wire that constitute an electrostatic shield and then passes the elliptical collector electrode to fall on the test specimen which is placed over the front of the chamber. The emission was measured with 1100-0 aluminum specimens without being subjected to fatigue deformation.

Some of the test parameters that have been studied are specimen temperature, excitation sources, test environment, surface preparation and previous history of the specimen.

Tests show that a few degrees change in specimen temperature can cause a large change in the electron current. Temperature rise of 30 or 40°F can increase the current to several times the original value. Specimen temperature must be stabilized or at least controlled to obtain steady current.

Intensity of the short-wave ultraviolet light or other excitation source must be maintained constant if test results are to be repeatable. The spacing between the lamp and the specimen has been held quite constant during the test. The lamp is operated from a constant voltage source and has been tested to assure that intensity has not changed greatly with age. All of the lamps on hand were compared and found to have very similar intensity.

Excitation by visible light, long-wave ultraviolet and laser beam have been investigated briefly with little success.

Pressure or density of the gas surrounding the specimen has a very strong effect on the measured electron current. The test system was used to measure exoelectron current while pressure in the bell jar was varied from atmospheric to about 10^{-2} torr. Within this range of pressure the current appears to be roughly inversely proportional to the absolute pressure. It is not known at present whether this is because of the gas pressure on the surface of the specimen or because the air molecules impede the flow of charges from the surface to the collector electrode.

Surface condition and surface preparation are very important since exoelectron emission initiates from the surface. Thin films of oil or grease

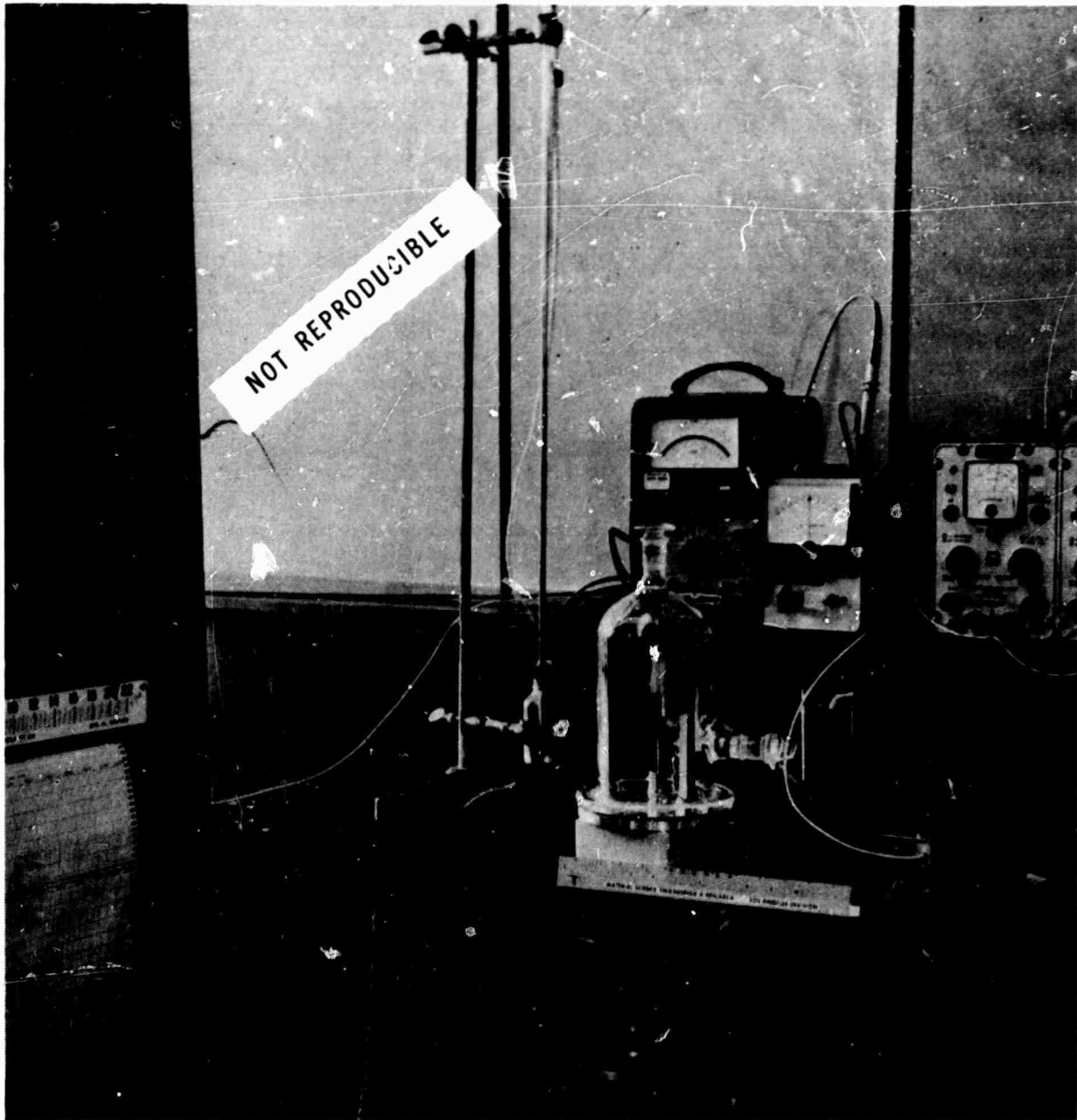


Figure 19. Equipment for Measuring Exoelectron Emission of Unstressed Material in Air

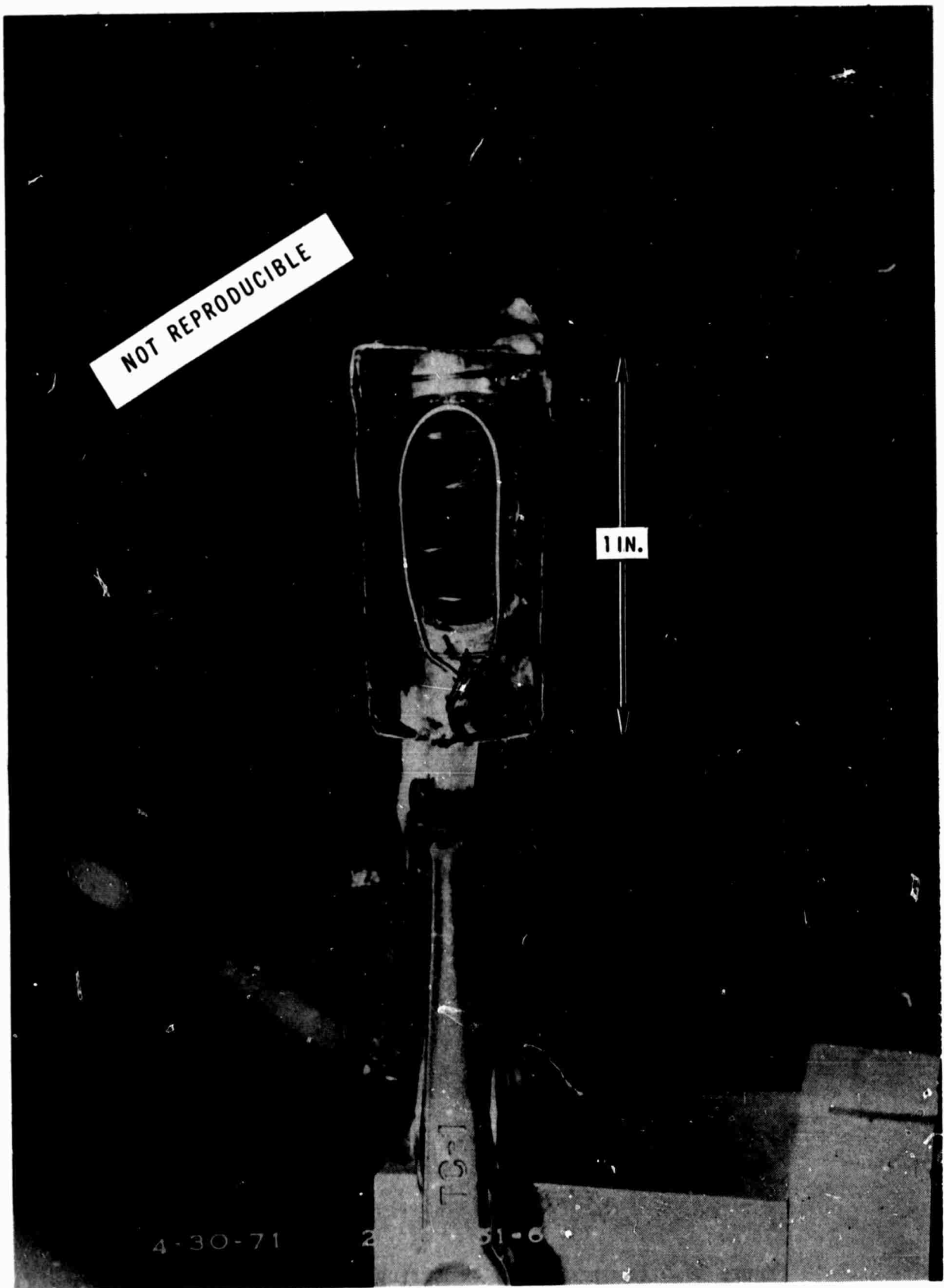


Figure 20. Photograph of Electron-Collecting Electrode

tend to inhibit the electrons and must be removed if all specimens are to be brought to standard condition. Scratches or abrasions on the surface are areas of stress concentration and produce highly localized emission. This may mask data from fatigue patterns on the test part.

Measurements have been made before and after cleaning the specimen by several methods. The presence of fumes from solvents, such as MEK or acetone, tend to change the electron current readings. This effect seems to be temporary but it is possible that solvent may influence a measurement after it has apparently evaporated. Other cleansing agents such as detergents might also leave a residue.

Another mechanism has been observed which may affect long term tests. Parafin has been used as a stop-off coating to prevent background emission from surfaces other than the specimen. After a period of days or weeks under ultraviolet irradiation the parafin seems to be partially decomposed into a viscous yellow substance. It is possible that similar decomposition process might occur when an oil or dirt film is present on the specimen. The effects are unpredictable.

Specimens to be used for evaluation were chem-milled to remove the old surface. All specimens were thus put into a standard condition before measurements. In one series of tests the same specimen was chem-milled and tested several times. After the first chem-milling process had removed about 0.002 inch from all of the surface the emission current followed a pattern of rather wide excursion and required several hours to stabilize. After the second and third etch the current variation was much smaller and current was stabilized much more quickly. This would indicate that surface characteristics may extend to depths of several thousandths of an inch.

The history or time sequence of a specimen has a strong effect on the exoelectron emission. Tests show that if two aluminum specimens are chem-milled and one is tested immediately while the other is allowed to stand in air for several days, their emission patterns will be different. Very likely this is due to formation of the oxide layer.

As a source of exoelectrons, the metal surface seems to have a memory. If a surface is tested under steady conditions the electron current may change with time but tends toward some stable value. When a test parameter is changed, such as temperature, ultraviolet excitation or accelerating voltage, the current will also immediately change. The current will then slowly move toward a new stable value. If the parameters are then returned to the original value, the current will never return to exactly the value it would have had if there were no interruption.

A two-axis scanning system has been used to map the exoelectron emission intensity over the surfaces of sheet metal panels. In one demonstration a scribe was used to scratch the letters AFML on an aluminum sheet. Figure 21 shows the panel taped to the scanning table, and shows the electron detector system the ultraviolet light source at the left. In the background is the pattern produced by an X-Y recorder showing the distribution of intensity of the electron current from the surface. Since high localized emission is produced by scratches or cracks, the scratched letters AFML were faithfully and distinctly reproduced on the graph. Although rather crude in the present form, its purpose is to show the feasibility of mapping fatigue damage or stress patterns from the surface of a metal. A system is in the planning stages which would adapt this method to an existing C-scan recorder using electro-sensitive recording paper.

The resolution or detail that can be achieved is dependent on several factors, two of which are speed of response and size of the sampled area. In the present system the size of the spot under test has been limited by allowing the ultraviolet light to pass through an aperture about 1/16 inch in diameter. Most of the electron current at any instant can be considered to come from the surface directly under the aperture. Literature has been obtained describing a commercially available light source capable of producing a very small, high intensity spot of short-wave ultraviolet. An alternative method for attaining high resolution is to flood the surface with light but use a pickup probe that accepts electron current only from a small spot on the surface. At present this method seems less promising.

A second determination in attaining good detail in the recording is the speed of response of the measuring system relative to the scanning rate. If system response is slow then the scanning rate must also be slow, so that the information thus collected can be accurately correlated with the area from which it is obtained. System response has been improved by using driven shields or guards and undoubtedly further improvements can be made. Efficient stimulation and collection of the electron current also improve the response of the system because larger current, which have shorter time constants, can be used.

DISCUSSION

Exoelectron emission occurs in vacuum from both statically and dynamically deformed 1100-0 aluminum. Emission from metal deformed statically in tension has previously been demonstrated, using a Geiger-Müller counter or electron multiplier. However, some additional information on emission behavior has been obtained. For example, the peak emission is reported to

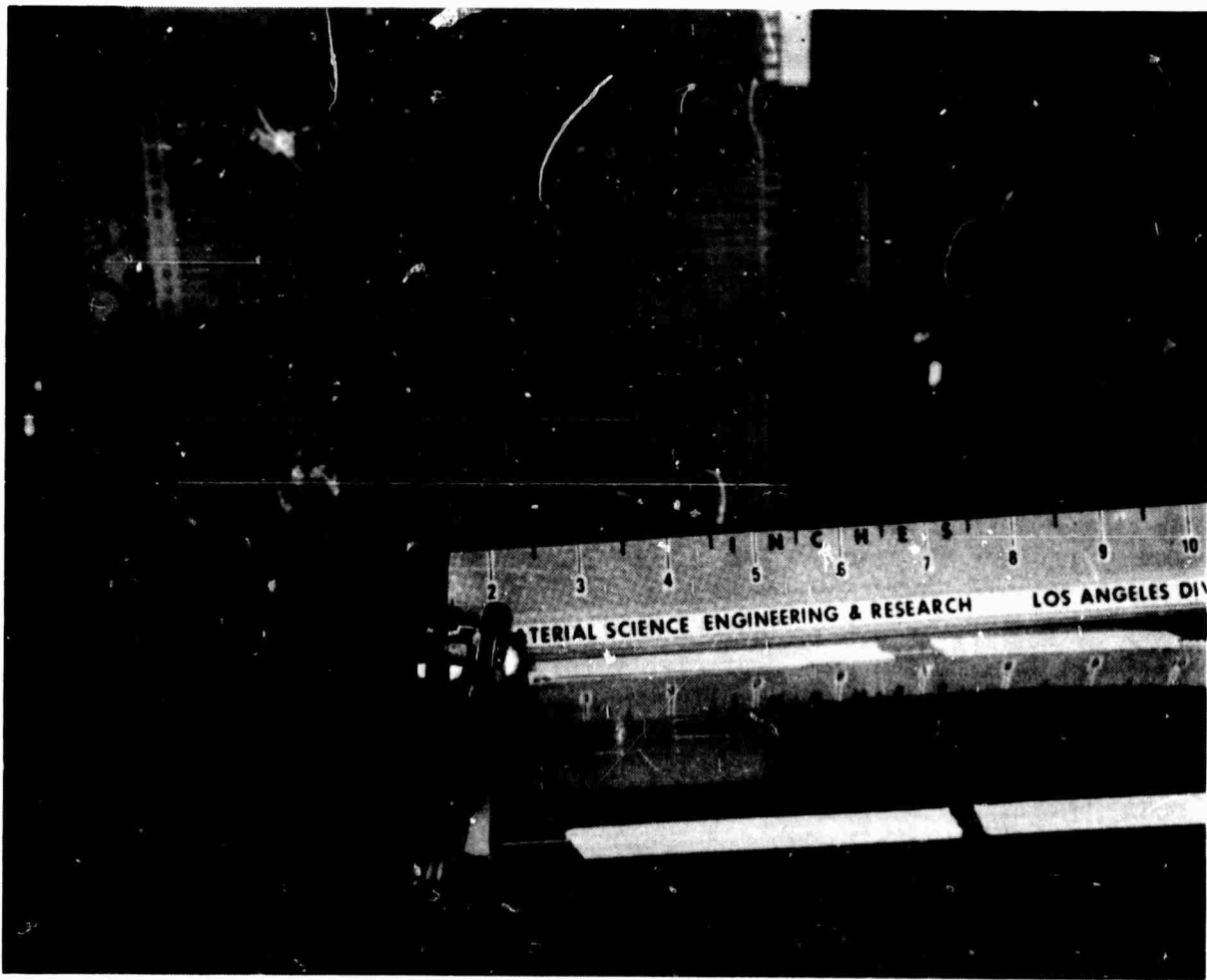
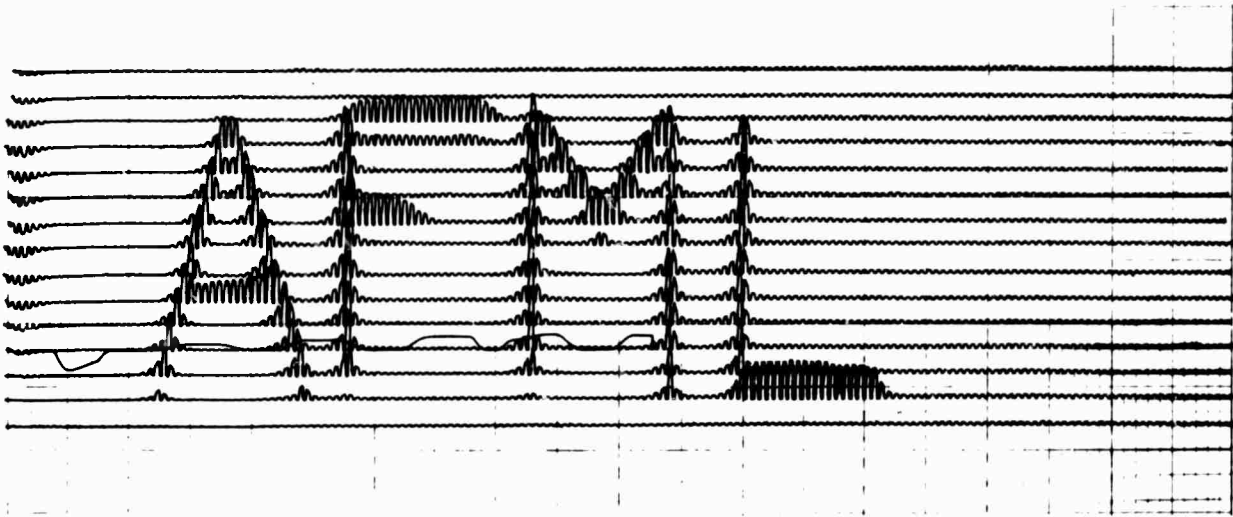


Figure 21. Exoelectron Emission Scanning System and Record

occur during (Hempel et al, 1964) or after (von Voss and Brotzen, 1959) deformation, depending on the loading time. As shown in figure 9, emission peak occurs only after the maximum stress is reached. The time to reach peak emission is about twice the time to reach maximum tensile load. Figure 9 further shows that, if a load is released and applied again before the emission decays to the background level, the total emission on the second loading is about the same as the emission on the first loading. It would appear from this test that a relationship might exist between total emission during a loading cycle and the stress time of that cycle.

Exoelectron emission by fatigue deformation in vacuum has been reported (Grosskreutz and Benson, 1963; Hempel et al, 1964; Krogstad and Moss, 1965; Bogachev et al, 1966; Mints and Kortov, 1967; Mints et al, 1968). The intensity generally increases with the number of cycles. After it reaches a saturated value, the emission decreases slowly until specimen failure. A rapid rise of intensity shortly before failure has also been observed. This rise is attributed to the formation of fatigue cracks. Results of the exoelectron emission tests on 1100-0 aluminum both in vacuum and in air are in agreement with this general description.

There are several similarities of exoelectron emission behavior of fatigue-stressed 1100-0 aluminum in vacuum and in air, among which are: (1) both emission curves exhibit an early rapid rise followed by a rapid, then slower, fall; and (2) there is a final rise in intensity before specimen failure. The fall of emission intensity, however, does not go below the background level in the vacuum tests. This might be attributed to the limitation of sensitivity of the particular electron multiplier.

The only difference in emission behavior is the apparent effect of applied stress level. The emission intensity appears to be dependent upon the stress in vacuum but independent of it in air. Figure 22 shows that the higher the stress, the stronger the emission (after deduction of the background level) becomes. The time in reaching the strongest emission is delayed if the stress is reduced (figure 23). However, the emission in air, as illustrated in figures 15, 16 and 18, is not influenced by the applied stress. Magnitudes of the emission current can vary appreciably for the specimens subject to equal stressing and same surface preparation.

As shown in figures 11 and 12, the initial stage of emission in vacuum has been tentatively defined as a period which ends as soon as the intensity of emission falls to the background level. Since the presence of this stage is thought to be associated with the limited sensitivity of the measuring instruments, it can hardly be related to the total fatigue life. Furthermore, duration of this stage is very short, being less than ten percent and one percent of the total life at high stress (above 11,000 psi) and low stress

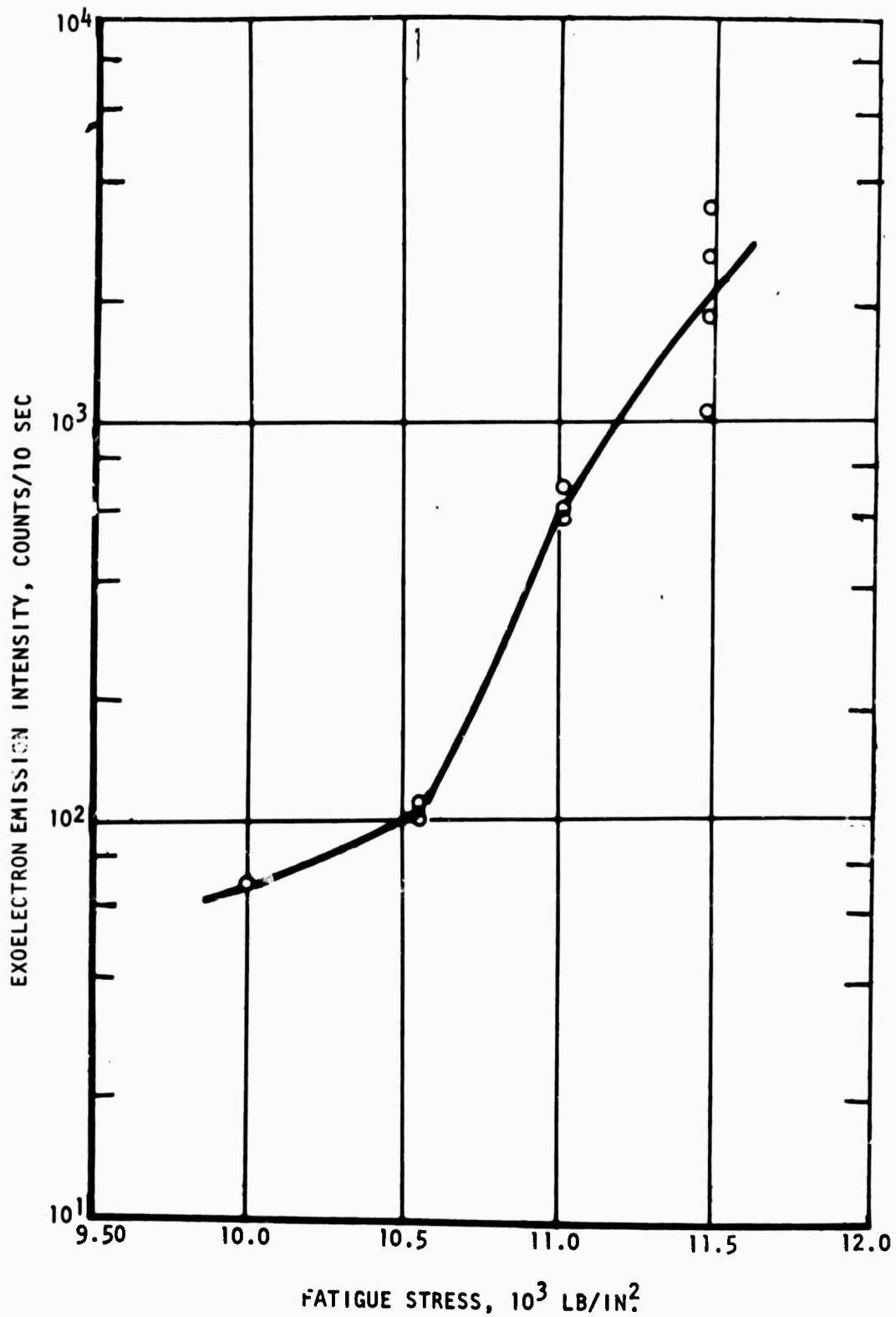


Figure 22. Relation of the Strongest Exoelectron Emission Intensity in Vacuum to Fatigue Stress for 1100-0 Aluminum

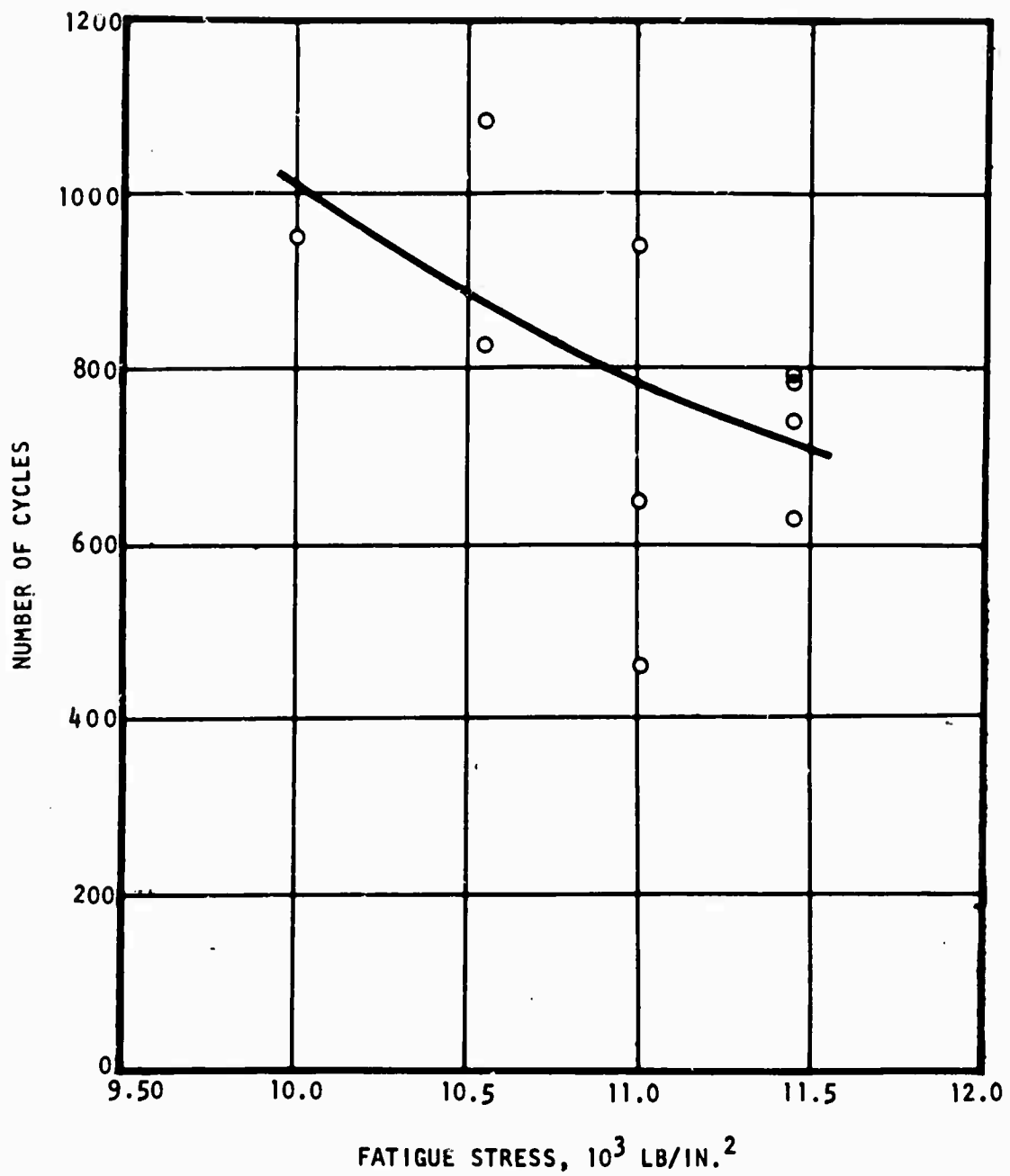


Figure 23. Relation of the Time at Which the Strongest Exoelectron Emission Intensity in Vacuum Occurs to Fatigue Stress for 1100-0 Aluminum

(below 11,000 psi), respectively. Changes of emission intensity within this stage cannot be used to predict the happenings in the long remaining safe life.

No such initial emission stage is present in an exoelectron emission curve in air. Once the intensity falls to the background level, it decreases further with increasing number of cycles before it rises again toward the end of the test. Moreover, the emission is not influenced by the applied stress. Regardless of the stress level, the current rises rapidly only in the first few hundred cycles. Since little fatigue damage is expected in such very short time, the rising portion of the emission curve was not included in the current analysis. An examination of figure 15 reveals that, after elapse of the first 1,000 cycles, the emission curves tend to have similar decreasing trend. Therefore, the change of emission current was computed with reference to the current at 1,000 cycles rather than the background level prior to test.

At the stress level of 11,000 psi, the fatigue life of the 1100-aluminum specimens of source B varies (table III), but, on the conservative side, a lower limit of life can be obtained from the two shorter lives for specimens 74 and 88. The average value of approximately 3×10^5 cycles was, therefore, considered to be the typical fatigue life at 11,000 psi. The actual life used in analysis is 2.99×10^5 cycles so that, by the subtraction of 1,000 cycles, the reference current is now the value at these cycles. The emission current at various numbers of cycles corresponding to certain percentages of life for the four specimens was noted on the record tape and the percent of current change relative to the value at 1,000 cycles were computed and plotted versus the percentage of fatigue life in figure 24. Data points for specimens 80, 82, and 88 gather in a group; however, the data for specimen 74 does not fit and the reason for this discrepancy was not apparent.

A conservative estimated average fatigue life at the stress level of 10,540 psi (table III) is set at 4×10^5 cycles. Again, the subtraction of 1,000 cycles results to a life 3.99×10^5 cycles for the analysis. Changes of the emission current for specimen 86 are computed and also plotted in figure 24. The data points again fall in the group formed by those for specimens 80, 82, and 88. The emission data for specimen 85 are not analyzed since magnitudes of the current are excessively large in comparison with those for all other specimens tested at different stress levels. It is not certain why specimen 85 had a very strong emission by fatigue deformation at relatively low stress level.

At 11,400 psi, the fatigue life for specimen 78 is about one-fourth the life for specimen 71. The rather short life may be ascribed to overstressing due to malfunctioning of the solenoid valve in the hydraulic system, which failed at the end of this test. The fatigue life at 11,400 psi was set at

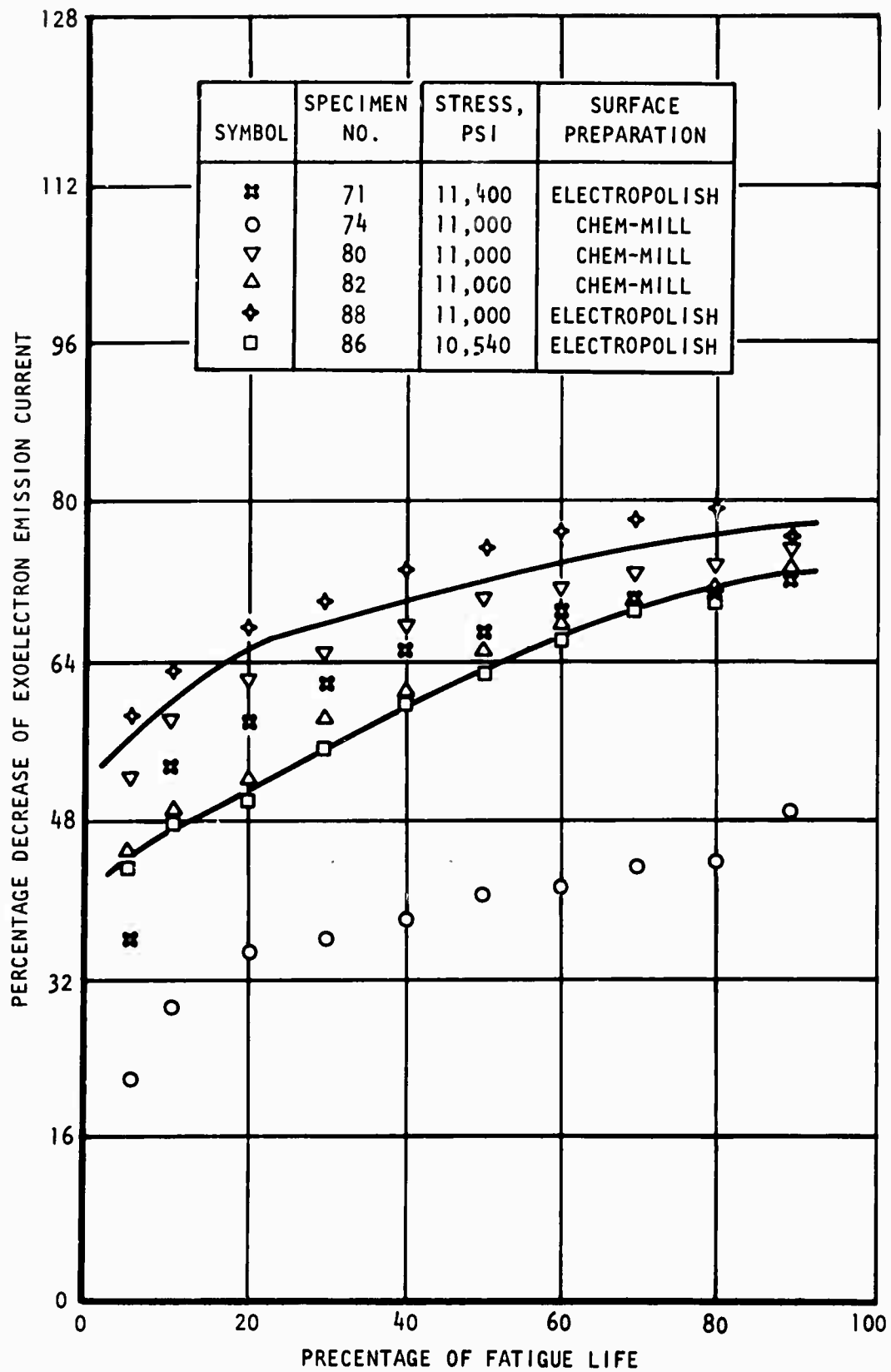


Figure 24. Relation of Percentage Decrease of Exoelectron Current to Percentage of Fatigue Life for 1100-0 Aluminum of Source B

5×10^4 cycles close to the life for specimen 71. The reference of emission current is shifted to 500 cycles since both specimens 71 and 78 emitted about the same amount current at 500 cycles (figure 16). The life for analysis is consequently 4.95×10^4 cycles. The change of current with fatigue life for specimen 71 is also included in figure 24.

Table III shows that at about the same stress level, the 1100-0 aluminum of source A has longer fatigue life than the life of the aluminum of source B. Hence the analysis of the emission curves for the former was separated from that of the latter, but the same details were followed in both cases.

The averages of fatigue life at 11,650, 11,450 and 11,000 psi for the 1100-0 aluminum of source A were computed from those specimens having comparatively shorter lives. The values are, respectively 51.3×10^4 , 78.5×10^4 and 2×10^6 cycles. The basis to which the change of emission current was referred was still the current at 1,000 cycles. The resulting computation is graphically illustrated in figure 25. It is noted that, regardless of the applied stress, most of the data points again fall within a band which yields a relation of the change of emission current with percentage of fatigue life. The data of a few specimens were not analyzed either because the fatigue life was shorter than the average value or because, like specimen 96, the individual emission behavior was different from the generalized behavior observed in most specimens.

Though they have about the same tensile properties, the 1100-0 aluminum from both sources A and B are quite different in their fatigue behavior. It is thus not surprising that the change in emission current also differs. Nevertheless, the overall shape of the curves relating the change of emission current to the spent fatigue life in figures 24 and 25 is quite similar. Both exhibit a rapid change in the early part (up to about 30 percent of life) of the fatigue process.

Figures 24 and 25 show that it is possible to predict the remaining safe fatigue life of 1100-0 aluminum by estimating the change of exoelectron emission current at the end of the spent life, if the change is based upon the current at the first few hundreds or thousands of cycles when the current decreases steadily after its initial rapid rise and fall. It is believed that the relation of the emission current change to the percentage of fatigue life should be independent of applied stress levels. A number of specimens subject to fatigue deformation at differing stress levels would after the elapse of various numbers of cycles, exhibit the same percentage change of current. A single curve should then tell what the percentages of life have been spent at these cycles. The remaining safe life can, therefore, be easily estimated. A trend approaching this idealized relation is clearly shown in both figures 24 and 25, even though in each figure a band instead of a single curve is drawn

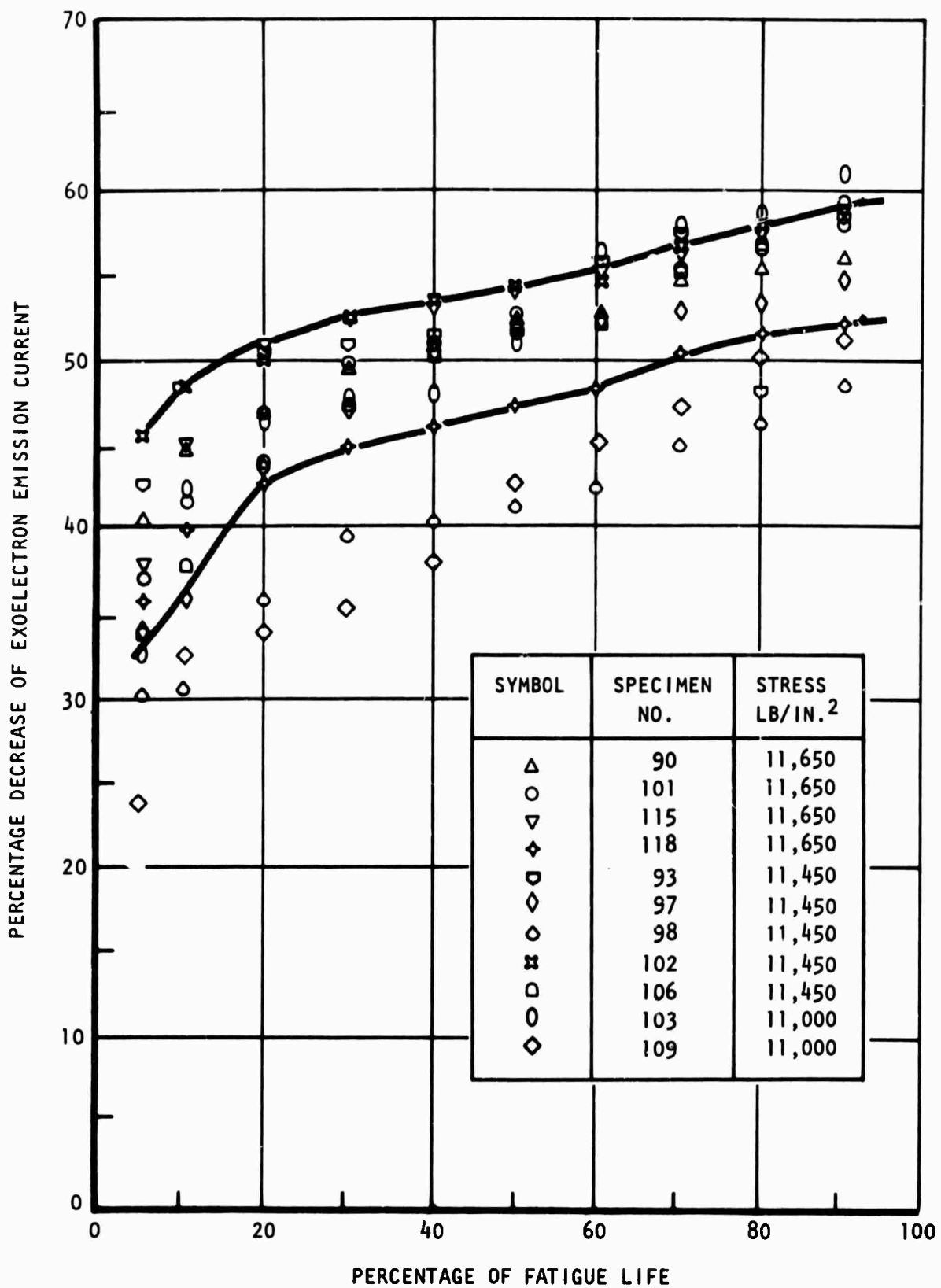


Figure 25. Relation of Percentage Decrease of Exoelectron Current to Percentage of Fatigue Life for 1100-0 Aluminum of Source A

to cover most of the data points. Therefore, the measurement of exoelectron emission in air during fatigue stressing is a promising tool for detecting early fatigue damage and assessing the remaining safe life at least for 1100-0 aluminum.

It should be noted, however, that the measurement of emission current in air must be made while the fatigued specimen is irradiated with ultraviolet light. Tests in vacuum indicate that the emission depends very much on light condition: no emission in complete darkness, and considerable increase of emission under ultraviolet light. Evidently additional energy is required for the electrons to emit from a deformed aluminum surface, as suggested by Pimbley and Francis (1961). Such a relationship between exoelectron emission and incident light energies has also been noticed in abraded and deformed metal surfaces, such as Al, Cu, Ni, Sn, and Zn (Conrad and Levy, 1961).

The experiment with different illumination in vacuum also explains the failure of detecting exoelectron by luminescence of the phosphor because the tests were carried out in darkness.

In contrast to 1100-0 aluminum, no appreciable increase in exoelectron emission current above the background level was observed in air in fatigue tests on 7075-T6 aluminum alloy, heat-treated D6AC steel and annealed 6Al-4V titanium alloy. It is therefore not known whether the emission was lacking or very weak, when the current was measured using the measuring system developed in this program. Probably the emission behavior of these three materials are influenced by the mode of deformation, the type of detection equipment, the measuring technique, the test environment including stimulation and other factors.

SECTION VI

ACOUSTIC EMISSION MEASUREMENTS

TEST SYSTEM

The acoustic emission measurement system included general laboratory type instruments combined to amplify, detect, display and count low level electrical signals. The system is shown in block diagram form in Figure 26. The acoustic emission from the specimen during fatigue test was detected using a Dunegan acoustic emission transducer No. D-1408. This transducer is electrically shielded and has a differential output making it less susceptible to electrical noise. The transducer has a narrow bandwidth with a resonance frequency at approximately 210 KHz. The transducer was held in position near the grip portion of the specimen by a spring clip as shown in figure 8 and was acoustically coupled to the specimen surface using Apiezon-N grease.

The acoustic signal from the transducer is amplified by an oscilloscope preamplifier, fed into a counter, and recorded as the number of acoustic pulses. The time interval between printing (which is either 10^1 , 10^2 , 10^3 or 10^4 fatigue cycles) is controlled in a similar manner as the printing of the digital voltmeter readings for exoelectron emission measurements. The printed number of counts indicates the total number of events that have taken place within the selected time interval. In the case of exoelectron emission, however, the recorded digital voltmeter reading is a measure of the current at the time of printing.

As needed, the electrical equivalent of the acoustic emission could be further analyzed in terms of the number of events occurring in any one cycle by converting the AC signal to DC and recording the signal on a high speed oscillographic type recorder. Each deflection on the recording graph indicated the detection of an acoustic event, and the height of the deflection is a measure of the acoustic emission energy.

TEST METHOD AND RESULTS

The acoustic emission measurements on 1100-0 aluminum specimens were conducted concurrently with exoelectron emission tests in air. The acoustic emission transducer was coupled to one face of the test section of the specimen, whereas the other face was illuminated with ultraviolet light to stimulate exoelectron emission (figure 8). During the first 1,000 or 2,000 cycles, the acoustic emission was recorded in every 10 or 100 cycles so that the number of counts represented all the events that had taken place in the selected cycles. After the elapse of these cycles, the emission was recorded

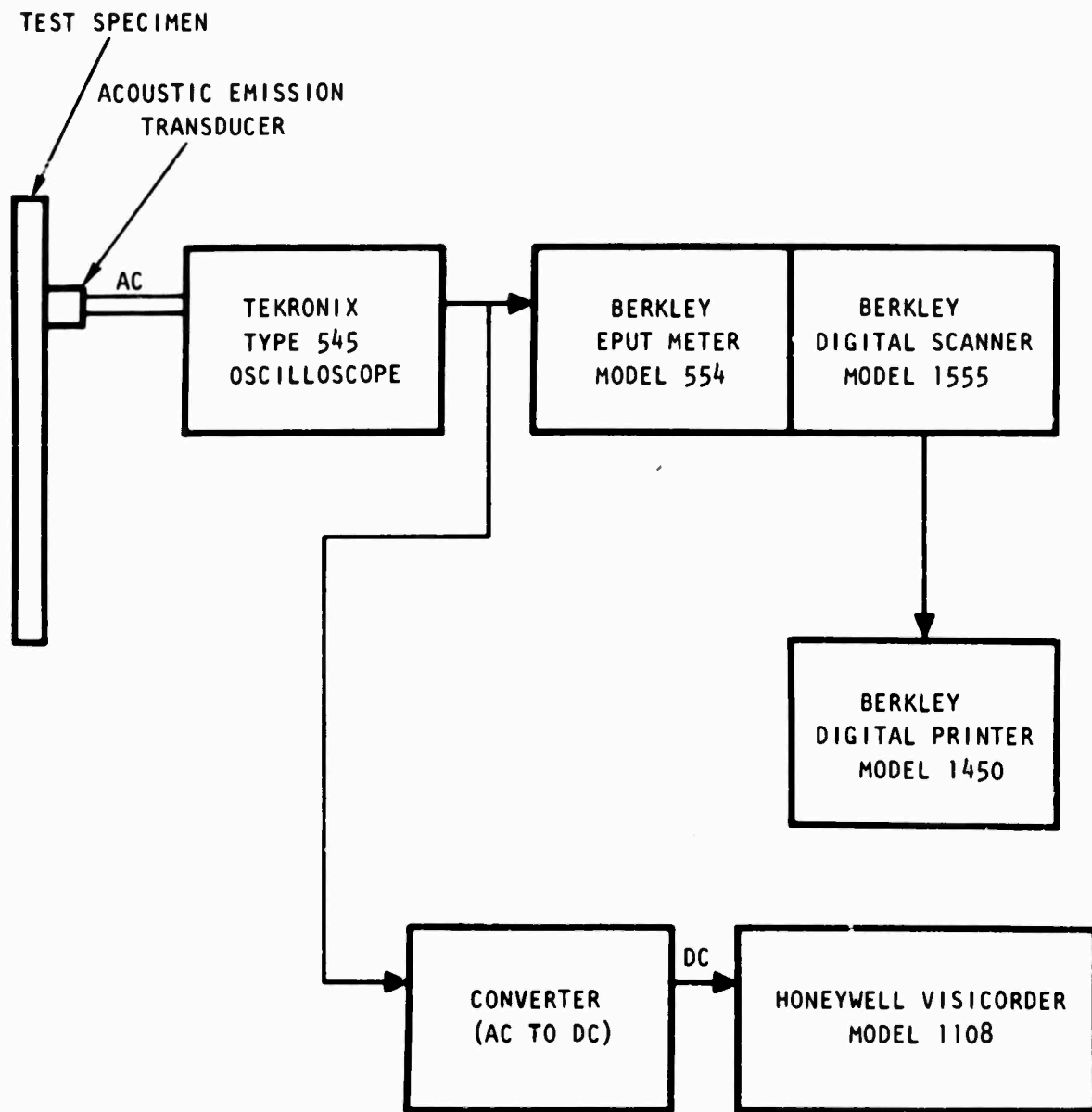


Figure 26. Block Diagram of Acoustic Emission Measurement System

throughout the remainder of the fatigue process at 1,000 cycle increments. The acoustic emission at a given number of cycles was then the total number of counts measured in a 1,000 cycle period prior to printing.

For the tests on the 1100-0 aluminum specimens of source B, because of the large mechanical and electrical surges generated by the operating 4-way solenoid valve, the background noise was fairly high, even though the specimen and the acoustic emission transducer were enclosed in a glass chamber. The emission intensity, measured in number of counts, can change an order of magnitude several times in the specimen life. Table IV summarizes these changes for all the eight specimens of source B. The hydraulic load system was then modified from a square to sinusoidal pressure curve by the replacement of the solenoid valve with a servo-drive system and the intensities of both mechanical and electrical surges in cycling were significantly reduced. As a result, the background noise level for acoustic emission measurements was also reduced.

Figure 27 illustrates two representative acoustic emission curves for 1100-0 aluminum specimens of source A subjected to fatigue stressing at 11,650 psi. It is seen that the emission intensity, expressed in terms of cumulative number of counts, changed slowly in the early part of the fatigue process. With further cycling, however, the intensity suddenly increased, making a significant change in the slope of the emission curve in figure 27. Henceforth, the change of acoustic intensity followed closely this new higher rate until the specimen failed.

The acoustic emission curves for 1100-0 aluminum subjected to fatigue stressing at 11,450 psi in figure 28 are similar to the curves at the higher stress level of 11,650 psi (figure 27), since the marked change in the slope is again noted. Such change in slope is also found in the emission curves for specimens at a lower stress level of 11,000 psi.

DISCUSSION

Table IV shows that at a high stress level of 11,400 psi, the acoustic emission intensity of 1100-0 aluminum of source B is fairly high throughout the entire life. An increase of one decade in emission from three to four orders of magnitude occurs before half of the life has been spent. At lower stress levels of 11,000 and 10,540 psi, the emission intensity is not only somewhat weaker, but it undergoes several changes in order of magnitude. In comparing the data presented in table IV, it is evident that in seven of the eight tests, the acoustic intensity changed by an order of magnitude during the period of 8 to 30 percent of the specimen fatigue life. Since this is the first significant change noted, it offers a potential test for early fatigue damage. The reason for the apparently random variation of the acoustic emission, which occurs after the initial major change and before that emission obviously associated with the crack propagation and specimen failure, was not established.

TABLE IV. SUMMARY OF ACOUSTIC EMISSION DATA FOR 1100-0 ALUMINUM OF SOURCE B
IN FATIGUE TEST IN AIR

Specimen No.	Stress, psi	Change of Acoustic Emission by Order of Magnitude	Percentage of Fatigue Life at Start of Emission Change
71	11,400	1 to 3 3 to 4	30.0 45.0
78	11,400	3 to 4	8.3
74	11,000	1 to 2 2 to 3 3 to 4	29.0 45.5 60.8
80	11,000	1 to 2 2 to 3 3 to 2 2 to 1 1 to 2 2 to 3 3 to 1 1 to 4	20.1 28.7 40.6 46.7 74.6 82.1 84.3 100.0
82	11,000	1 to 2 2 to 1 1 to 2 2 to 3 3 to 4	0.13 1.4 4.4 6.8 11.8
88	11,000	1 to 2 2 to 1 1 to 3	9.2 9.9 100.0
85	10,540	1 to 4 4 to 3 3 to 2 2 to 4	21.9 34.1 39.4 100.0
86	10,540	1 to 3	100.0

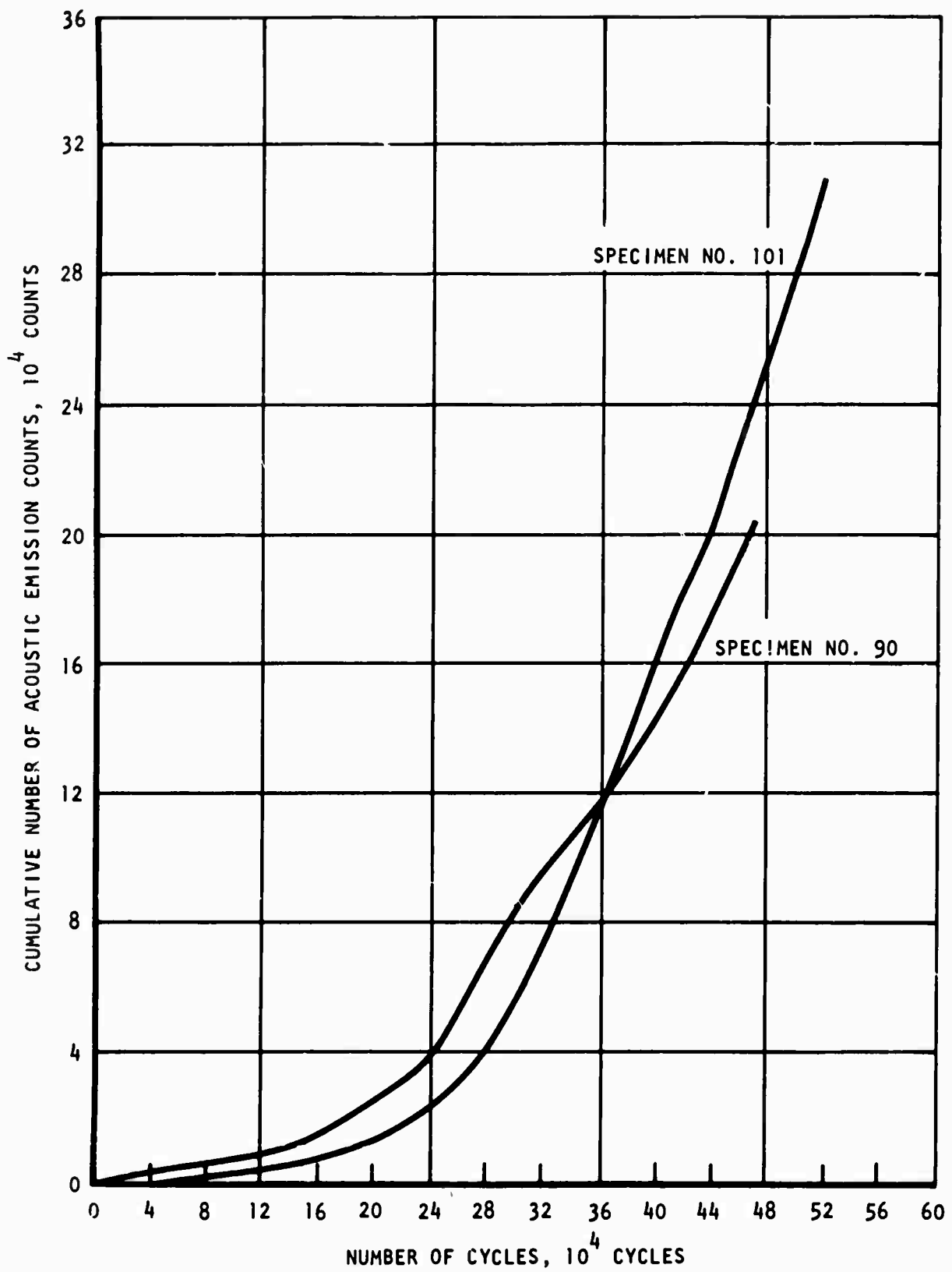


Figure 27. Acoustic Emission of 1100-0 Aluminum in Fatigue Test in Air at 11,650 lb/in.²

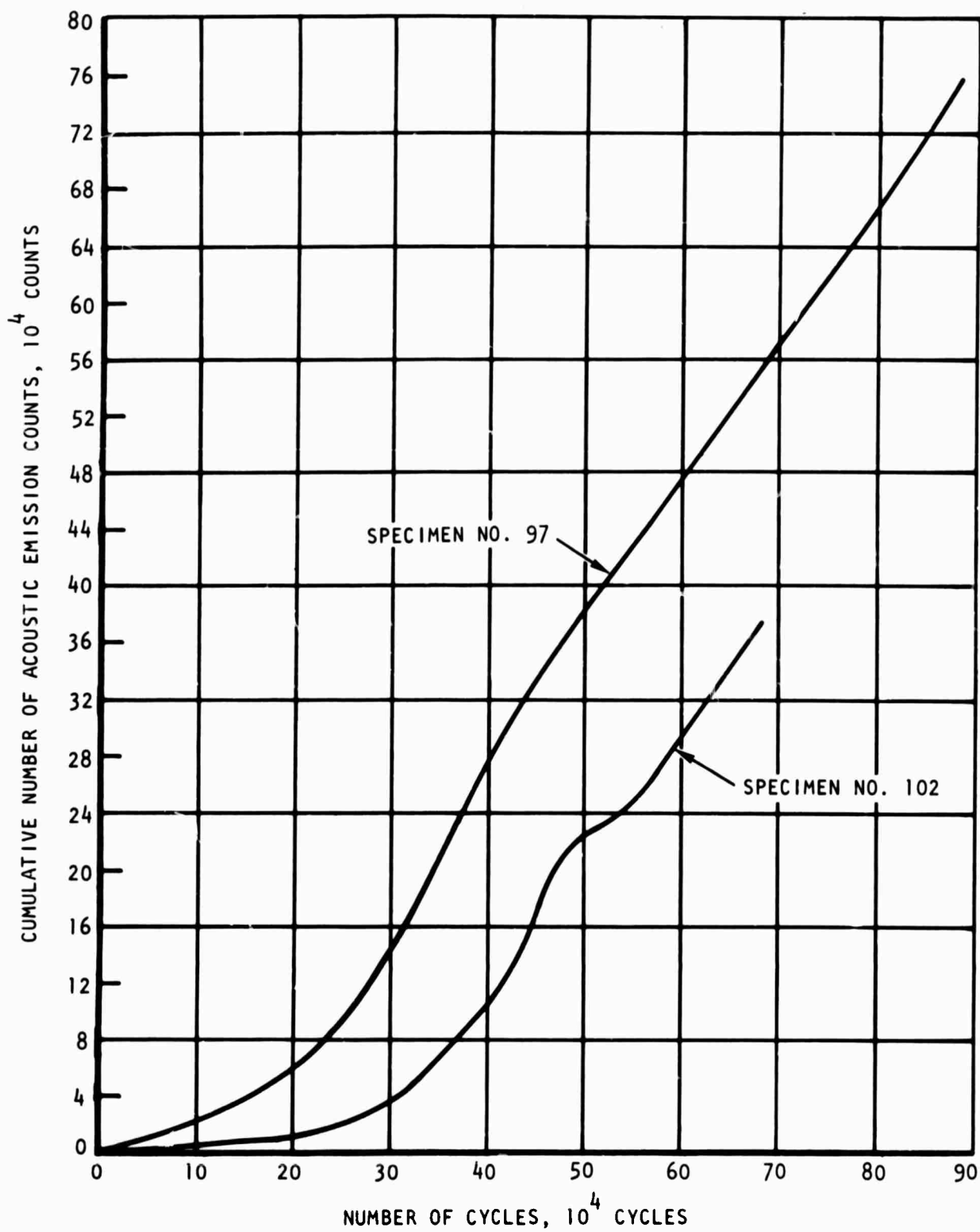


Figure 28. Acoustic Emission of 1100-0 Aluminum in Fatigue Test in Air at 11,450 lb/in.²

The change in slope of the acoustic emission curves for 1100-0 aluminum of source A (figures 27 and 28) becomes even more evident when the changes of acoustic emission counts with spent fatigue life were analyzed. Data for plotting figures 27 and 28 were thus presented in another manner in figure 29 indicating the relation of the change in acoustic emission intensity in number of counts with percentage of fatigue life. Unlike the analysis performed in exoelectron emission measurement, the actual total fatigue life of each specimen was used for computing the percentages. The marked change in slope of the curves for specimens 90 and 101 of figure 27 and for specimens 97 and 102 of figure 28 occurs, respectively, at 45, 46, 30 and 43 percent of their fatigue life. Results of the same analysis performed for other 1100-0 aluminum specimens of source A at the two stress levels are given in table V. It is seen that regardless of stress level, the acoustic emission curves experiences a significant change in slope at less than 50 percent of the fatigue life of the material. At a lower stress level of 11,000 psi, however, the change in slope appears to shift to a higher percentage of fatigue life. The two curves for specimens 109 and 114 in figure 30 show the change to occur respectively at 65 and 75 percent of their life. The change in another specimen (No. 96 in table V) also falls at about 65 percent of the life.

The abrupt change in slope of the acoustic emission curve for 1100-0 aluminum under fatigue deformation offers a possibility of utilizing acoustic emission to assess fatigue damage and estimate remaining safe fatigue life. Ideally, this change is not dependent upon applied stress level. Though results in table V do not indicate this idealized condition, they are still very useful toward developing nondestructive test method for detecting fatigue damage.

The acoustic emission from 7075-T6 aluminum alloy, heat-treated D6AC steel and annealed 6Al-4V titanium alloy specimens in fatigue deformation were also measured at various stress levels. When the data were plotted in a manner similar to that in figures 29 and 30 the resulting curves are roughly linear from zero to 100 percent of fatigue life. The approximate linearity of the curves suggests that the measurement included only background noise and obscured any emission from the material.

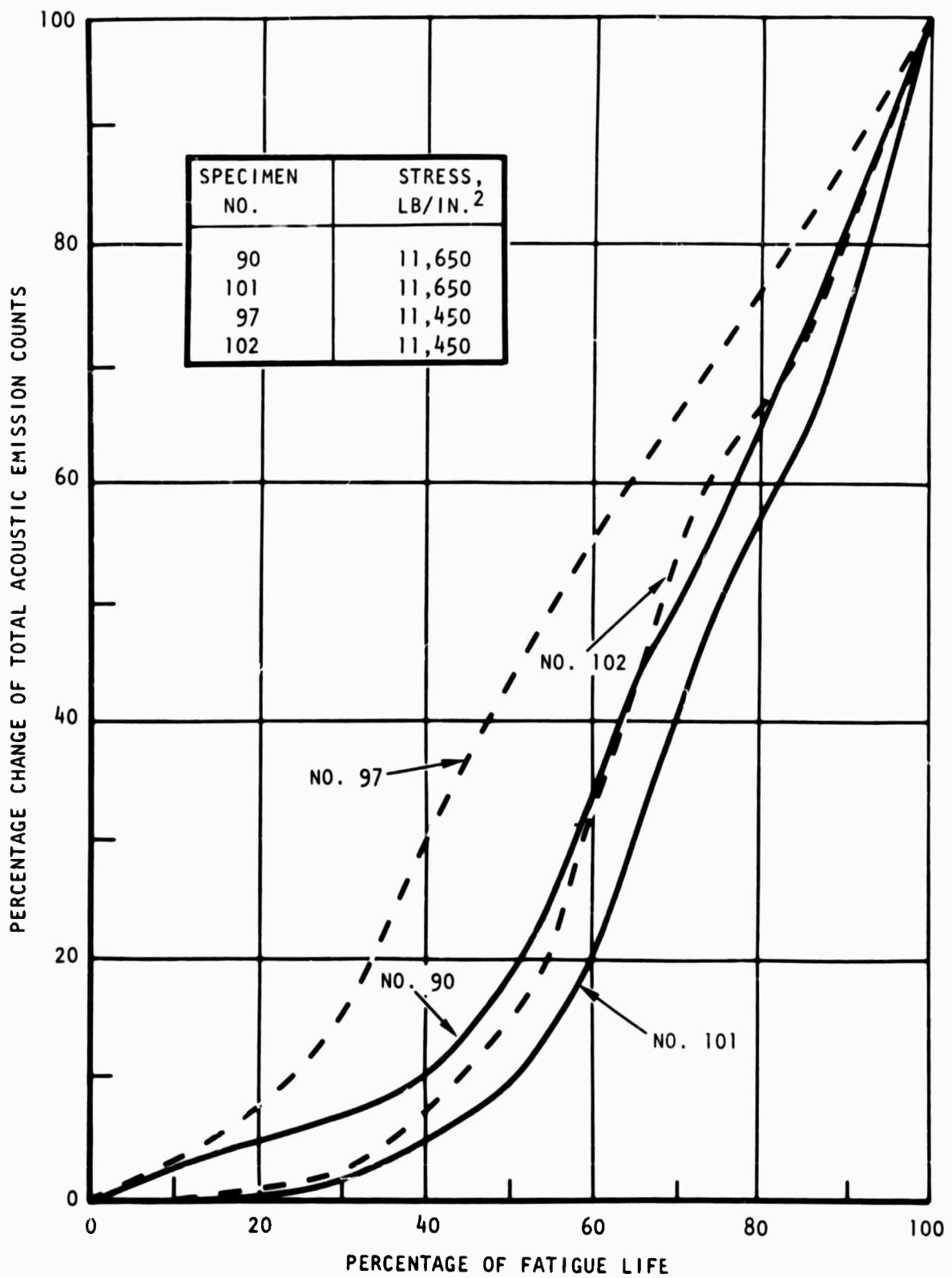


Figure 29. Relationship Between Acoustic Emission and Fatigue Life of 1100-0 Aluminum at Two Stress Levels

TABLE V. CHANGE IN SLOPE OF ACOUSTIC EMISSION CURVE FOR 1100-0 ALUMINUM OF SOURCE A IN FATIGUE TEST IN AIR

Specimen No.	Stress, psi	Percentage of Life at Change of Slope	No. of Cycles at Failure
90	11,650	45	472,800
101		46	521,960
110		45	185,200
115		33	684,130
118		50	544,020
93		11,450	30
97	30		1,273,350
98	32		488,080
99	28		681,090
102	43		981,350
106	30		1,316,500
107	35		507,780
96	11,000	65	3,326,060
103		*	2,017,600
109		65	1,914,620
114		75	851,430

*The acoustic emission data are not available on account of malfunction of the counter in test.

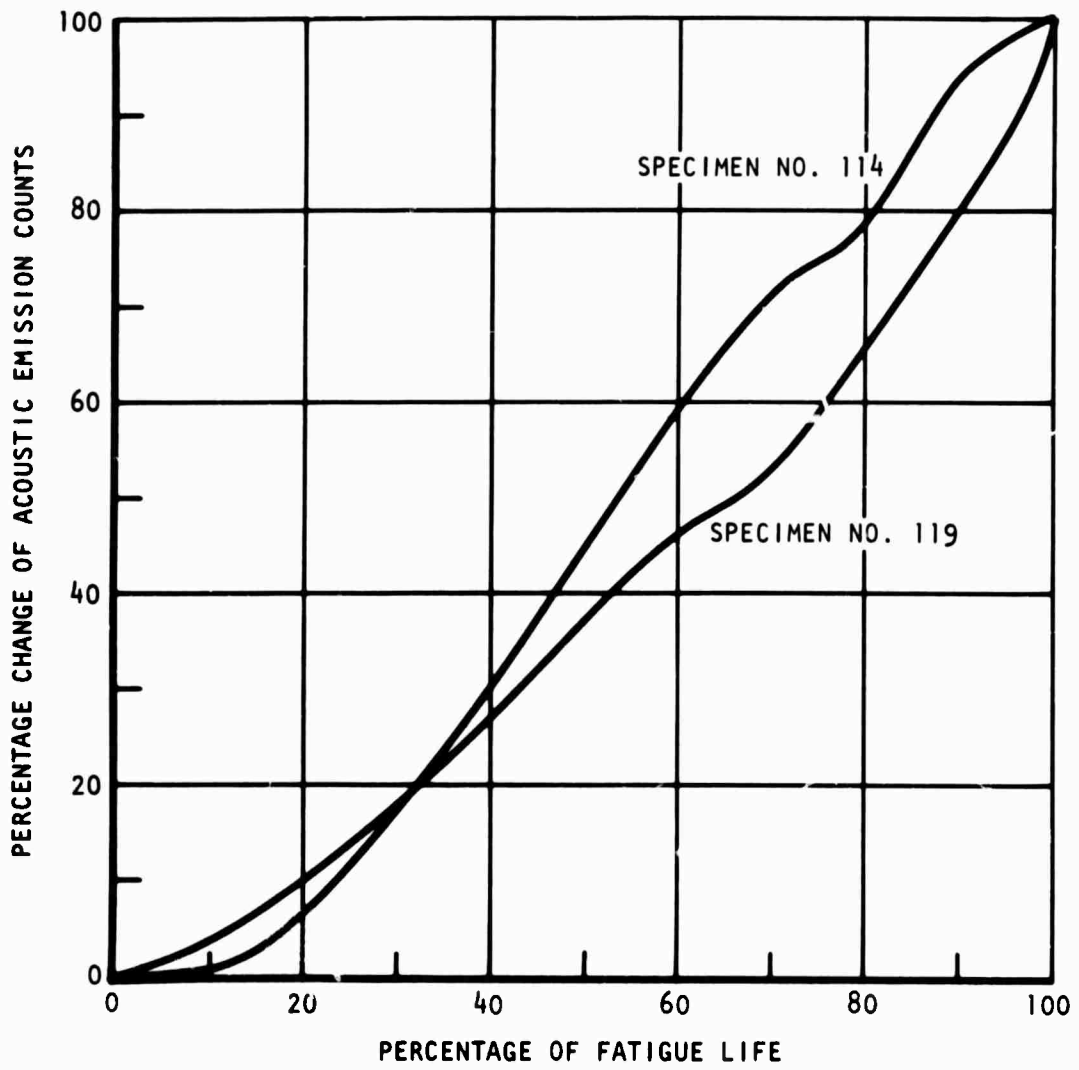


Figure 30. Relationship Between Acoustic Emission and Fatigue Life of 1100-0 Aluminum at 11,000 lb/in.²

SECTION VII

ULTRASONIC SURFACE WAVE MEASUREMENTS

TEST SYSTEMS

The initial ultrasonic measurements were performed using a precision velocity system shown in figure 31. By using the oscilloscope in the main sweep delay mode, it is possible to display the desired signal and observe pulse superposition. When superposition is achieved (by adjusting the sine-wave generator frequency), the actual frequency is monitored on the counter. Based on this accurate frequency data, it is possible to calculate ultrasonic surface velocity with high precision.

For attenuation measurement using the conventional system, the transducer was moved in a manner similar to the velocity measurement. A portion of the signal displayed on the reflectoscope was gated and amplified to an ac voltmeter. Difference between voltmeter readings at the two transducer locations was an indication of attenuation. Measurements were made at 1 and 5 MHz frequencies.

Because of problem of acoustic coupling encountered in using two transducers in the conventional ultrasonic wave measurements, the laser probe technique was later employed to replace the receiving transducer. The surface wave was generated by commercial wedge transducers driven by 10 μ sec, 200-volt RF bursts from an Arenberg pulsed oscillator. The transducer was centered in one end of the specimen and so directed that energy would propagate through the test section (figure 32). A laser probe and the associated electronic device were used to determine the amplitude of the surface vibration as well as its phase relative to that of the driving electrical signal. Attenuation was measured by noting the change of amplitude with distance from the source. Velocity was obtained by noting the distance in which the phase changed by 2π , i.e., the wavelength, and computing the phase velocity, v , according to the relation $v = \lambda f$, where f is the average frequency of the rf burst. The laser detection technique depends on reflecting light from the specimen surface and the surface reflectivity of the fatigued specimen was quite poor. However, a thin coat of a lightweight oil spread on the surface was found to improve the reflectivity and the signals obtained were then of sufficient amplitude and reproducibility to accurately study the ultrasonic behavior of the specimen.

Two wedge transducers were used to launch surface wave into test specimens. They were a variable angle wedge transducer (Sperry type SV2, style 57A8946) operating at 3.4 MHz and a fixed angle wedge transducer (Automation

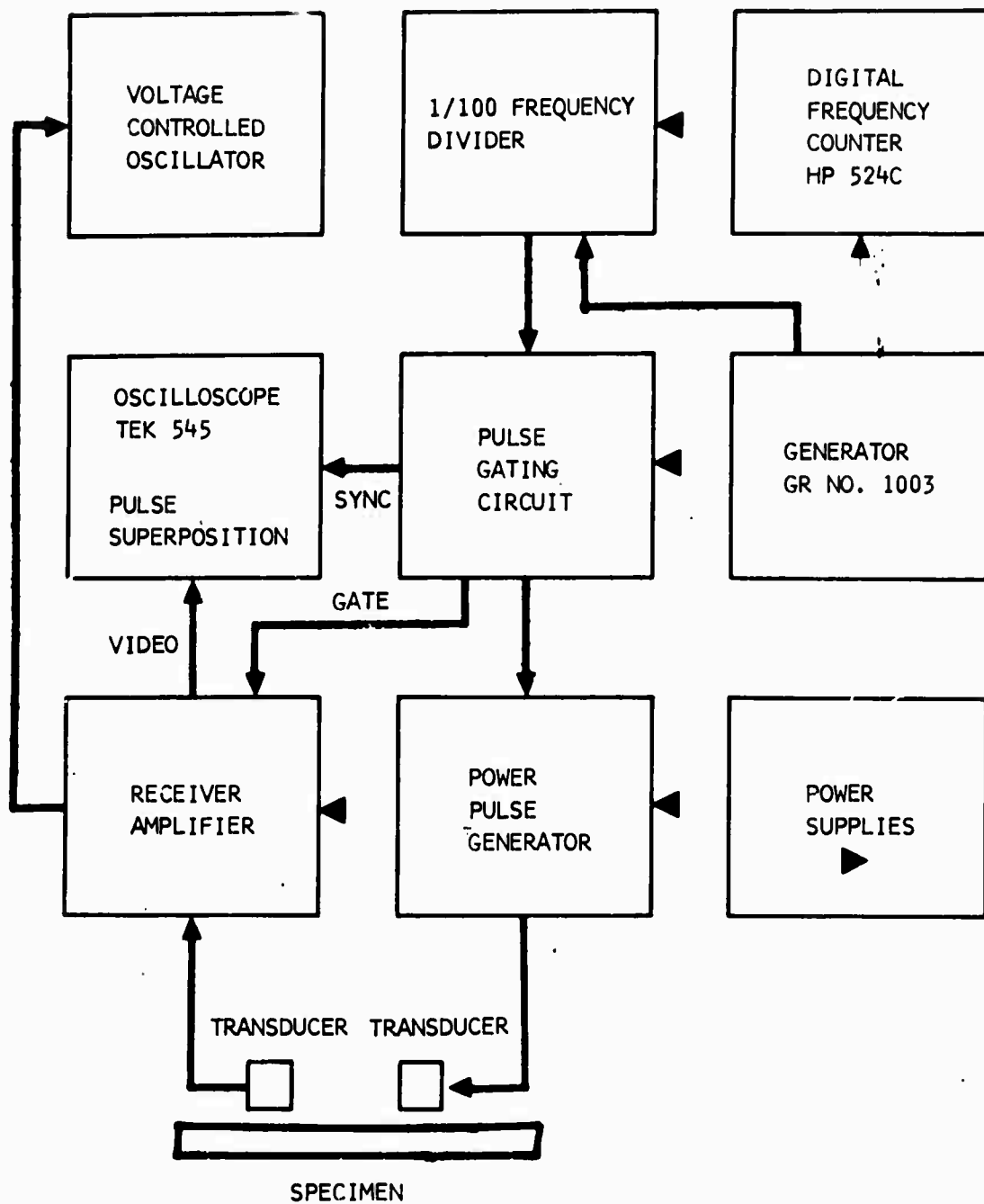


Figure 31. Block Diagram of the Precision Ultrasonic Wave Velocity System

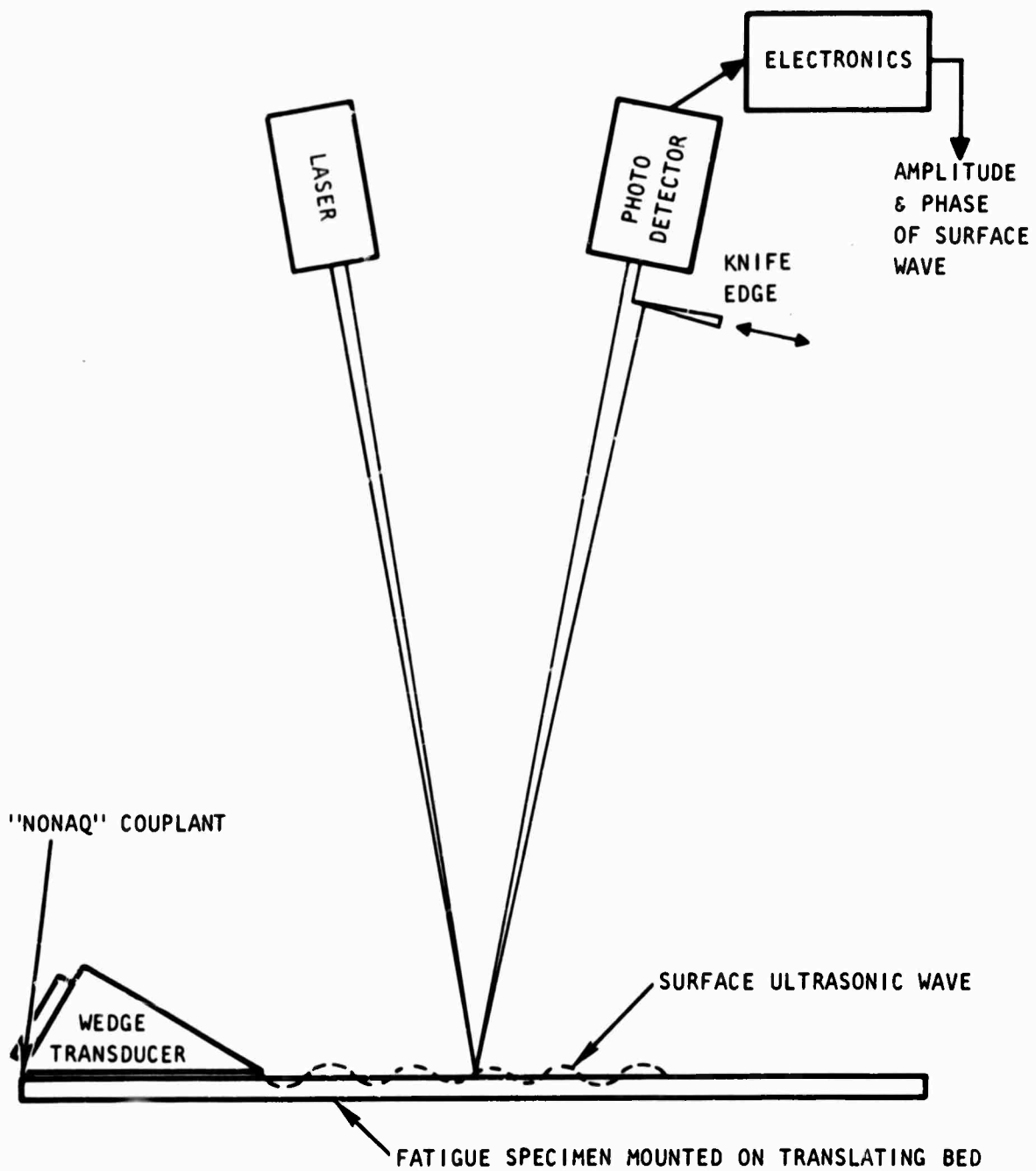


Figure 32. Schematic Diagram of Ultrasonic Surface Wave Measuring System

Industries type SMZ, style 57A3084 90°R) operating at 10 MHz. At 3.4 MHz the variable angle wedge transducer was adjusted to give maximum coupling to the surface acoustic mode. This adjustment was accomplished by choosing the angle which gave the largest signal transmitted along the specimen at the surface wave velocity.

TEST RESULTS AND DISCUSSION

Initial surface velocity measurements using two transducers were carried out on a control specimen and five 1100-aluminum specimens which had undergone fatigue deformation for 30, 50, 70, 80, and 90 percent specimen life at a maximum stress of 11,500 psi. Results obtained from both the conventional system and the precision measurement system at 2.25 MHz fall in the ranges illustrated in figure 33. A comparison of the change in attenuation in the family of these specimens is shown in figure 34. The ordinate is the ratio of the voltage difference at 5 to 1 MHz. The scatter in figures 33 and 34 was mainly due to the use of SAE 30 oil as couplant. Heavyweight oil couplant is reliable for detecting cracks. For velocity or attenuation measurement, however, one no longer looks for the presence or absence of a responding signal, but one must resolve and define the waveform and cycles of that signal. Any minute variation in coupling pressure or thickness has a marked effect on the waveform. It is necessary to use a coupling medium to eliminate air from the transducer-specimen interface with compatible acoustic impedance and yet to be sufficiently fluid to insure removal of all air bubbles. Furthermore, any changes in the couplant thickness affect both the acoustic pulse transit time and the amount of energy transferred to the specimen. A coupling medium under the trade name Aroclor 1260, manufactured by Monsanto Chemical Co., proved superior in terms of data reproducibility. The trend of the curve shown in figure 34 was confirmed.

Both figures 33 and 34 indicate a gradual reversal of fatigue life to surface wave velocity and fatigue life to attenuation ratio trend at about 50-percent specimen life. However, owing to the wide scatter of the experimental data, it is not certain whether there is a perceptible change in velocity or attenuation between the control specimen and the specimen which had spent 20 percent of its fatigue life based on 4.0×10^5 cycles.

The frequencies (1 to 5 MHz) chosen were dictated by the availability of suitable transducers. The depth of penetration of surface waves is about one wavelength, which in the present case is about 0.05 inch, much larger than the depth of the fatigue-affected zone determined by metallography. The present results, however, are somewhat similar to those observed by Herlescu and coworkers (1967) on steel in bending fatigue.

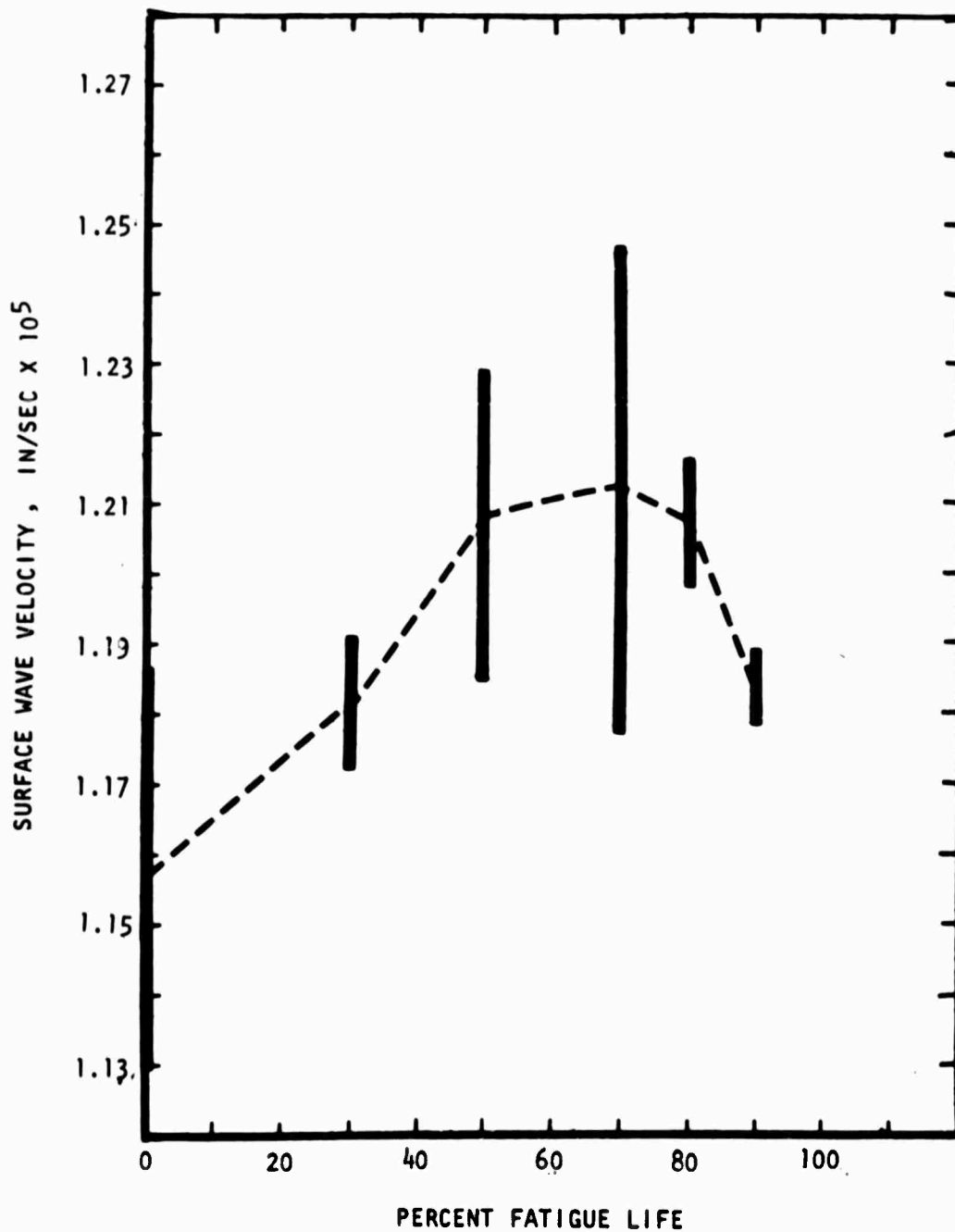


Figure 33. Relationship Between Surface Wave Velocity and Fatigue Life of 1100-0 Aluminum

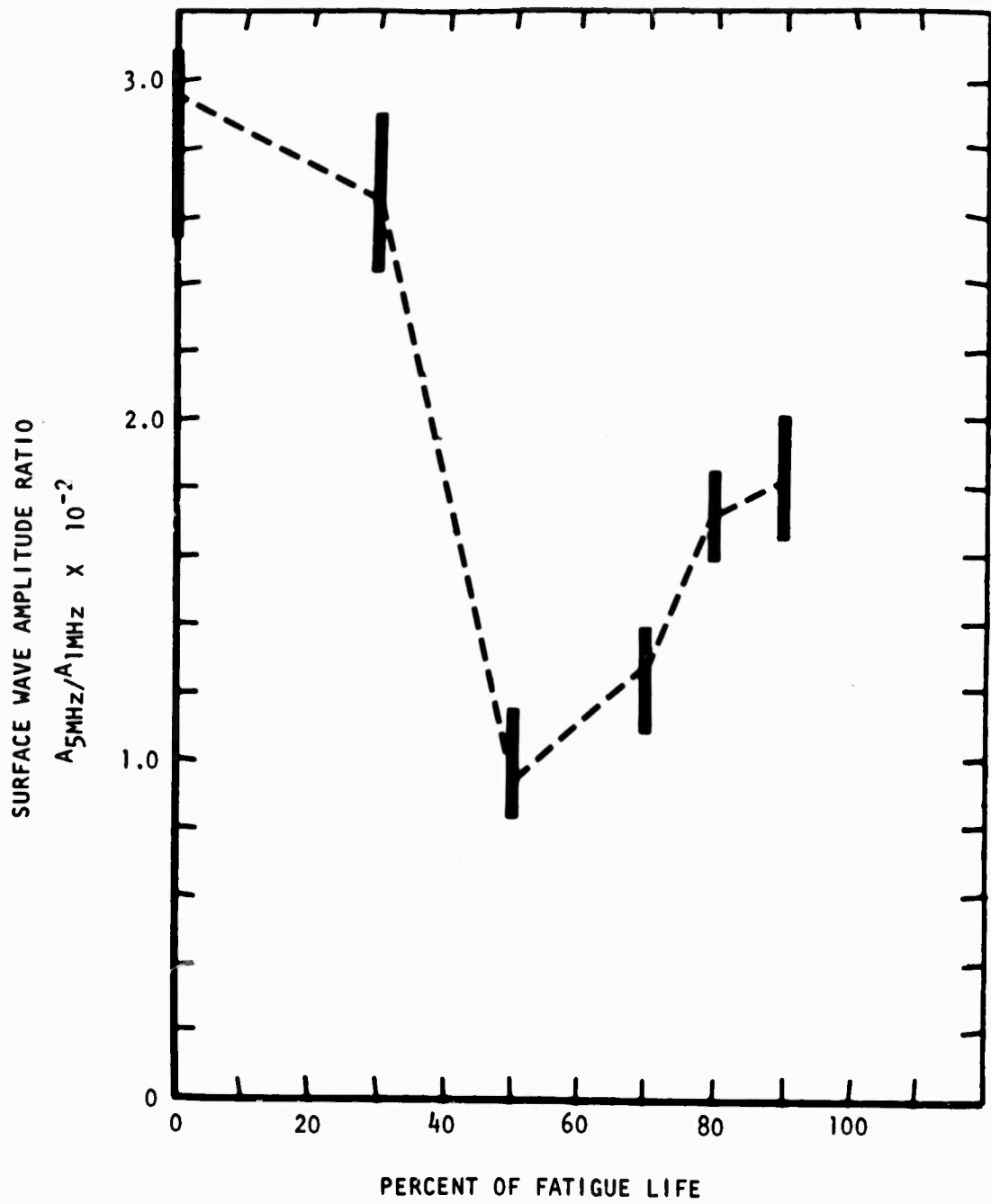


Figure 34. Relationship Between Surface Wave Attenuation and Fatigue Life of 1100-0 Aluminum

The laser probe technique was applied in measuring both attenuation and velocity of ultrasonic surface wave propagating in 7075-T6 aluminum alloy specimens which had been subjected to fatigue loading at a stress of 40,000 or 60,000 psi for different numbers of cycles.

The surface wave velocity for three specimens with measurement precision better than 0.5 percent, using the variable angle wedge transducer at 3.4 MHz, is shown below.

<u>Specimen No.</u>	<u>Stress, psi</u>	<u>No. of Cycles</u>	<u>Surface Wave Velocity, 10⁵ cm/sec</u>
1	40,000	40,000	2.88 ±0.001
6	60,000	8,250	2.95 ±0.001
13	60,000	8,250	2.89 ±0.001

The difference between specimens 1 and 13 is less than the experimental error. Since the fatigue history of the two specimens is quite different, it appears that no correlation exists within the 0.5 percent velocity precision of these measurements. The anomalously high velocities measured in specimen 6 have not yet been explained. However, it was noted that this high average velocity was due primarily to a locally high velocity in the region where the specimen width changed from one inch at the end to about 1/2 inch in the center section. No change in velocity with position was noted in the other specimens.

Since the velocity measurements were quite time consuming and did not show great promise at this frequency, the effort was then directed towards attenuation measurements. Difficulties were encountered due to apparent interference effects between some unspecified wave and the surface wave of interest. This is illustrated in figure 35 where the amplitude is plotted as a function of position along the specimen. At points near the transducer, the amplitude fluctuates rapidly. This fluctuation decreases with distance, and it is evident that a precise determination of attenuation is difficult. If one notes that the beat period is about 8 wave-lengths and assumes that the result is caused by the beating of 2 waves of velocity differences Δv , then it may be readily shown that $\Delta v/v = 1/8 = 0.125$. For aluminum, the difference between bulk shear and surface velocity is 0.2×10^5 cm/sec so $\Delta v/v \approx (0.2/3) = 0.067$. This differs by a factor of 2 from the measured result but does suggest that energy injected in the form of bulk shear waves may contribute to the measurement difficulty.

Despite the obvious problem, it was felt important to attempt an attenuation measurement on all of the specimens to see if a correlation did in fact exist. The amplitude of the surface wave energy was measured at four points along each specimen, two points near the ends of the test section and two points near specimen center. For consistency the results were taken at

the local maxima nearest to the point chosen. (For example, at $n = 55$ rather than $n = 60$ in figure 35). These points were then fitted to an exponential curve using a least square fit computer program.

The results of this attenuation measurement are presented in table VI. One set of data was taken on each face of each specimen, and the average of the two taken as the attenuation value for that specimen. The specimens are grouped according to their nominal fatigue condition and the average value for a given group determined. It is this value of attenuation, which represents the average of six nominally identical experiments, which shows a correlation with fatigue. This correlation is graphically illustrated in figure 36. At 40,000 psi attenuations for the specimens which had been subjected up to 5 percent of the fatigue life are clearly separated from those for the specimens which had undergone further cycling. The variation of attenuation at 60,000 psi was not well defined due to the limited number of tests.

Attenuation measurement was also made using the fixed angle wedge transducer at 10 MHz. This should decrease the penetration distance of the surface wave and hence increase the influence of fatigue damage on attenuation. The results are also given in table VI and figure 36. Again the correlation between attenuation and fatigue cycles previously determined at 3.4 MHz is also noted here.

The tests results at 10 MHz do not show an improvement in establishing a relationship with fatigue presumably due to interference effects. Some simple diagnostic experiments were performed, using the laser probe, to understand in greater detail the origin of these effects. The data in figure 35 indicates an interference or beating effect is observed but does not conclusively determine its origin. A number of possible causes were considered. First, the fact that the specimen has finite thickness might introduce Lamb wave modes of velocities near the surface wave velocity and cause interference. Secondly, interference might arise due to the finite and varying width of the specimen, and thirdly, interference might occur if both bulk and surface waves are excited by the wedge transducers.

The first possibility can be quickly dispelled by reference to the literature, where Victorov (1967) discusses the relation of Lamb and Rayleigh (surface) waves. He shows that if one attempts to excite a surface wave on the upper surface of a plate of finite thickness $2d$, a quasi-Rayleigh wave occurs in which the energy is localized near the upper surface only for distances much less than $N\lambda_R$ from the transducer (this wave is in fact the linear combination of the symmetric and antisymmetric Lamb modes of the plate). At

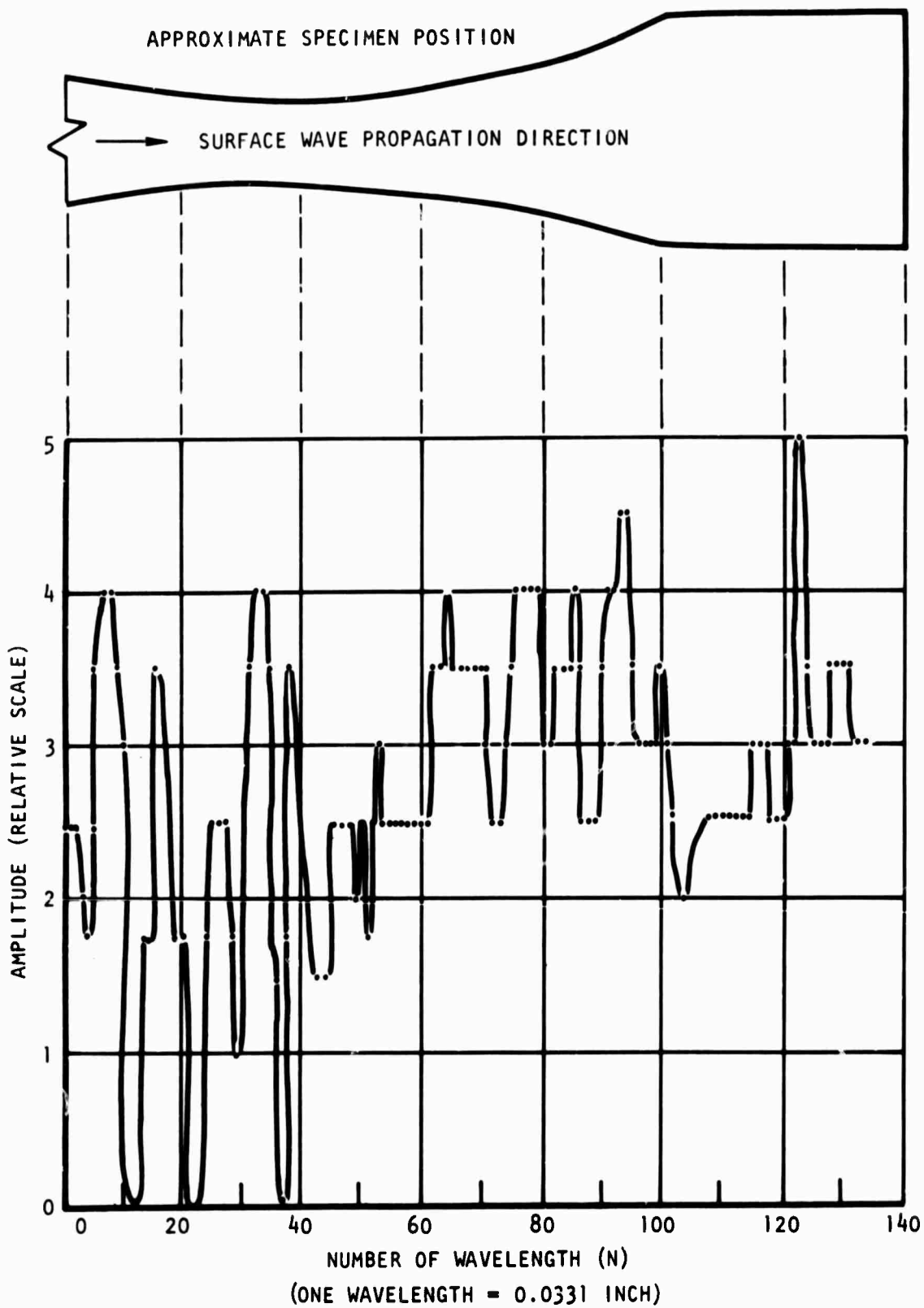


Figure 35. Amplitude as a Function of Specimen Position Showing Interference Effects at 3.4 MHz Frequency in Fatigue-Stressed 7075-T6 Aluminum Alloy

TABLE VI. SURFACE WAVE ATTENUATION IN FATIGUE-STRESSED 7075-T6 ALUMINUM ALLOY

Specimen No.	Stress, psi	No. of Cycles	Percentage of Fatigue Life*	Attenuation, neper/cm									
				3.4 MHz				10 MHz					
				One Side	Other Side	Average	Group Average	One Side	Other Side	Average	Group Average		
15	0	0	0	0.003	0.105	0.054			0.086	0.003	0.045		
1	40,000	40,000	1.6	-0.067	0.021	-0.024	0.047	0.047	0.076	0.229	0.153		
28	40,000	50,000	2	0.058	0.120	0.087			0.083	0.033	0.058		
16				0.038	0.047	0.042			0.142	0.076	0.109		
19	40,000	125,000	5	0.135	0.097	0.106	0.094	0.094	0.080	0.146	0.113		
26				0.186	0.062	0.124			0.229	0.025	0.127		
7				-0.014	0.011	0.002			0.101	0.026	0.064		
11	40,000	250,000	10	0.170	0.081	0.126	0.082	0.082	0.109	0.097	0.098		
18				0.153	0.082	0.118			0.110	0.146	0.128		
8	40,000	625,000	25	0.190	0.050	0.121			-0.001	0.308	0.153		
14				0.061	0.118	0.091	0.105	0.105	-0.30	0.030	0		
3				0.070	0.126	0.098			0.157	0.156	0.157		
12	60,000	3,300	10	0.121	0.035	0.078	0.081	0.081	0.092	0.057	0.075		
23				0.055	0.076	0.066			0.159	0.115	0.137		
6				0.098	0.126	0.112			0.078	0.080	0.079		
13	60,000	8,250	25	-0.007	0.031	0.012	0.069	0.069	0.139	0.225	0.182		
22				0.111	0.052	0.082			0.196	-0.010	0.093		

*The percentage of fatigue life was based on an average life of 2.5×10^6 and 3.3×10^4 cycles at 40,000 and 60,000 psi, respectively.

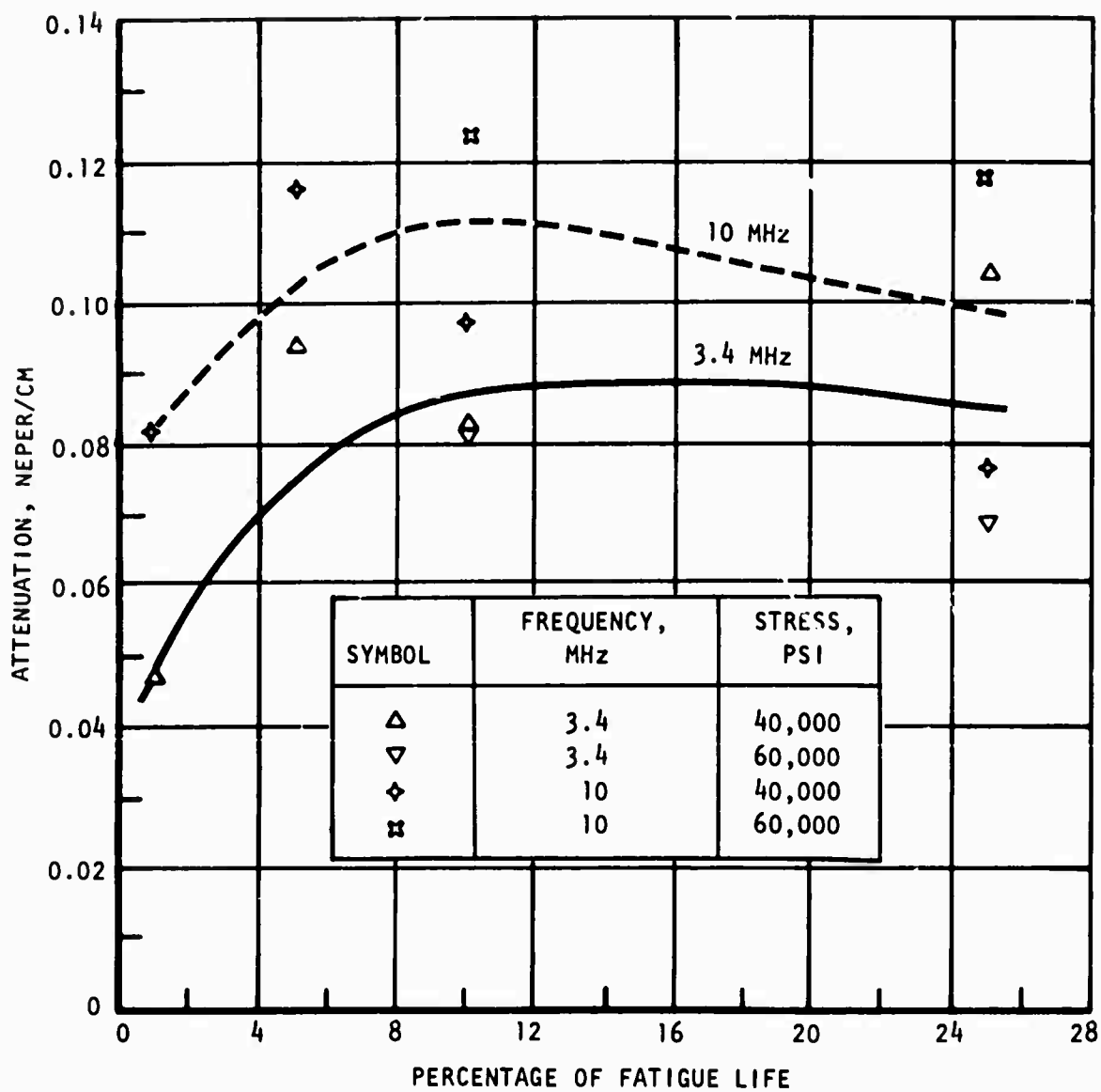


Figure 21. Attenuation of Surface Wave in Fatigue-Stressed 7075-T6 Aluminum Alloy

the distance $N\lambda_R$ a destructive interference phenomenon occurs which eliminates the Rayleigh type wave. N is given by the expression:

$$N = \left[\frac{1}{4} + \frac{1}{8(1-\eta_R^2)} + \frac{1}{8(1-\eta_R^2\xi^2)} - \frac{1}{2-\eta_R^2} \right] \exp \left(2k_R d \sqrt{1-\eta_R^2} \right)$$

where

$$\eta_R = v_R/v_s$$

$$k_R = \omega/v_R$$

$$\omega = 2\pi \times \text{frequency}$$

$$\xi = v_s/v_L$$

v_s = shear wave velocity, v_L = longitudinal wave velocity, and

v_R = surface wave velocity

with an accuracy of 10% for $2d/\lambda_R > 2.5$. From the present experimental case, $2d = 0.86''$. At 3.4 MHz, $2d/\lambda_R = 2.55$ and thus $N = 150$. At 10 MHz, $2d/\lambda_R = 7.55$ and $N = 107$. Thus at 3.4 MHz destructive interference would occur 12.8 cm (5.05 in.) from the transducer. At 10 MHz the number would be on the order of 2 km or over a mile. This then establishes that deviations from Rayleigh wave propagation due to the finite thickness of the sample was not the cause of the observed interference.

The second possibility, interference due to the finite and varying width of the specimen was dispelled by using the same transducer and laser probe to study propagation in an infinitely wide plate of the same thickness as the fatigued specimens. The same interference effects were observed. It cannot be ruled out that the width of the specimen produces some effects, but this is certainly not the worst source of interference.

Elimination of these possibilities suggests that in fact bulk waves were injected by the wedge transducers and that these experienced multiple reflections between the upper and lower surfaces of the fatigued specimens. This was in fact verified at 10 MHz by using the laser probe to study the lower surface (opposite the transducer) of the specimens. It was found that a

significant amount of energy was present, with amplitudes ranging roughly from 1/4 to 1/2 that on the upper surface. This energy first appears directly under the transducer and propagates in the same direction as the surface wave on the upper surface.

A detailed explanation of this phenomena has not been obtained, but a number of observations suggest that it results from an excitation of bulk shear wave as well as surface wave by the wedge transducers. As a first check on this idea, the velocity of the wave on the lower surface of specimen 28 was measured at 10 MHz. A value of 3.20×10^5 cm/sec was observed which is on the order of but slightly in excess of the shear velocity in aluminum (3.11×10^5 cm/sec). As a check, the velocity was measured on the upper surface. Halfway along the length a value of 3.04×10^5 cm/sec was observed, while at the far end away from the transducer the value of 3.12×10^5 cm/sec was obtained. These results suggest that a mixture of the surface and bulk shear modes are present on the upper surface. At the middle, they are both present and of comparable amplitude. An average wavelength, or velocity, is measured. Away from the transducer the bulk wave is dominant since surface defects cause the surface wave to attenuate more rapidly.

The result that a large amount of bulk energy is launched by the wedge transducer is surprising in view of predictions that excitation of bulk wave is 20 to 30 dB lower than excitation of surface wave (Victorov, 1967). However experimental investigations using a commercial variable angle wedge at 3.4 MHz indicate that the half power angular bandwidth for excitation of Lamb waves in a plate is on the order of 5° to 10° . Since the theoretical wedge angles for excitation of the surface wave and grazing shear wave in aluminum by a lucite wedge with longitudinal transducer are 67° and 59° , respectively, and thus differ by only 8° , the excitation of both waves is not surprising.

Since it was well established that energy exists on the bottom and presumably in the bulk of the fatigue-stressed specimen, several approaches were considered. First, a few wedge and comb transducers were fabricated with different properties in an attempt to decrease the coupling to the bulk modes, but no improvement was obtained.

Secondly, it was tried to decrease the interference effects by altering the elastic boundary conditions at the lower surface. The specimen was placed in a water bath with the lower surface in contact with the water but the upper surface on which the surface wave propagates free. If the energy on the lower surface were in the form of a surface wave, it would be rapidly attenuated in a distance on the order of 10 wavelengths by radiation into the water (Victorov, 1967). Some change in the interference effects were in fact observed when the water level was raised to touch the lower surface, but the situation was not markedly improved. Hence it may be concluded that energy does in fact fill the bulk of the specimen.

Thirdly, the specimen was bonded to the surface of a large aluminum block with phenyl salicylate (Salol). In the case of a perfect bond, the bulk energy would radiate into the larger block rather than be reflected within the fatigued specimen. In fact, however, it was impossible to obtain a satisfactory bond without altering the surface of the specimen and this approach was abandoned.

As a final experiment, it was decided to verify that the method proposed would provide a good means of measuring surface wave attenuation if the interference effects were avoided by some means. Figure 37 shows a plot of the attenuation of 10 MHz surface wave on the surface of a very thick aluminum block which had been turned smooth in a lathe and polished flat on a surface plate. A number of fluctuations still exist which may be, in part, a result of the presence of the oil film. Nevertheless, a well defined measure of attenuation is obtained. It is interesting to note that this value of 0.3 n/cm is larger than that observed and tabulated in table VI. This again suggests that the surface wave was dominant near the transducer in those measurements but that bulk waves become increasingly dominant at greater distances due to their lower attenuation. This is of course strictly hypothetical since the metallurgical history and composition of the large aluminum block was unknown.

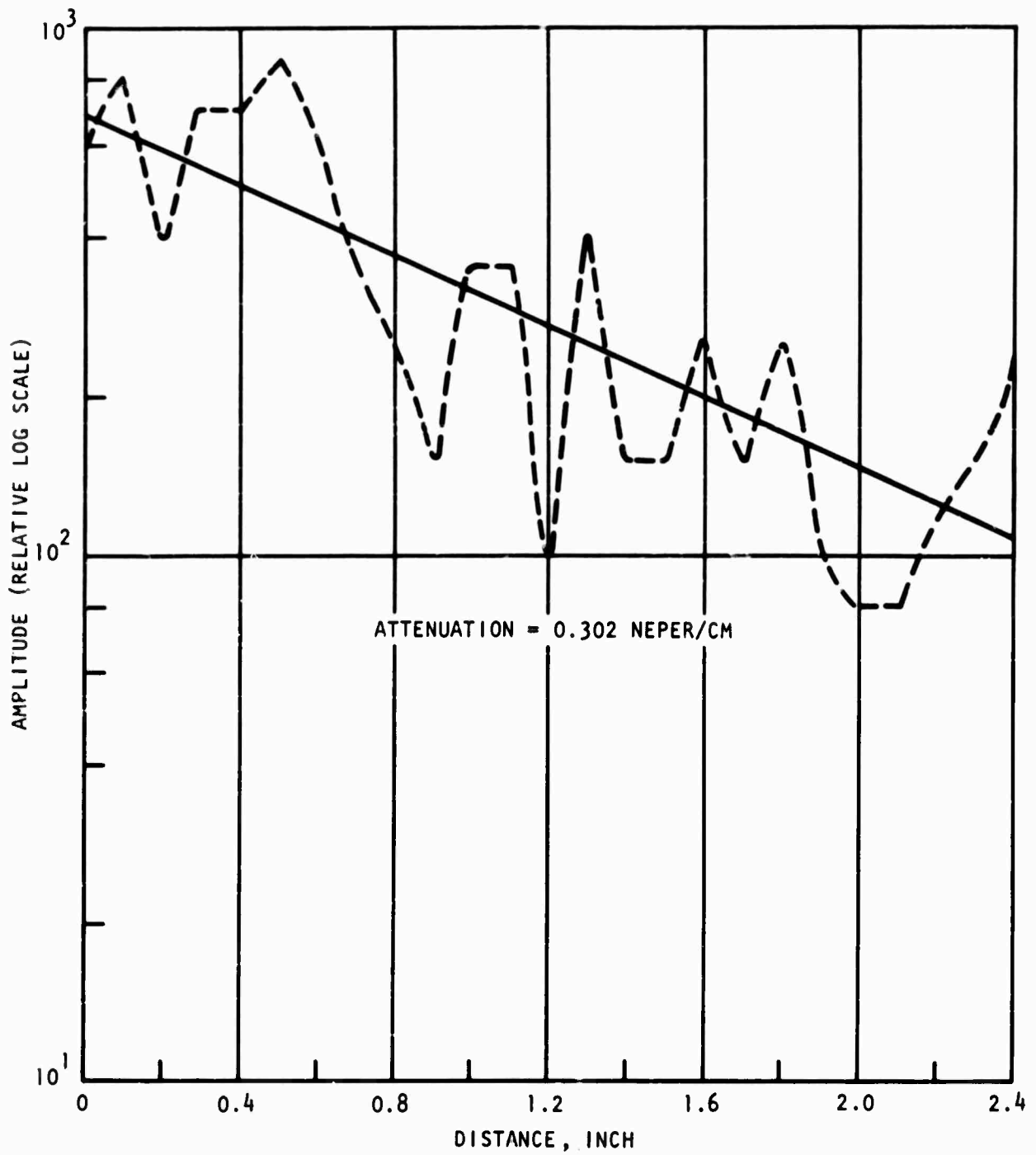


Figure 37. Surface Wave Attenuation at 10 MHz Frequency in a Thick Aluminum Block

SECTION VIII

MATERIAL CHARACTERIZATION

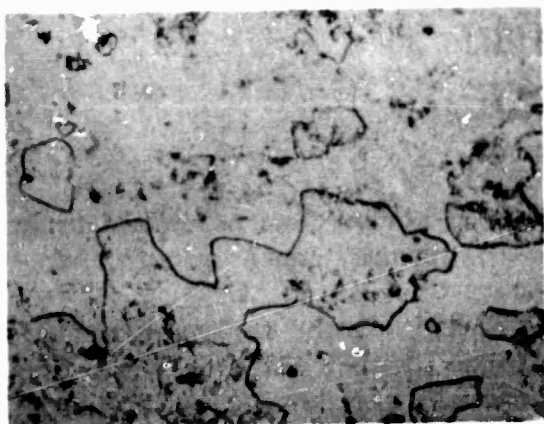
A systematic examination of the fatigued surface was performed to attempt to characterize the early damage in terms of nature, depth, growth, etc.

The early appearance of slip lines or bands on the fatigue-stressed surface does not necessarily indicate fatigue damage, since only the persistent slip (slip bands that are resistant to removal) are thought to be the potential nucleation sites for fatigue cracks (Thompson et al, 1956). The physical evidence of fatigue damage is therefore the presence of persistent slip bands in the surface layer. The depth of these bands is generally less than a few hundred microns as measured at approximately one-half of the fatigue life. It is therefore concluded that early fatigue damage can be related to depth of this fatigue-affected layer.

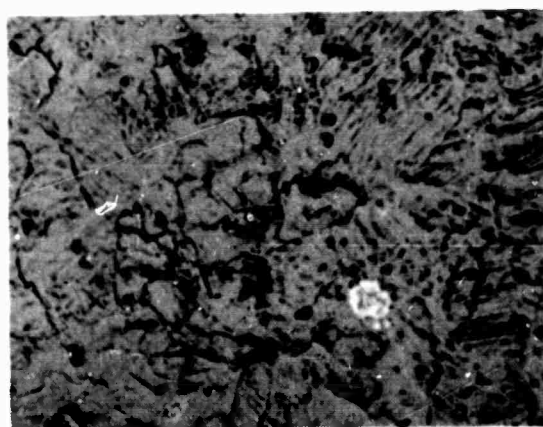
METALLOGRAPHY

Metallographic examination using an optical microscope and an electron microscope was conducted on a control and five 1100-0 aluminum specimens, which had been subject to fatigue stressing at 11,500 psi for 1.2, 2.0, 2.8, 3.2, and 3.6×10^5 cycles. The results are shown in figures 38 and 39. The control surface shows a relatively smooth grain structure. The fatigued specimen surfaces exhibit considerable evidence of slip and indications of intrusions and extrusions even at the lowest fatigue exposure of 1.2×10^5 cycles. Penetrant tests, however, did not reveal any indication of surface cracks.

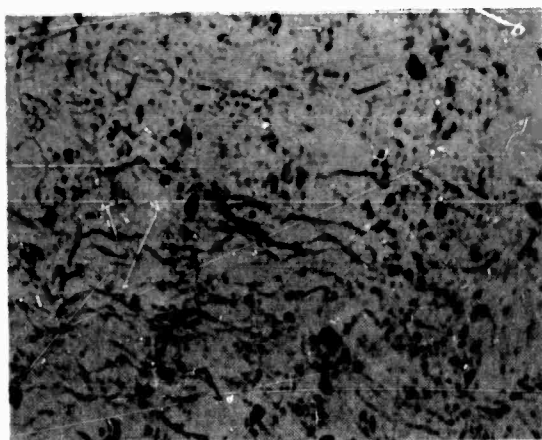
To gain some idea of the depth affected by the surface slip movement, the electropolished surfaces of two 1100-0 aluminum specimens, which had been fatigue-stressed at a stress of 11,450 psi for 800 and 3.0×10^4 cycles, were examined by means of a secondary electron emission microscope. During this examination, the surface layer was progressively etched off by means of an argon bombardment until all traces of slip line structure had disappeared. Details are shown in figures 40 and 41. The specimens were then removed from the microscope and mounted, so that the cross section could be polished across the area exposed to the argon ions. The depth of attack was then measured by means of a reticule microscope objective. The depth of attack for the specimen subject to fatigue stressing for 800 cycles was too shallow to measure accurately, while that for the specimen which had undergone 3.0×10^4 cycles was approximately 10 μm .



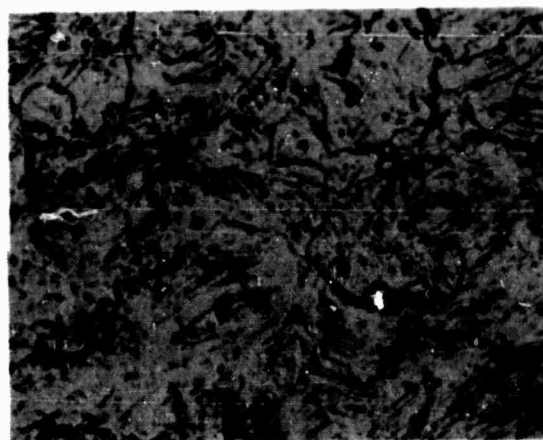
Control, 0 Cycle



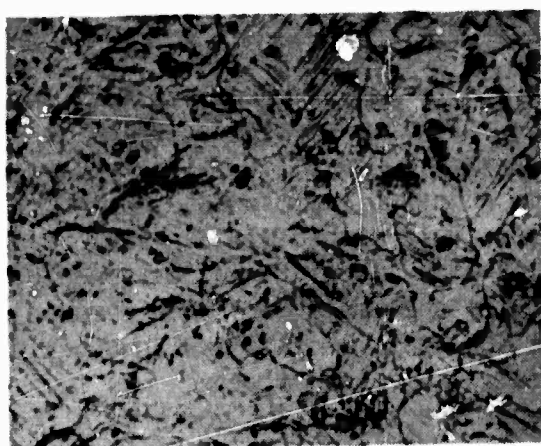
2.8×10^5 Cycles



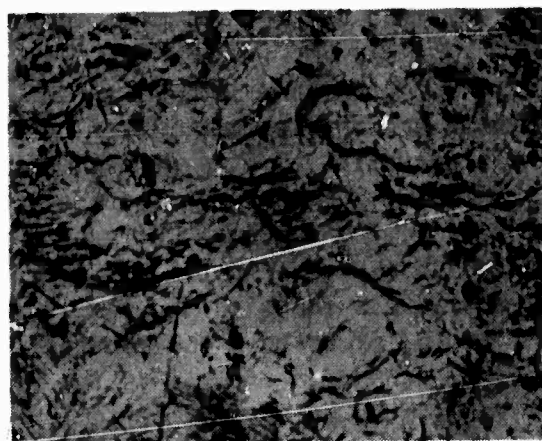
1.2×10^5 Cycles



3.2×10^5 Cycles



2.0×10^5 Cycles

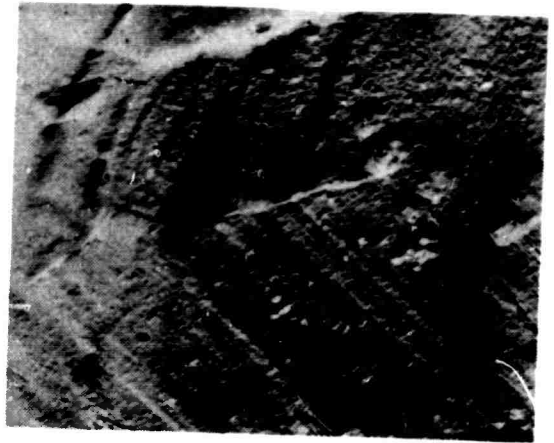


3.6×10^5 Cycles

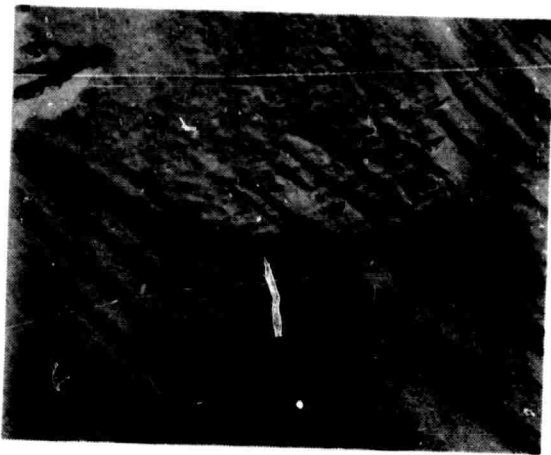
Figure 38. Optical Micrographs of Fatigue-Stressed 1100-0 Aluminum at 11,500 lb/in.² (250X)



Control, 0 Cycle



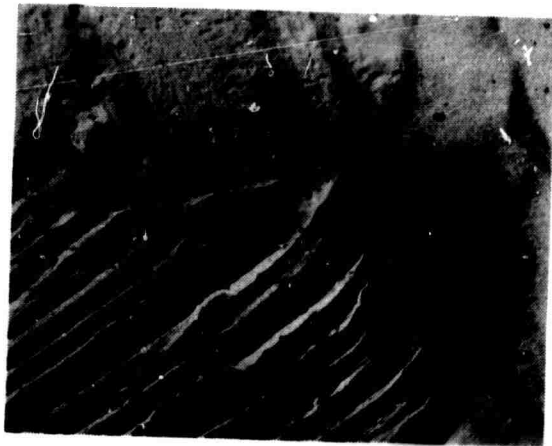
2.8×10^5 Cycles



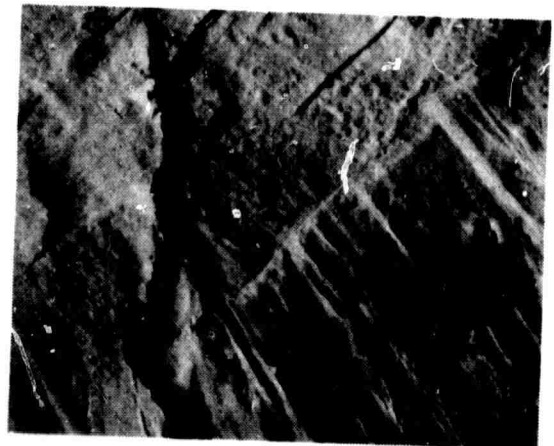
1.2×10^5 Cycles



3.2×10^5 Cycles

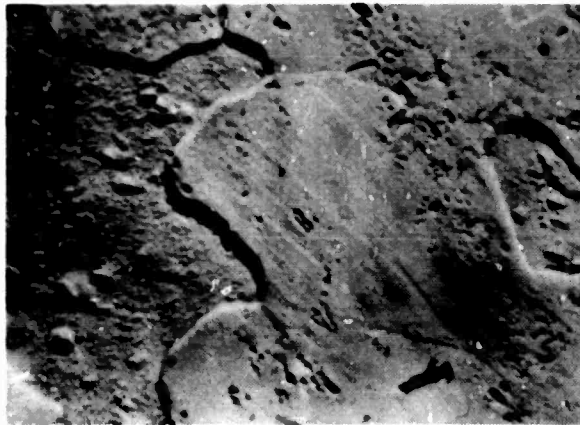


2.0×10^5 Cycles

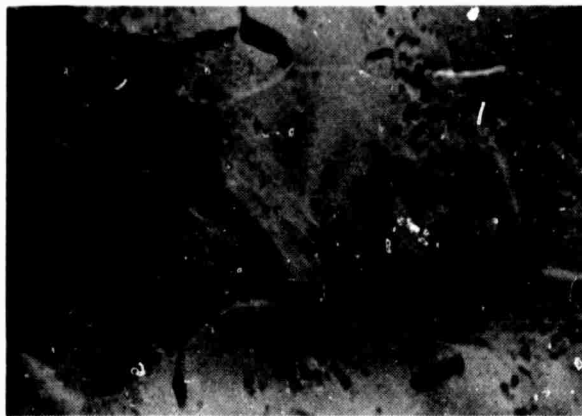


3.6×10^5 Cycles

Figure 39. Electron Micrographs of Fatigue-Stressed 1100-0 Aluminum
- at 11,500 lb/in.² (2500X)



As Fatigued

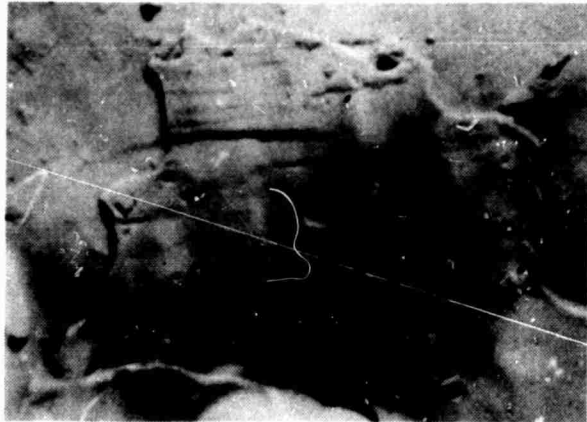


Argon Etch for 50 Minutes

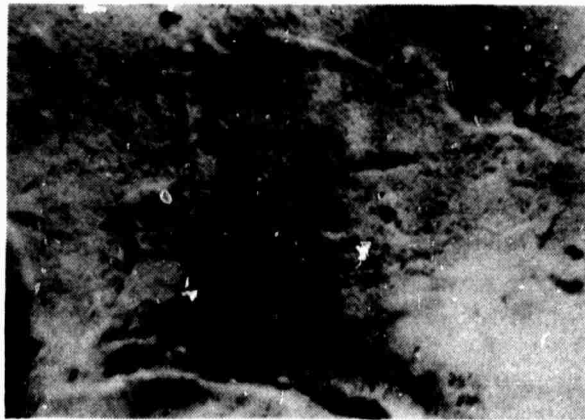


Argon Etch for 2 Hours 35 Minutes

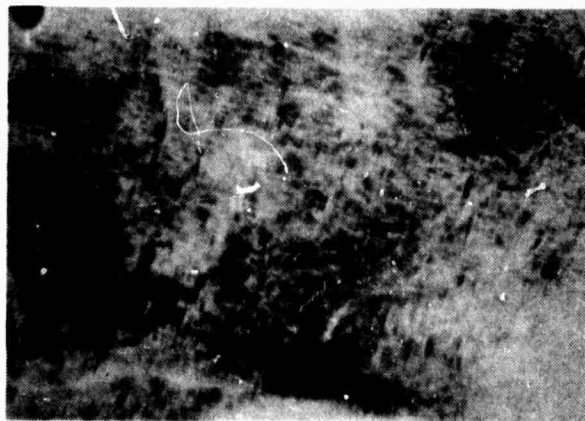
Figure 40. Secondary Electron Emission Micrographs at 550 X of Fatigue-Stressed 1100-0 Aluminum at 11,450 psi for 800 Cycles



As Fatigued



Argon Etch for 50 Minutes



Argon Etch for 3 Hours 58 Minutes

Figure 41. Secondary Electron Emission Micrographs at 550X of Fatigue-Stressed 1100-0 Aluminum at 11,450 psi for 3×10^4 Cycles

To be certain that the depth of the fatigue effects was removed, the test sections of five additional 1100-0 aluminum specimens which had been fatigue-stressed at 11,000 psi for 5×10^3 , 1×10^4 , 5×10^4 , 1×10^5 and 2×10^5 cycles were also examined. They were electropolished in a methanol-nitric acid bath and withdrawn periodically from the bath for examination with an optical microscope. The fatigue-affected layer was thought to have been removed by electropolish when no slip bands were evident under the microscope at a magnification of 250 and the microstructure on the surface had reverted to the structure prior to fatigue test. The thickness of the removed layer was determined from specimen thickness measurements before and after electropolishing. The surface layer measurements (table VII) did not appear to be directly proportional to the fatigue life.

Metallographic studies of 1100-0 aluminum reveal that slip striations appear very early on the surface. For example, at a stress of 11,000 psi slip bands could be observed on the surface of the specimen having been cyclically stressed for 5×10^3 cycles, which correspond roughly to 1.7 percent of the total life.

The affected surface layer data shown in table VII do not indicate a relationship between fatigue time and the thickness of the fatigue-affected layer. In addition, the layer depth appears to reach the final value early in the process. In analyzing this data, it was noted that in the course of repeated electropolishing, an oxide film forms on the surface of the 1100-0 aluminum when withdrawn from the bath for metallographic examination. This film then obstructs subsequent polishing when the piece was returned to the bath. Further, some excess metal could have been removed during the attempt to remove the oxide and the piece could have been overpolished. Despite overpolish, however, the measured depths do not vary greatly; the average value is about 60 microns. This investigation thus reveals that increasing fatigue damage is confined to a surface layer, and does not penetrate beyond this layer until subsequent cracking occurs and the specimen fails.

SURFACE ANALYSIS

Since fatigue damage is a surface phenomenon, knowledge of the changes of certain surface-sensitive properties effected by fatigue loading might reveal some clues to the damage suffered by the metal in fatigue. Characterization of a metal surface can be made with surface potential difference and ellipsometry. Surface potential difference or difference in work function between a metal specimen and a reference surface yields information concerning dielectric properties of films or contamination on the metal surface. Since work function of a metal is influenced by plastic deformation (Andreev and Palige', 1962 and 1964) and probably also by fatigue stressing, the measured surface potential difference might also be related to fatigue damage.

TABLE VII. DEPTH OF SURFACE LAYER REMOVED BY ELECTROPOLISY FROM FATIGUE-STRESSED 1100-0 ALUMINUM SPECIMENS

Specimen No.	No. of Cycles	Percentage of Fatigue Life*	Depth of Surface Layer, microns
79	5×10^3	1.7	75
72	1×10^4	3.3	55
70	5×10^4	16.6	61
75	1×10^5	33.3	76
87	2×10^5	66.7	39

*The percentage of fatigue life was based on an average life of 3×10^5 cycles at 11,000 psi.

Characterization of the surfaces of both 7075-T6 aluminum alloy specimens and annealed D6AC steel specimens which had been subjected to fatiguing at various stress levels for differing numbers of cycles were made with surface potential difference and ellipsometry.

Surface Potential Difference

The surface potential difference between the metal and a reference surface can be measured by a high impedance electrometer in a circuit connecting the specimen with the reference surface shown in figure 42. A radioactive substance sealed behind a steel foil on the reference electrode ionizes the air between the reference electrode and the specimen and allows a current to flow between them. This current is detected by the electrometer. The voltage reading from the electrometer will yield surface potential difference directly if the electrometer resistance is much greater than the air gap resistance.

Surface potential difference between fatigue-stressed 7075-T6 aluminum alloy specimen and a reference electrode (figure 42) was measured at the center of the specimen on both sides a number of times. The average value is given in table VIII and plotted versus the number of fatigue cycles in figure 43. The surface potential in negative value appears to decrease with increasing number of cycles at the lower stress level 40,000 psi. However, as the cycling proceeds further (after 2×10^5 cycles) the potential difference tends to increase in negative value again. At the higher stress level 60,000 psi, the limited amount of data also indicates a decreasing surface potential with increase of fatigue cycling. The role played by applied stress itself is yet to be resolved, since the effects of other variables also present on the specimen surface are not known.

The difference in surface potential, ϕ , can be expressed by the equation:

$$\Delta\phi = (W_s - W_R) + \Delta\phi_s + (\Delta\phi_d + \Delta\phi_o + \Delta\phi_w + \Delta\phi_g)$$

where

W_s and W_R = work function of the metal and reference electrode, respectively

$\Delta\phi_s$ = effect of applied fatigue stress and number of cycles

$\Delta\phi_d$ = effect of initial surface damage prior to fatigue test

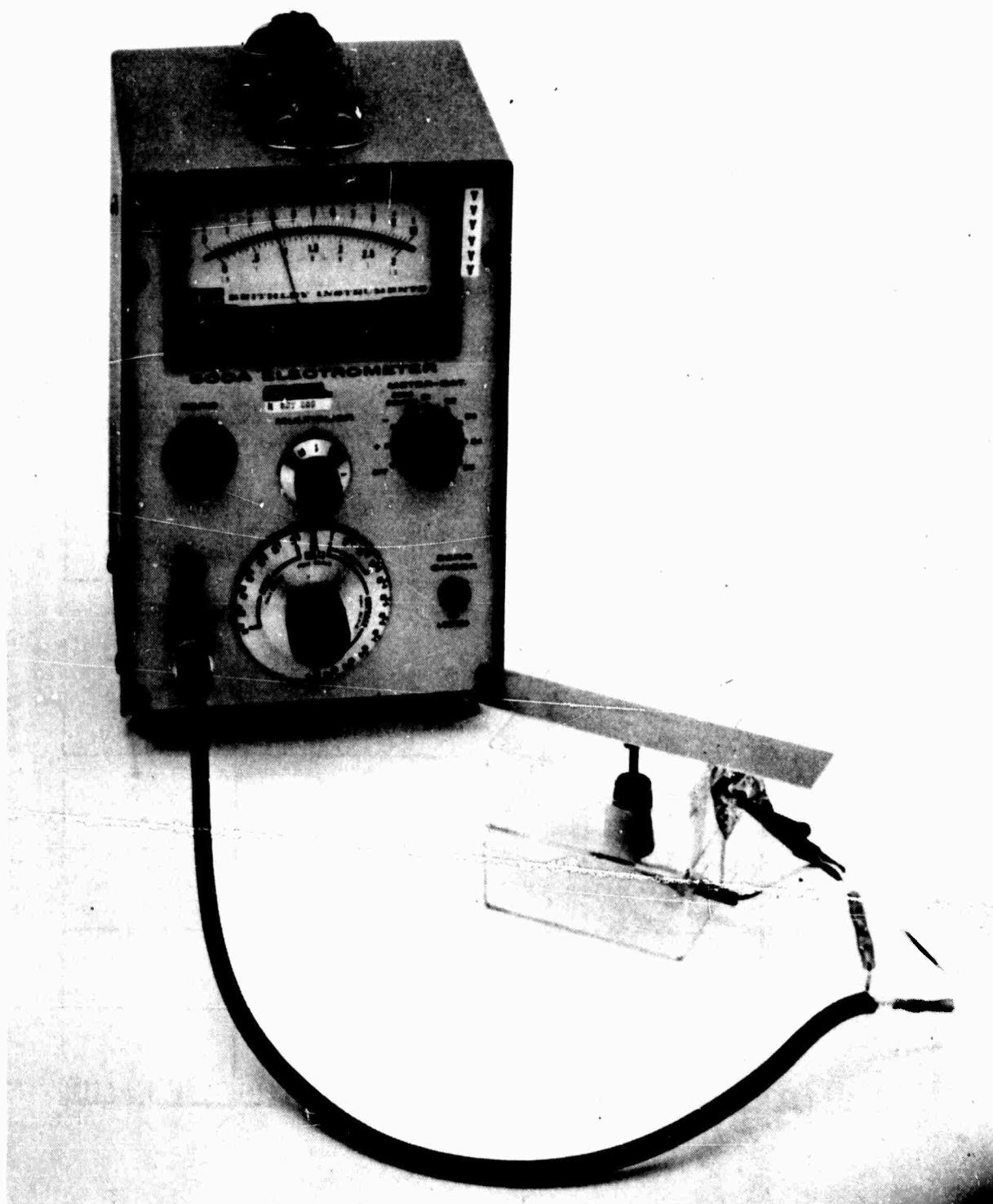


Figure 42. Photograph of Instrument for Measurement of Surface Potential Difference

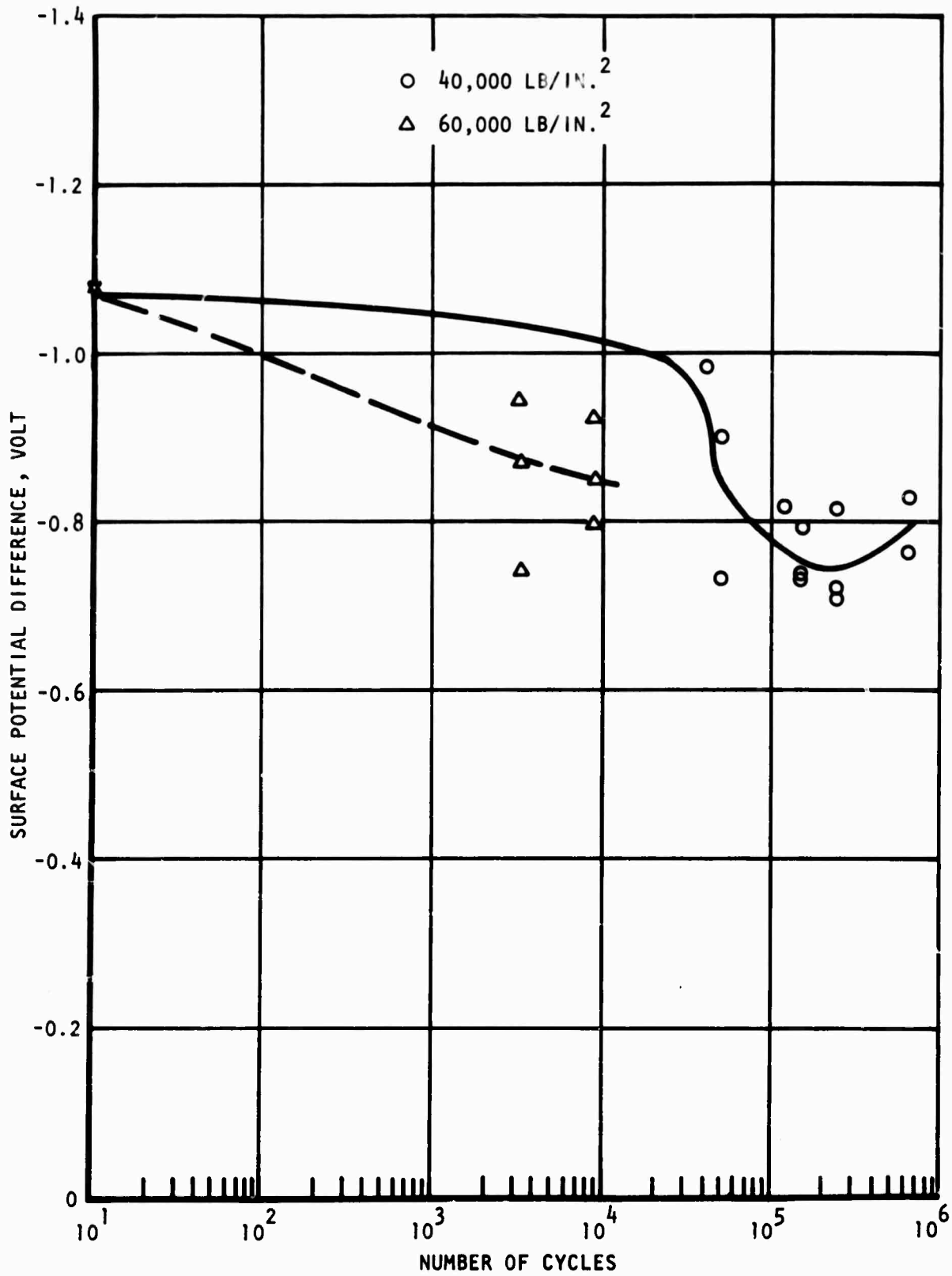


Figure 43. Surface Potential Difference of Fatigue-Stressed 7075-T6 Aluminum Alloy Specimens

$\Delta\phi_o$ = effect of oxide layer

$\Delta\phi_w$ = effect of absorbed water

$\Delta\phi_g$ = effect of grease and dirt

At any rate, the apparent changes of surface potential difference with stress in table VIII for 7075-T6 aluminum alloy are orders of magnitude greater than that observed by French and Beams (1970) for copper and nickel (about 1 to 3 millivolts).

All of the terms in brackets are already present on the metal surface prior to fatigue test. Their presence defines the initial surface condition, and surface condition can vary from specimen to specimen. To demonstrate the effect of surface condition on surface potential difference, a piece of aluminum plate about 1/8 inch thick was handled in differing ways and the surface potential difference was measured after each handling. The handling history and the accompanying surface potential difference are listed in table IX. These results indicate that, for a chem-milled aluminum specimen, rolling, rubbing or cyclic stressing causes a layer of surface damage to form that has a larger negative surface potential difference than in the chem-milled state. To show that the damage layer is very thin, note in table IX that rubbing aluminum foil with dry Kimwipe tissue on one side changes ϕ from -0.58 to -0.96 while the other side remains at -0.62.

The width in the test section of each specimen changes continuously along the length on account of the presence of the 6-inch radius notch. The cross-sectional area normal to the applied stress as well as the degree of fatigue damage would consequently vary in the test section. Center of the specimen where the cross-sectional area is smallest should suffer heaviest fatigue damage. The damage would become less and less toward each end of the test section. Since figure 43 indicates a change of surface potential difference with number of cycles and presumably also with fatigue damage, a survey of surface potential difference along the length of a fatigued specimen may also map the variation in the extent of accrued damage. Hence the surface potential difference was measured on specimen 6 which had been fatigued stressed at 60,000 psi for 8,250 cycles. The potential difference profile before and after cleaning with acetone is plotted in figure 44. The smooth dashed curve after cleaning shows the increased effect of fatigue stressing and hence damage at the center. The sharp increase in negative value of the potential difference at specimen end reflects the highly stressed area where the specimen was tightly clamped in test. The irregular curve before cleaning probably arises from a different surface condition, since oxide, dirt or water vapor could have accumulated on the fatigued surface

TABLE VIII. SURFACE POTENTIAL DIFFERENCE AND ELLIPSONOMETRY DATA FOR FATIGUE-STRESSED 7075-T6 ALUMINUM ALLOY

Specimen No.	Stress, psi	No. of Cycles	Surface Potential Difference, volt			Phase Shift, Degree	Ellipsometry Data		
			One Side	Other Side	Average		\tan^{-1} (Amplitude Ratio)	Film Thickness, Å	Refractive Index
15	0	0	1.05	1.09	1.07	13.83	38.65	130	
1		40,000	0.92	1.05	0.99	7.3	41.1	120	2.00
24		50,000	0.69	0.78	0.74	1.4	41.6	208	1.95
28		50,000	0.95	0.84	0.90	13.8	45.3	100	
27		111,500	0.94	0.77	0.83	13.9	44.5	100	
16		125,000	0.76	0.75	0.76	11.0	44.6	130	2.00
19		125,000	0.77	0.71	0.74	8.9	43.8	160	2.00
26	40,000	125,000	0.85	0.73	0.79	14.5	44.6	95	
7		250,000	0.70		0.70	10.7	42.6	130	2.35
11		250,000	0.72		0.72	12.8	41.8	88	2.15
18		250,000	0.78	0.85	0.82	18.3	44.3	60	
8		625,000	0.76		0.76	12.9	42.9	109	2.93
14		625,000	0.85	0.81	0.83	-10.1	42.1	440	
3		3,300	0.72	0.77	0.75	-5.0	41.3	187	2.96
12		3,300	0.95		0.95	5.9	43.7	428	1.4
23		3,300	0.85	0.90	0.88	7.0	39.4	200	
6	60,000	8,250	0.85		0.85	12.4	42.4	99	2.77
13		8,250	0.91	0.94	0.93	8.0	42.9	196	1.9
22		8,250	0.70	0.69	0.80	14.9	45.3	118	

TABLE IX. EFFECTS OF HANDLING ON SURFACE POTENTIAL DIFFERENCE

Material	Handling History	Surface Potential Difference, volt
Aluminum plate 1/8 inch thick	Dirty in as-received condition Cleaned with acetone Chem-milled for 2 minutes at room temperature Chem-milled for 2 minutes at 160°F Chem-milled for 5 minutes at 160°F Chem-milled for 10 minutes at 160°F Rubbed hard with dry Kimwipe tissue Chem-milled for 3 minutes at 160°F Bent plate 3 times Bent plate 4 times Cleaned with acetone Rolled to 0.03 inch thick Cleaned with acetone Chem-milled for 3 minutes at 100°F	-1.25 -1.50 -0.90 -0.85 -0.80 -0.80 -1.25 -0.80 -0.93 -1.40 -1.25 -1.60 -1.30 -1.10
Aluminum foil	Smooth and clean Wiped hard with dry Kimwipe tissue	-0.58 -0.96
Aluminum foil	Smooth and clean Wrinkled then stretched out	-0.55 -1.30
Type 304 stainless steel 1/16 inch thick	Dirty in as-received condition Cleaned with acetone Chem-milled for 2 minutes at room temperature Chem-milled for 2 minutes at 160°F	-0.32 -0.12 -0.42 -0.58

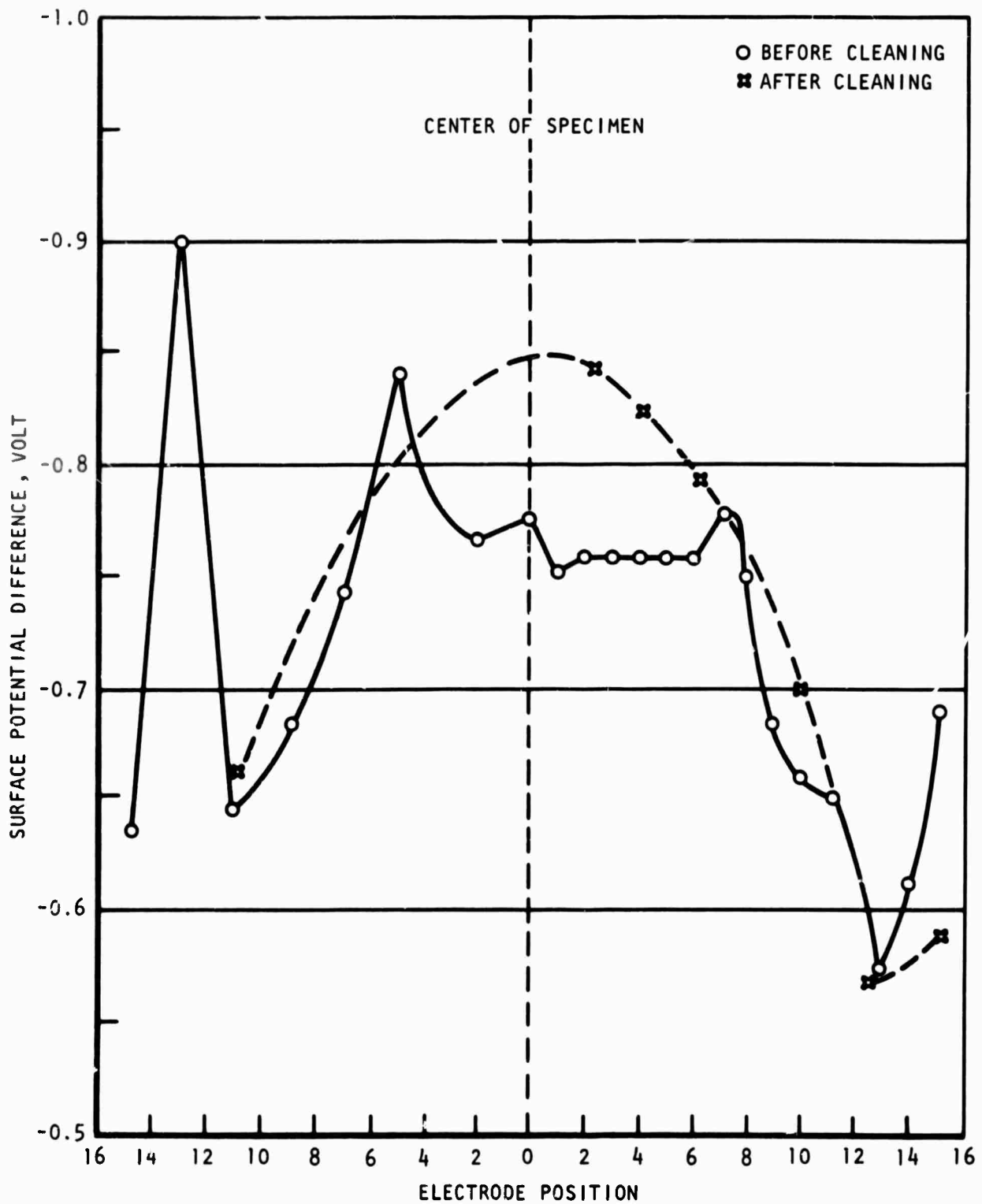


Figure 44. Variation of Surface Potential Difference Along Length of Fatigue-Stressed 7075-T6 Aluminum Alloy Specimen No. 6

layer in storage prior to measurement. The same measurements were again made on another specimen (No. 13) of identically fatigue-stressed state (figure 45). The difference between curves 1 and 2 reflects the change from day to another, whereas the difference between curves 2 and 3 shows the effect of cleaning with acetone. If larger negative values of surface potential difference reflect the effect of fatigue, the distribution along specimen 13 is not as symmetrical as for specimen 6. The reason for such difference is not clear. However, figure 44 offers a possibility of detecting highly fatigued regions by scanning the surface of a structure component and noting the variation of surface potential difference.

Surface potential difference between annealed D6AC steel specimens and the reference electrode was also measured. The results are given in table X. Some variation of the potential difference with number of cycles is noted but no correlation can be deduced.

Ellipsometry

Ellipsometry yields information about the thickness and optical constants (refractive index and absorption coefficient) of films on metals. The plane polarized light in an ellipsometric measurement is reflected from a surface and the light becomes elliptically polarized. This interaction with the surface causes both a phase shift in the normal and parallel components of the polarized light and a change in the ratio of the amplitudes. Analysis of these changes for a clean surface allows one to determine the complex refractive index of the surface. When a film is on the surface, an analysis allows one to determine the film thickness and its refractive index. A type 43603-200E manual photo-electric ellipsometer manufactured by O.C. Rudolph & Sons Inc., was used in the measurement.

Two ellipsometric parameters were measured. They are phase shift, p , and amplitude ratio, a . The results for 7075-T6 aluminum alloy specimens and annealed D6AC steel specimens are shown in tables VIII and X respectively. Large differences exist between the ellipsometry parameters ($p \sim 10$ to 15 , and $a \sim 39$ to 45) for 7075-T6 aluminum alloy, but no correlation with the number of cycles exists. This indicates that the film thickness and refractive index vary much.

Correlation is also not noted for annealed D6AC steel specimens, unlike 7075-T6 aluminum alloy, the ellipsometry parameters for the steel do not change appreciably with the number of cycles. The average oxide film thickness is 115 \AA and the refractive index is approximately 1.3.

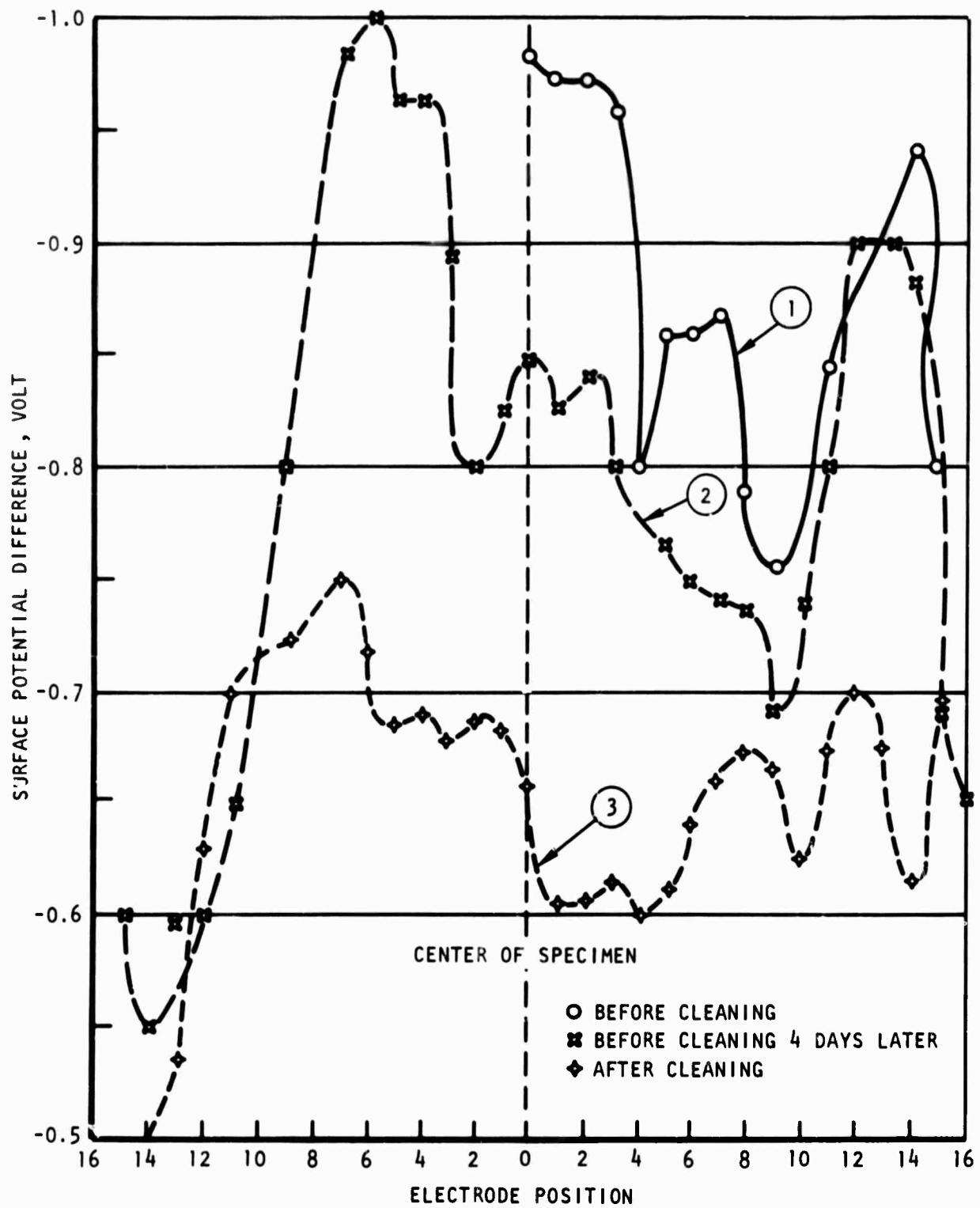


Figure 45. Variation of Surface Potential Difference Along Length of Fatigue-Stressed 7075-T6 Aluminum Alloy Specimen No. 13

TABLE X. SURFACE POTENTIAL DIFFERENCE AND ELLIPSONOMETRY DATA FOR FATIGUE-STRESSED ANNEALED D6AC STEEL

Specimen No.	Stress, psi	No. of Cycles	Surface Potential Difference, volt			Ellipsometry Data					
			One Side	Other Side	Average	One Side			Other Side		
						Phase Shift, Degree	tan ⁻¹ (Amplitude Ratio)	Phase Shift, Degree	tan ⁻¹ (Amplitude Ratio)		
16		200,000	0.22	0.22	0.22	12.57	32.62	8.65	33.15		
17		200,000	0.34	0.30	0.32	11.50	32.74	13.28	32.80		
4		215,000	0.28	0.38	0.33	12.40	32.42	11.90	32.64		
29		306,000	0.28	0.30	0.29	12.68	32.64	13.42	32.24		
22		391,000	0.50	0.26	0.28	10.94	33.56	12.85	33.03		
20	70,000	428,000	0.34	0.29	0.32	10.70	34.00	12.88	32.97		
2		502,000	0.36	0.34	0.35	12.39	32.82	12.73	32.93		
25		1,075,000				12.50	33.38	12.74	33.22		
5		1,190,000	0.27	0.20	0.24	11.84	32.67	11.90	32.98		
8		2,500,000	0.35	0.34	0.35	12.04	33.55	11.03			
27		2,500,000	0.34	0.30	0.32						
1		3,950	0.29	0.32	0.31	12.70	32.86	13.60	33.24		
3		3,950	0.22	0.23	0.23	12.34	32.82	13.16	33.27		
19		5,000	0.24	0.28	0.26	12.05	32.51	12.61	32.42		
9		9,000	0.26	0.24	0.25	12.30	32.71	11.18	32.64		
24		9,000	0.23	0.24	0.24	12.46	32.48	13.68	32.96		
26	80,000	9,000	0.36	0.46	0.41	11.69	32.86	11.95	32.75		
12		20,000	0.25	0.26	0.26	9.82	32.12	11.30	33.24		
21		20,000	0.31	0.34	0.33	11.13	30.68	13.58	33.41		
30		20,000	0.32	0.43	0.38	12.24	32.28	13.82	33.13		

Since ultraviolet light was used as a stimulator for exoelectron emission, the possible accelerated oxidation of the metal surface by ozone in air might influence the emission process. The effect of ultraviolet light on the oxide layer of 1100-0 aluminum was investigated by ellipsometry. The thickness of the oxide layer and its refractive index of a chem-milled specimen were measured to be respectively 32 Å and 2.5. After the specimen was exposed to ultraviolet light for 143 hours, both the thickness and the index were found unchanged within experimental error. It thus appears that ultraviolet light has little, if any, effect on further growth of the oxide film on 1100-0 aluminum. However, ultraviolet light affects surface potential difference by changing its value from -0.20 to +0.20 volt after 143-hour exposure which could be significant since the change is in the order of 100 percent, however the reason for the change is not known.

Section IX

CONCLUSIONS AND RECOMMENDATIONS

CONCLUSIONS

The program has successfully achieved a number of the original objectives; i.e., the theoretical and empirical establishment of the nature and extent of the metallurgical characteristics of the fatigue-affected zone on the surface of a material, the relating of the mechanical-metallurgical properties of a fatigue-damaged material with potential measurement parameters and associated test methods, the evaluation and development of several nondestructive test (NDT) methods showing direct correlations with the extent of fatigue damage, and the initial characterization studies of three test methods (exoelectron emission, ultrasonic surface wave, and acoustic emission) under laboratory conditions. Additional characterization and development efforts are needed to further advance these methods to the state of practical application to air vehicle structures under field service conditions.

Among the various physical properties that undergo change in fatigue stressing, the emission of electrons from the material and the propagation of elastic waves in the material are considered to be most potentially suitable for assessing the fatigue damage.

Electrons are emitted from a material under fatigue stressing. Emission can also occur after cessation of the deformation upon the application of a stimulant such as heat, ultraviolet energy, etc. Recent laboratory tests conducted under this program and by the University of Arizona indicate that the exoelectron emission may be characterized in terms of changes in the surface characteristics of the material and used to estimate the remaining life of the material. The measurement technique is considered to be at a rather advanced state of experimental verification, and additional effort is necessary to complete the surface characterization correlation by including the effects of vehicle fatigue loading and environment, the development of a practical in-field measurement instrument system, and evaluation of the system on actual vehicle materials and structures.

The response of material in fatigue to elastic wave propagation has been investigated by the introduction of ultrasonic surface waves to the material during or after fatigue deformation. Both the velocity and attenuation of the wave have been found to vary with the spent life of the material. The remaining safe life can thus be estimated if the whole life is known. Since fatigue damage occurs only at the surface layer, surface wave measurements at high frequencies should be used so that the depth of wave penetration is of the order of 1 wavelength.

The acoustic emission from the fatigue specimens was measured concurrently with exoelectron emission tests; the intensity of the acoustic emission, expressed in number of counts in 1,000 fatigue cycles, varied by several orders of magnitudes during the fatigue tests. A relationship was observed between the significant change in the slope of the emission curve and the percent of fatigue life. The change occurs at less than 50 percent of the fatigue life and offers a possible early fatigue damage warning.

RECOMMENDATIONS

Future efforts should be directed toward the further development of one or more of the most promising NDT methods evaluated under the current effort based on the applicability of the method to determine cumulative fatigue damage in currently used aerospace materials. The development should be directed toward a prototype system for the prediction of safe life on actual parts and structures. Consideration should be given to the further developing of an understanding of the interdependency of the testing parameters, physical conditions, and material conditions environment.

The further characterization of a metal surface can be made with an extension of the ellipsometry and surface potential difference (SPD) measurements initiated in the current study. Ellipsometry yields information about the thickness and optical constants (refractive index and absorption coefficient) of films on metals. SPD yields information concerning dielectric properties of films or contamination on the metal surface. Since these characteristics change markedly as a function of fatigue, such measurements may be used as nondestructive indicators of fatigue damage or as research tools to improve the reliability of tests more easily adaptable to field service. Instrumentation for field testing could be developed using ellipsometry and SPD once correlations between these surface sensitive properties and fatigue damage are established.

Additional specimens should be prepared from 7075 aluminum alloy, D6AC steel, and ELI grade 6Al-4V titanium alloy materials. The quantity of specimens for tensile fatigue loading should be sufficient to establish a statistically reliable confidence level in the NDT technique evaluation. Structural test specimens for NDT system evaluation should include titanium and aluminum bonded and welded structures. In addition, actual air vehicle structures should be used to finally evaluate and characterize the NDT methods.

Future NDT development effort should be concentrated on the exoelectron emission measurement method based on its potential at this time; however, the same general development consideration and effort should be applied to the ultrasonic and acoustic emission measurement methods. The NDT method development should be related to the surface characterization studies in terms of (1) further establishing the measurement mechanism, (2) defining the need for

surface preparation, and (3) the requirements for inspection periods and scanning rates. The test measurement equipment should be evaluated in terms of reliability in fatigue measurement, the ability to reliably predict remaining life, and the relative influence of external and environmental parameters. Consideration should also be given to automation of the test method and its suitability for in-the-field usage.

The continuation of complementary metallographic studies with the NDT development is essential to correlate and characterize the NDT results with the actual fatigue mechanisms and physical manifestations.

BLANK PAGE

APPENDIX I
BIBLIOGRAPHY RELATING TO EXOELECTRON EMISSION

APPLICATION OF THE METHOD OF EXOELECTRON EMISSION IN METAL SCIENCE

I. N. Bogachev, R. I. Mints, and V. S. Kortov

Metal Science and Heat Treatment, July-August 1966, pp 591-594

MATERIAL

Fe-Ni alloy, Fe-Mn alloy, and 1Kh18N8 stainless steel

SPECIMEN PREPARATION

Cleaning and etching

EXCITING CONDITION

Static pressing with a cone with a 90-degree angle on a 5-ton press

Dynamic loading by impact from a free-falling cone weighing 20 kg from a height of 0.5 m

Microimpact

Microindentation using 100 g load

Cyclic stressing

DETECTION EQUIPMENT

BFL end-window counter with mica window having minimum thickness less than 1 mg/cm^2 , operating between 2×10^{-3} and 2×10^{-5} torr

Distance between specimen and nickel grid, which is placed 0.1 mm below the counter = 2.9 mm

Voltage between grid and specimen = 4 kv

RESULT

Variation of emission intensity after static or dynamic loading with time exhibits a maximum; time to reach the peak intensity depends on the specimen material tested.

Dynamic loading produces more intense emission peak than static loading.

Emission from grain may differ from emission from grain boundary.

Emission intensity of ferrite is greater than that of austenite which in turn is greater than that of martensite or epsilon carbide.

In cyclic stressing, 1Kh18N8 steel emission intensity increases with number of cycles and then decreases as cyclic stressing continues. Shape of the emission versus time curve depends on magnitude of the stress.

EXOLECTRONIC EMISSION DURING $\gamma = \epsilon$ TRANSFORMATIONS

I. N. Bogachev, V. F. Yegolayev, V. S. Kortov, and R. I. Mints
Physics of Metals and Metallography, Vol 23, 1967, pp 100-104

MATERIAL

Fe-Mn austenite alloy

SPECIMEN PREPARATION

EXCITING CONDITION

Phase transformation ($\gamma \rightleftharpoons \epsilon$)

DETECTION EQUIPMENT

End-window counter, operating at 2×10^{-5} torr with accelerating voltage 4 kv
Electron multiplier

RESULT

In the metastable condition, phase transformation of the alloy is accompanied by electron emission.

Emission intensity depends on the amount of ϵ phase and structural changes (formation of structural imperfections such as increased probability of stacking faults, microdistortions, and block fragmentation) during phase transformation.

Emission intensity varies with number of transformation cycles, the peak occurring after three cycles; subsequent cycles of transformation stabilize the austenite and structural imperfections, which is accompanied by a reduction in emission.

ON THE THEORY OF CHEMIELECTRON EMISSION OF METALS
A. Bohun, J. Sak, and M. Pšeničková
Czechoslovakia Journal of Physics, Vol 15, 1965, pp 667-677

MATERIAL

Li, Na, K, Rb, and Cs

SPECIMEN PREPARATION

Vacuum-deposited metal layer having about 65 cm^2 reacting surface area

EXCITING CONDITION

Reaction with halogens (Cl_2 , Br_2 , I_2) or oxygen

DETECTION EQUIPMENT

Lutz-Edelman electrometer

RESULT

The highest electron emission yield is measured for the reaction of chlorine with cesium.

The yield decreases from cesium to lithium (for the same halogen) and from chlorine to iodine (for the same alkaline metal).

At the beginning of the measurement, when the metal surface is clean, the yields do not depend on the temperature between 20° and -78° C .

The yield of the reaction of the alkaline metal-oxygen system is at least five orders lower than that of the reaction of chlorine with the corresponding metal.

ELECTRON EMISSION FROM ALUMINUM AFTER LOW-TEMPERATURE DEFORMATION

R. N. Claytor and F. R. Brotzen

Journal of Applied Physics, Vol 36, 1965, pp 3549-3555

MATERIAL

99.993 percent Al

SPECIMEN PREPARATION

0.020-inch-diameter wire annealed for 2 hours at 550° C

EXCITING CONDITION

Tensile loading at -140° C to a strain 7.5 of 12 percent, then allowed to warm up (0.27° C/sec) while measurement being taken

DETECTION EQUIPMENT

Open-window Geiger-Müller counter containing 99 percent He and 1 percent methane at 0.5 atmospheric pressure

Distance between window and specimen = 5 mm

Potential between counter case and specimen = 45 v

300-watt incandescent reflector spotlight placed 18 inches from specimen

RESULT

Variation of emission rate with temperature exhibits a peak in the general temperature range (210°-230° K) same as that for the drop in electrical resistivity and the release of stored energy, suggesting that point defect migration plays an important role in emission by plastic deformation. Migration energy of the point defect involved in emission is about 0.44 ev, which coincides closely with the energies for annealing of defects introduced in aluminum by quenching from elevated temperatures and by electron bombardment.

ELECTRON EMISSION FROM ALUMINUM AFTER QUENCHING
R. N. Claytor, J. E. Gragg, and F. R. Brotzen
Journal of Applied Physics, Vol 37, 1966, pp 149-152

MATERIAL

99.993 percent Al

SPECIMEN PREPARATION

0.020-inch-diameter wire

3/4 inch square x 0.020 inch thick

EXCITING CONDITION

Heating by alternating current the wire specimen to 300°-400° C at a pressure about 100 μ m Hg in a chamber containing the Geiger-Müller counter and quenching the specimen by the counter gas to room temperature
Heating the plate specimen in a furnace to 300°-400° C at a less than 50 μ m Hg pressure and quenching the specimen in ice-brine solution.

DETECTION EQUIPMENT

Open-window Geiger-Müller counter containing 99 percent He and 1 percent methane

RESULT

Only little or no emission is observed without illumination of the specimen. Except for the initial portion, the emission decay curve for the quenched wire is almost identical to the curve for the quenched plate. Emission occurs after quenching because of the creation and diffusion of point defects toward the surface.

PHOTOEMISSION FROM METAL SURFACES MEASURED WITH GEIGER COUNTERS

M. A. Conrad and S. Levy

Nature, Vol 189, 1961, pp 887-889

MATERIAL

Commercial purity Al, Cu, Ni, Sn, and Zn

SPECIMEN PREPARATION

1 inch diameter x 1/4 inch thickness

EXCITING CONDITION

Abrasion, filing, polishing, or compression

A grating monochromator and an incandescent ribbon lamp as the light source

DETECTION EQUIPMENT

Windowless Geiger-flow counter containing 98.5 percent He and 1.5 percent isobutane

Specimen forming a part of the cathode

Distance between anode and specimen = 3/4 inch

RESULT

No detectable emission from abraded or deformed metal surfaces in complete darkness suggests that the mechanism of the Russell effect cannot be explained by the action of delayed electrons detectable in a Geiger counter. Photoelectric wavelength thresholds of the metals are in the near ultraviolet region of the light spectrum; they differ slightly for the different metals.

X-ray irradiation of metals does not induce delayed electron emission but strongly deactivates the materials with respect to photoemission.

EXOELECTRON EMISSION DURING OXYGEN CHEMISORPTION AT CLEAN NICKEL SURFACES

T. A. Delchar

Journal of Applied Physics, Vol 38, 1967, pp 2403-2404

MATERIAL

Ni

SPECIMEN PREPARATION

Evaporated film deposited on walls of a cell having a very low electrical capacity ($0.1 \mu\mu$ F)

EXCITING CONDITION

Addition of spectroscopically pure oxygen to 10^{-10} torr vacuum

DETECTION EQUIPMENT

Dc amplifier connected to the ionization gage grid in the cell

RESULT

Each oxygen addition at 77° K is accompanied by a burst of electrons with the yield about 10^{-9} electron per adsorbed molecule.
Number of electrons ejected at room temperature depends on the time allowed to elapse between oxygen additions: higher yield at increased dose interval because time is required for incorporation of oxygen in the nickel lattice which does not occur significantly at 77° K.
Oxygen chemisorption causes electron emission from nickel surfaces.

INVESTIGATION OF EXOELECTRONIC EMISSION DUE TO SLIDING FRICTION

V. D. Evdokimov

Soviet Physics - Doklady, Vol 12, 1968, pp 732-734

MATERIAL

Steel 25, steel 45, cast iron SCH-32, and aluminum

SPECIMEN PREPARATION

Specimen in the form of a ring 60 x 50 x 15 mm

EXCITING CONDITION

Specimen subject to dry one-directional or reversing friction against a bar of steel 40 with a 90.5 m/min sliding velocity under a normal load of 13.2 kg in a duration of 10 minutes.

Ultraviolet lamp OJ-18 with filter UFS-1 for steel and cast iron and with an additional BS-12 filter for aluminum

DETECTION EQUIPMENT

Open surface counter

RESULT

Emission of electrons from the metal surface after reversing friction is greater than emission after one-directional friction. The process of rubbing reduces the work of electron escape by locally increasing the lattice energy. Reversing friction, by increasing the surface of metal and the number of its various defects, should reduce the work function to a greater degree than does one-directional friction. Hence, exoemission after reversing friction is more intense than after one-directional friction.

Both emission decay curves for aluminum conform to hyperbolic law and show a sharp fall of the emission with time.

Emission of electrons for steel 25 also decreases with time.

Exoemission for steel 45 and cast iron increases initially and latter decreases steeply with time.

The tendency for inflections on the decay curve to appear increasing with decreasing plasticity of the material.

Chemisorption of oxygen and the influence of the oxide film on the work function play a significant role in shaping the decay curve.

INVESTIGATION OF EXOELECTRONIC EMISSION OF SURFACE
LAYERS DURING SLIDING FRICTION

V. D. Evdokimov

Soviet Physics - Doklady, Vol 13, 1968, pp 475-477

MATERIAL

Steel 25 and steel 45

SPECIMEN PREPARATION

Flat specimen (20 x 20 x 50 mm) and annular specimen (60 x 50 x 15 mm)

EXCITING CONDITION

Sliding friction at various normal loads but with a constant sliding rate
of 90.5 m/min

Ultraviolet light

DETECTION EQUIPMENT

Open-type transducer

RESULT

The intensity of exoelectron emission during sliding friction increases
steadily with time, reaching a stabilized state in a few minutes.

The intensity increases with increase of normal load at the start of friction,
but later it slows down and finally it even diminishes.

Under a steady-state sliding condition, the least load corresponds to the
highest exoelectron emission.

There is a relationship between exoelectron emission and microhardness: the
higher the microhardness, the higher the intensity of emission.

Variation of exoelectron emission and microhardness with normal load and time
is attributed to the formation of structural defects in the surface layers
of metals during friction. In the course of plastic deformation, the
generation of dislocation gradually diminishes and steady state sets in.
Both working hardening and relaxation occur simultaneously in this state.
Further increase in the normal load raises the temperature of the friction
surface, thus intensifying relaxation and reducing work hardening and the
density of defects in the deformed lattice, giving a corresponding
reduction in the level of exoelectron emission as well as the microhardness.

AUTOR DIOGRAPHY OF FATIGUE FRACTURE IN ALUMINUM
J. C. Grosskreutz
Journal of Applied Physics, Vol 33, 1962, pp 2653-2654

MATERIAL

99.99 percent Al

SPECIMEN PREPARATION

EXCITING CONDITION

Push-pull fatigue loading at constant strain (± 0.002) for 50,000 cycles
(approximately 10 percent of expected life)

DETECTION EQUIPMENT

Stripping emulsion on specimen surface and 18-hour exposure time in total
darkness

RESULT

Photographic image is a faithful replica of the slip band and crack structure
induced by fatigue loading.

THE EMISSION OF EXOELECTRONS FROM ALUMINUM DURING FATIGUE

J. C. Grosskreutz and D. K. Benson

NASA CR-57918, 1963

MATERIAL

Pure Al and 2S alloy

SPECIMEN PREPARATION

EXCITING CONDITION

Constant stress fatigue loading at 400 cps and a pressure of $2-5 \times 10^{-5}$ torr
in complete darkness

Unidirectional tensile straining at 10^{-6} to 10^{-9} torr

DETECTION EQUIPMENT

Snooper-scope image converter tube

AR.10 stripping emulsion, Kodak SWR vacuum ultraviolet film, and Tri-X
film placed over zinc sulphide phosphor

14-stage electron multiplier having a current gain about 10^6

RESULT

There is no detectable image using AR.10 stripping emulsion and Kodak SWR
film after fatiguing 3.5×10^6 cycles and between 10^5 and 2×10^6 cycles,
respectively; negative result is also obtained from Tri-X film with zinc
sulphide phosphor.

When the electron multiplier is used, emission is observed 5 minutes after
start of the fatigue test; the emission rate varies widely with increasing
number of cycles but tends to rise near end of the test (about 4.36×10^5
cycles in 18 minutes) due to formation of macrocracks; failure of the
specimen occurs after 8×10^5 cycles.

No emission from aluminum with oxide coating subject to unidirectional
tensile straining at 10^{-6} or 10^{-9} torr even when the specimen is
illuminated during test; emission rate after 10 percent strain is about
 10^2 electrons/cm²-sec, a very low figure.

UNTERSUCHUNGEN ÜBER DIE EXOELEKTRONEN-EMISSION MECHANISCH BEANSPRUCHTER METALLE

M. Hempel, A. Kochendörfer, and A. Tietze

Archiv für das Eisenhüttenwesen, Vol 35, 1964, pp 465-474

MATERIAL

99.989 percent Al and 0.09 percent C steel

SPECIMEN PREPARATION

Al specimens: 7 mm thick, annealed in air for 1/2 hour at 350° C

Steel specimens: 15 mm thick, annealed in vacuum (10^{-2} torr) for 1/2 hour at 930° C

Electropolishing before test

EXCITING CONDITION

Tensile-tensile fatigue loading with lower stress at 0.5 kg/mm^2

Static tensile loading to 4 kg/mm^2 corresponding at 5.25 percent strain

Illuminated with unfiltered incandescent lamp at 250, 275, or 300 ma with wavelengths longer than $0.33 \mu\text{m}$ but shorter than $0.5 \mu\text{m}$

DETECTION EQUIPMENT

17-stage electron multiplier operating at 10^{-4} torr

Distance between specimen and multiplier end facing first dynode = 2 cm

RESULT

For Al:

Emission intensity reaches a plateau in $0.5\text{-}5.1 \text{ kg/mm}^2$ fatigue loading 10 to 15 minutes after start of test (test duration = 35 minutes) and decreases after test but is still way above the background level in 1 hour.

Emission intensity increases with increase of fatigue stress range but the intensity is more or less independent of stress range in the first 1.3×10^5 cycles; no emission is observed at a stress range of 2 kg/mm^2 .

Emission starts after static loading to 1.25 percent strain with illumination using 275 or 300 ma, but the emission intensity at 300 ma is much greater than that at 275 ma.

Little emission is observed in the absence of illumination even at 10 percent strain in static loading.

Emission in static loading starts at a stress of 2 kg/mm^2 , increases rapidly until end of the test at 4 kg/mm^2 , and decreases slowly thereafter.

Surface treatment affects the rate of emission: Emission rate of electropolished specimen is greater than the rate of electropolished and anodized (in 0.1 N NaOH) specimen which in turn is greater than the rate of electropolished and heated (350° C in air for 1/2 hour or 500° C in vacuum for 1/2 hour) specimen.

Emission intensity increases with increase of temperature (18 to 100° C).

For steel:

No emission intensity above the background level is observed in both fatigue test and tensile test using illumination with wavelengths longer than $0.33 \mu\text{m}$, regardless of different heat treatments.

EXOLECTRONIC EMISSION AS A METHOD OF STUDYING THE DEFORMED SURFACE
OF METALS

V. S. Kortov and R. I. Mints

Physics of Metals and Metallography, Vol 19, 1965, pp 72-76

MATERIAL

Al, 1Kh18N8 steel, and bronze

SPECIMEN PREPARATION

Cleaning and etching

EXCITING CONDITION

Abrading Al surface with emery paper

Hydraulic shock for 40 minutes on steel

Diamond pyramid (200 g load) indentation on bronze

DETECTION EQUIPMENT

BFL end-window counter with mica window having minimum thickness not less than
1 mg/cm², operating between 2×10^{-3} and 2×10^{-5} torr

Distance between specimen and Ni grid, which is placed 0.1 mm below the
counter, = 2.9 mm

Voltage between grid and specimen = 4 kv

RESULT

Emission intensity of Al increases with increase of accelerating voltage
between grid and specimen.

Emission curve for 1Kh18N8 steel exhibits a maximum, but no such peak is
observed in the curve for bronze.

Emission intensity of ferrite is greater than the intensity of austenite
which in turn is greater than that of martensite.

ELECTRON EMISSION DURING METAL FATIGUE

R. S. Krogstad and R. W. Moss

Proceedings of the Symposium on Physics and Nondestructive Testing
September 28-30, 1965, Dayton, Ohio, pp 9-21

MATERIAL

Al, Au, Fe, Ni, and Ti

SPECIMEN PREPARATION

Electropolish

EXCITING CONDITION

Torsional fatigue

DETECTION EQUIPMENT

Phosphor film deposited on transparent stannous oxide conducting film, which is lined over the inner surface of a glass cylinder containing the specimen
13-stage photomultiplier

RESULT

Except for Al, emission from other metals tested starts after a few hundred cycles, followed by a series of emission events.

Frequency with which the emission events occur increases to a maximum (at about one-third of fatigue life) and then decreases slowly until specimen fails.

Duration of an emission event (less than 5×10^{-6} sec) is several orders of magnitude too short to ascribe to chemisorption.

The observed emission from gold which has no stable oxide coating is incompatible with the concept of emission by thermal dissociation of deformation-induced electron levels.

Since a large number of electrons (about 10^4) are involved in emission, it is difficult to assume vacancy annihilation as the mechanism of electron ejection from metal surface.

Tentative mechanism of emission: Energy associated with the stress fields around dislocations in the slip process. Emission occurs if this energy exceeds work function, and it is also transferred to an electron.

Based on this mechanism, calculation shows that there is no emission from Al.

EXOEMISSION FROM GROUND SURFACES OF GERMANIUM AND SILICON
V. I. Kryuk, R. I. Mints, and V. S. Kortov
Soviet Physics - Solid State, Vol 8, 1966, pp 1295-1296

MATERIAL

Single-crystal Ge, single-crystal Si, and polycrystalline Si

SPECIMEN PREPARATION

Area of etched specimen = 3.5 cm^2

EXCITING CONDITION

Grinding with emery cloth for 1 minute

Soft ultraviolet light which does not cause photoelectric emission

DETECTION EQUIPMENT

Electron multiplier operating at 10^{-5} torr and 3.2 kv

RESULTS

No emission is observed from undeformed metal surfaces.

Emission intensity varies with accelerating voltage and wavelength of the illumination, but nature of the decay curve remains practically the same.

Ge shows more intense and more rapid emission decay than Si.

Kinetic characteristics of emission are closely associated with the diffusion of vacancies to the surface; the lower mobility of vacancies in Si is indicated by the activation energy Q for self-diffusion in Si and Ge, which proceeds by a vacancy mechanism ($Q = 86\text{-}100 \text{ kcal/mol}$ and 54 kcal/mol for Si and Ge, respectively).

EFFECT OF TEMPERATURE ON THE EMISSION OF ELECTRONS FROM
ABRADED SURFACES OF BERYLLIUM, CALCIUM, ALUMINUM,
AND MAGNESIUM

T. C. Ku and W. T. Pimbley

Journal of Applied Physics, Vol 32, 1961, pp 124-125

MATERIAL

Al, Be, Ca, and Mg

SPECIMEN PREPARATION

EXCITING CONDITION

Abrading and then placed in counter

Abrading, placed in counter to start counting, and then withdrawing from counter to store in liquid nitrogen for 2,260 seconds before placing back into counter

Abrading, placed in counter to start counting, and then withdrawing from counter to store at 550° C for 120 seconds before placing back into counter

White light or zirconium arc lamp as the light source

DETECTION EQUIPMENT

Open-window Geiger-Müller counter containing 98.7 percent He and 1.3 percent butane

Specimen at a negative potential of 50 v with respect to the grid at aperture of the counter

RESULT

Under identical experimental conditions, the rate of emission from Be is approximately one-third the rate from Al, and the rate of emission from Ca is about twice that from Al.

There is no measurable emission when the light is shut off.

Emission rate decreases or increases respectively with decrease or increase of temperature.

Emission is thought to be influenced by diffusion of vacancy so that the condition of emission is that the sum of potential energy released by vacancy and photon energy is equal to or greater than photoelectric work function.

EXOELECTRON EMISSION DUE TO ULTRASONIC IRRADIATION
J. A. M. Langenecker and D. B. Ray
Journal of Applied Physics, Vol 35, 1964, pp 2586-2588

MATERIAL

99.999 percent Al, 2024 and 6061 Al alloys

SPECIMEN PREPARATION

12 mm diameter specimen annealed for 4 hours at 450° C and oven-cooled under inert atmosphere (96 percent N and 4 percent H)
Standard cleaning, no effort to restrict oxide formation

EXCITING CONDITION

Filing, abrading with steel brush (2 seconds) or carborundum paper
Ultrasonic irradiation using transducer with intensity 0-100 W/cm² and frequency 20 KHz

DETECTION EQUIPMENT

Windowless flow counter containing 98.5 percent He, 1 percent isobutane and 0.5 percent butadiene

RESULT

Abrading with steel brush yields good reproducibility
Ultrasound causes increase in emission rate for 6061 Al alloy; the higher the ultrasound intensity (20-45 W/cm²), the higher is the emission rate
Without light stimulation, emission from pure Al is at the background level; a very small increase of emission is observed during the application of ultrasound (intensity not greater than 45 W/cm²). 2024 Al alloy shows no emission intensity above the background level.
6061 Al alloy has to be heated to 320° K to produce the same emission intensity as produced at 297° K with the application of ultrasound of 45 W/cm² intensity.

EFFECT OF TEMPERATURE AND AIR HUMIDITY ON THE PHOTOSTIMULATED
EXOELECTRON EMISSION FROM OXIDE FILMS ON ALUMINUM

T. Lewowski

Journal of Applied Physics, Vol 33, 1962, pp 2393-2394

MATERIAL

Al

SPECIMEN PREPARATION

EXCITING CONDITION

Abrading

(6 v, 20 w) tungsten bulb

DETECTION EQUIPMENT

Open Geiger counter operating at atmospheric pressure

Both counter and specimen in a closed chamber

RESULT

Emission intensity is maximum while the temperature of the abraded specimen is increased to about 400° C.

If the specimen at 400° C falls rapidly to room temperature, the emission intensity decreases, passes through a minimum, afterwards a maximum, and decays again.

The rate of this decay varies with air humidity; it is much faster in the moist than in the dry atmosphere.

Emission is associated with the presence of an oxide layer. Because of the very higroscopic properties of alumina, the electrical character of the oxide layer might be changed with the humidity of air.

DIE ELEKTRONENEMISSION BEARBEITETER METALLOBERFLÄCHEN

J. Lohff

Die Naturwissenschaften, Vol 44, 1957, pp 228

MATERIAL

Al

SPECIMEN PREPARATION

EXCITING CONDITION

Abrading with steel brush at 5×10^{-4} torr oxygen pressure

DETECTION EQUIPMENT

Electron multiplier

RESULT

When the system is suddenly evacuated after the emission decay proceeds for a period, the emission drops rapidly. Later when the original oxygen pressure is restored, the emission rises to a level substantially lower than the level at the time of evacuation.

The processes, such as changes of defect structure in the oxide layer and the metal, taking place in the specimen during evacuation are thought to affect the subsequent emission rate.

DIE ELEKTRONENEMISSION BEI DER OXYDATION MECHANISCH
BEARBEITETER METALLOBERFLÄCHEN

J. Lohff

Zeitschrift für Physik, Vol 146, 1956, pp 436-446

MATERIAL

Ag, Al, Au, Be, Cu, Fe, Mg, Pb, Pt, and Zn

SPECIMEN PREPARATION

EXCITING CONDITION

Abrading with steel brush at 22° C in oxygen pressure of 1×10^{-4} to 7×10^{-6} torr

DETECTION EQUIPMENT

Electron multiplier

RESULT

In the case of abraded Al, emission intensity at oxygen pressure of 10^{-4} torr is much greater than that at oxygen pressure of 7×10^{-6} torr.

Emission current from abraded Be, Mg, Pb, and Zn also depends on oxygen pressure.

Less than 2 electrons/cm²-sec emit from Ag, Au, Cu, Fe, and Pt at 10^{-5} and 5×10^{-4} torr 10 seconds after abrading.

In the case of abraded Zn, the emission reaches a maximum at various pressures before decay sets in; the higher the oxygen pressure, the higher is the emission peak and the shorter is the time to reach that peak.

Emission intensity of Zn at 22° C is greater than that at 100° C at various pressures; the same trend is noted for Al and Pb.

DIE ELEKTRONENEMISSION BEI DER PLASTISCHEN VERFORMUNG
VON ZINKKRISTALLEN

J. Lohff

Zeitschrift für Physik, Vol 145, 1956, pp 504-507

MATERIAL

99.9 percent Zn

SPECIMEN PREPARATION

3-3.5 mm diameter single crystal

EXCITING CONDITION

Tensile loading to maximum elongation 50 percent of original length at
 2×10^{-5} torr or at oxygen pressure 10^{-4} torr

DETECTION EQUIPMENT

Electron multiplier

RESULTS

Emission rate at 2×10^{-5} torr increases with increase of strain; under steady straining, emission rate increases and then decreases with time. There is practically no difference in emission for a given amount of straining (0.5 percent) at 2×10^{-5} torr or oxygen pressure 10^{-4} torr, suggesting that emission by tensile straining is independent of oxygen.

DIE ENERGIEVERTEILUNG DER ELEKTRONENEMISSION MECHANISCH
BEARBEITETER METALLOBERFLÄCHEN

J. Lohff

Zeitschrift für Naturforschung, Vol 12a, 1957, pp 267-268

MATERIAL

Al, Li, Mg, and Zn

SPECIMEN PREPARATION

Specimen surface area = 0.4 cm^2

EXCITING CONDITION

Abrading with steel brush at $1-5 \times 10^{-4}$ torr oxygen pressure or $5-7 \times 10^{-6}$ torr residual gas pressure

DETECTION EQUIPMENT

Electron multiplier

RESULT

The average energy of exoelectron emission is determined by the number of electrons per second versus grid potential curve. The average energy of emission for Al and Zn is independent of oxygen pressure and is 0.20 and 0.15 ev, respectively.

The average energy of emission for Li and Mg is slightly dependent upon pressure, but the value is in the neighborhood of 0.2 ev.

A POSSIBLE ORIGIN OF EXOELECTRON EMISSION IN PLASTICALLY DEFORMED METALS

A. H. Meleka and W. Barr

Nature, Vol 187, 1960, pp 232-233

MATERIAL

High purity Zn

SPECIMEN PREPARATION

Single crystal rod

Electropolished and thoroughly cleaned

EXCITING CONDITION

Static tensile straining

DETECTION EQUIPMENT

Kodak AR 10 stripping emulsion

Exposure time = 1 hour if commencing exposure within a few minutes of straining

RESULT

Black lines on emulsion correspond exactly to slip lines on the crystal surface.

Rows of individual spots resemble dislocation etch pits along slip lines.

It is suggested that the centers of emission are the points where dislocations terminate at the surface of the crystal.

THE TIME REQUIRED TO REACH MAXIMUM ELECTRON EMISSION FROM DEFORMED METALS

R. I. Mints and V. S. Kortov

Russian Metallurgy and Fuels (Mining), No. 2, 1967, pp 90-96

MATERIAL

High purity (99.93 percent) Al, Au, and Cu; Fe-Ni alloy; Fe-Mn alloy; and 1Kh18N8 stainless steel

SPECIMEN PREPARATION

Annealing, grinding, and electropolishing

EXCITING CONDITION

Grinding

Local static loading with a diamond pyramid using 100 g load

Microimpact loading

Cyclic loading

DETECTION EQUIPMENT

Electron multiplier

RESULT

Admission of air into the apparatus changes pressure from 2×10^{-5} to 2×10^{-4} torr, but emission current from ground Au and 1Kh18N8 steel is affected very little.

When air is admitted into the apparatus containing ground Al or Cu, a jump in emission current is noted, the effect on Al being more pronounced.

Emission from ground metal surface is therefore not entirely due to oxidation.

Admission of air during emission decay from locally indented Al surface has no effect on fall of emission, indicating that emission depends on size of the deformed area. This is also true of surfaces deformed by microimpact loading.

For equal amount of microimpact deformation, the time to reach peak emission for Fe-Mn alloy is longer than that for Fe-Ni alloy because high defect mobility in the latter leads to a shorter rise time.

Emission current depends on mobility of vacancy; vacancy mobility for Al is greater than that for Au, so the time reaching peak emission for micro-impacted Al surface is shorter than that for the similarly deformed Au surface.

Increase of amount of microimpact deformation generally increases the time reaching peak emission because increasing degree of hardening of surface decreases defect mobility.

During cyclic loading, Al emission intensity increases with number of cycles until microcracks develop. At the moment of microcrack formation, vacancies on the surface flow into the submicrocracks, leading to a decrease in electron emission. Further deformation produces fatigue cracks with a sharp increase in the number of vacancies, which are not dissipated, so there is an increase in electron emission directly prior to fracture.

EXOLECTRONIC EMISSION FROM AUSTENITIC STEELS
UNDER ALTERNATING CYCLES OF STRESS

R. I. Mints, V. S. Kortov, V. L. Aleksandrov and V. I. Kryuk
Physics of Metals and Metallography, Vol 26, 1968, pp 681-687

MATERIAL

Austenitic steels 30Kh10G10, 68Kh7N7, 1Kh18AG10, and 1Kh18N8

SPECIMEN PREPARATION

Specimen dimensions: 2 x 5 x 100 mm
Electropolishing in sulphophosphochromic bath

EXCITING CONDITION

Symmetrical bending fatigue at a frequency of 50 cycles/sec

DETECTION EQUIPMENT

Cu-Be electron multiplier operating at 2×10^{-5} torr
Accelerating potential on specimen = -300 v

RESULT

The emission intensity rises with increasing number of cycles, the biggest change in intensity occurring before the elapse of 10^5 cycles. Afterwards, the emission current grows more slowly. There is a tendency to saturation or even reduction at large number of cycles.

The kinetics of exoelectron emission is largely controlled by the applied stress level. The emission rate increases rapidly and its maximum level rises as the stress increases.

The shape of emission curve is explained on the basis of the hypothesis that its intensity is controlled by the number of defects contained in the surface layer of metal and its kinetics by their mobility.

Under the same conditions of stress, alloys 30Kh10G10 and 68Kh7N7, which undergo the greatest strengthening by fatigue deformation, have less emission than alloys 1Kh18N8 and 1Kh18AG10. The considerable strengthening of the former, which is due to phase and structure transformations, has the effect of pinning the defects generated, restricting the total number of active emission centers at the surface, and reducing their size.

There is an interrelation between the dissipation of mechanical energy and exoelectron emission. The internal friction of 35KhGF steel in temper-embrittled state is higher than in ductile state, and the emission intensity in fatigue process for the temper-embrittled state is correspondingly lower.

Exoelectron emission can be regarded as an electrical effect which is the result of the storing of deformation energy. Large dissipation of energy, indicated by internal friction measurement, reduces the fraction of stored energy and lowers the intensity of emission.

EXO-ELECTRON EMISSION FROM A MECHANICALLY TREATED SILICON SURFACE

R. I. Mints, V. S. Kortov, V. I. Kryuk, A. I. Tatarenkov, and I. A. Petrushkova
Soviet Physics - Semiconductors, Vol 1, 1968, pp 1535-1537

MATERIAL

n-type and p-type Si single crystals

SPECIMEN PREPARATION

30 mm diameter x 0.3 mm thickness cut along (111) plane

Washing specimen in acetone and alcohol after grinding

Exposing ground and washed specimens in air at room temperature for 1 month

EXCITING CONDITION

Grinding with green SiC powder or white electrocorundum which was elutriated in distilled water

Grinding with the same abrasive powders as above and additionally treating the specimens with SAM3 and SAM1 powders deposited on a cloth

Electric current pulse (150 v for 100 μ sec) as the stimulating agent

Negative potential at the specimen surface

DETECTION EQUIPMENT

Electron multiplier at 2×10^{-5} torr

Accelerating potential at the grid above the specimen = 250 v

RESULT

No emission occurs at room temperature or 250° C if no current passes through the specimen.

With excitation by current pulse, emission from the surface of p-type Si is roughly two orders of magnitude weaker than emission from n-type Si at room temperature.

All the n-type Si specimens after decay of emission exhibit exoemission peaks when the temperature is increased; the nature of the exoemission depends on the method of surface treatment with various abrasive powders.

Emission is observed if a specimen is excited with a current pulse before it is heated again.

However, the thermally stimulated emission after the passage of a current pulse is not observed when the direction of the exciting current is reversed in the case of n-type Si, for any polarity of the exciting voltage in p-type Si, and in specimens in which the surface layer disturbed by grinding with abrasive powders is removed by etching.

EXOEMISSION FROM ABRADED AND ETCHED ALUMINUM
R. K. Mueller and K. Pontinen
Journal of Applied Physics, Vol 35, 1964, pp 1500-1502

MATERIAL

99.4 percent Al and 2024 Al alloy

SPECIMEN PREPARATION

Annealing

Etched for several minutes in 1 percent HF and carefully washed and dried

EXCITING CONDITION

Abrading with No. 600 emery paper

Successive removal of surface layers by etching with 1/2 or 1 percent HF

Illumination with a fluorescent lamp

DETECTION EQUIPMENT

Geiger-Müller counter containing 93 percent argon and 7 percent ethyl alcohol,
operating at 100 torr and 850 v

Specimen at -6 v with respect to the grounded tube cathode

RESULT

Both Al and 2024 alloy yield similar result, suggesting that impurities have no effect on emission.

A 1-second etch in 1 percent HF is sufficient to recover 90 percent of original emission activity.

Compared with a freshly abraded specimen, an abraded specimen oxidized in air for 6 days exhibits a wider maximum of recovered activity, probably due to the added etching time necessary to break up and remove the oxide layer.

Pattern of emission decay with total time of etch for a freshly abraded specimen is similar to that for an abraded specimen after it is stored 8 days in the counter gas mixture.

Emission from a freshly abraded specimen and an abraded specimen stored in air for several days and then etched for 4 seconds in 1 percent HF decays with the same time constant.

Since aging does not affect significantly decay, it is unlikely that the transport of imperfections to the active surface is of importance for emission.

EFFECTS OF TEMPERATURE ON THE EXOEMISSION OF ELECTRONS
FROM ABRADED ALUMINUM SURFACES
W. T. Pimbley and E. E. Francis
Journal of Applied Physics, Vol 32, 1961, pp 1729-1733

MATERIAL

99.999 percent Al

SPECIMEN PREPARATION

26 gage thick

Standard cleaning technique without effort to restrict oxide formation

EXCITING CONDITION

Abrasion by four to five passes using 400 or 600 grade SiC paper
Zirconium arc source for illumination at low excitation or at lower temperature (temperature range = 9.9 to 44.4° C)

DETECTION EQUIPMENT

Windowless, open-end Geiger counter containing 98.7 percent He and 1.3 percent butane

Specimen at a negative potential of 50 v

RESULT

No count above the background count can be obtained from the abraded paper itself nor from the freshly clean, unabraded specimen.

The emission decay curve is composed of two exponential decays according to the expression $I = A \exp(-k_1 t) + B \exp(-k_2 t)$ where I is the emission intensity, t is the time, k_1 and k_2 are decay constants, and A and B are temperature-dependent constants.

The decay constant is related to the temperature according to $k = F \cdot \exp(-E/RT)$ where E , R , T , and F are the activation energy, the universal gas constant, the absolute temperature, and constant, respectively. Both the first and second decay constants have the same activation energy (about 5.6 kcal/mol). Vacancies are created by abrasion; emission depends on diffusion of vacancies in metal; emission intensity increases with increase of temperature because of increasing diffusion constant.

EXOELECTRON EMISSION FROM ABRADED METAL SURFACES
AT HIGH AND ULTRAHIGH VACUUMS

J. A. Ramsay

Journal of Applied Physics, Vol 37, 1966, pp 452-453

MATERIAL

Spectroscopically pure Al and pure Zn

SPECIMEN PREPARATION

EXCITING CONDITION

Abrading with stainless steel brush in vacuo (10^{-6} to 10^{-9} torr) for
2-3 seconds

Lamp

DETECTION EQUIPMENT

Be-Cu particle multiplier and electrometer

RESULT

There is a slight decrease in the intensity of peak emission at lower pressure ($0.7 - 50 \times 10^{-6}$ torr); maximum emission current = 10^{-15} amp. No emission is detected at 10^{-8} torr; subsequent increase of electrometer sensitivity and switching on and off of illumination yield a current about 2.5×10^{-18} amp.

At 2.7×10^{-9} torr, emission current is about 0.3 to 0.5×10^{-18} amp. Time reaching the emission peak is 10^3 to $10^4 \times 10^{-18}$ times greater than the time required to form a monolayer on clean metal surface in the case of Zn and is 10 to 100 times greater in the case of Al.

THE EMISSION OF ELECTRONS FROM ALUMINUM ABRADED IN ATMOSPHERES
OF AIR, OXYGEN, NITROGEN, AND WATER VAPOR

J. A. Ramsey

Surface Science, Vol 8, 1967, pp 313-322

MATERIAL

Pure Al

SPECIMEN PREPARATION

EXCITING CONDITION

Abrading with stainless steel brush in air, spectroscopically pure oxygen, spectroscopically pure nitrogen, and water vapor bled at pressure from 10^{-5} to 10^{-8} torr into a bakeable glass ultrahigh vacuum system. Illumination wavelength longer than 3450 Å.

DETECTION EQUIPMENT

Be-Cu particle multiplier and electrometer
Phillip 56002 omegatron for gas analysis

RESULT

Emission is negligible below 10^{-8} torr.

Exposure to air pressure 10^{-5} to 10^{-8} torr: t_{in} (incubation time) increases with decrease of pressure, t_m (time to peak emission) increases with decrease of pressure, and i_m (emission current peak) decreases with decrease of pressure.

Exposure to oxygen pressure 10^{-4} to 10^{-8} torr: Change of t_{in} is similar to that for the exposure to air; change of t_m is about one-fourth of that for the exposure to air; i_m is comparatively independent of pressure and is lower than i_m in air.

Exposure to nitrogen pressure 10^{-5} to 10^{-8} torr: Changes of t_{in} and t_m are longer than those for exposure to air and oxygen; i_m is comparable with i_m for exposure in oxygen.

Exposure to water vapor 10^{-5} to 10^{-8} torr: The initial stage of emission current vs time curve at 4×10^{-6} and 3×10^{-7} torr is comparable respectively to the initial stage of the same curve at 10^{-5} and 10^{-6} torr in air.

Time at onset of emission decay in water vapor becomes shorter when oxygen is admitted to the apparatus; the higher the pressure of admitted oxygen, the shorter is the time at onset of emission decay.

Initial growth stage of emission is thus due to the adsorption of water vapor; the subsequent decay is associated with the establishment of an oxide film.

SENSITIZED PHOTOELECTRIC EMISSION DURING OXIDATION OF ALUMINUM

J. A. Ramsey and G. F. J. Garlick

British Journal of Applied Physics, Vol 15, 1964, pp 1353-1360

MATERIAL

Pure Al and pure Zn

SPECIMEN PREPARATION

1 cm diameter

Degreasing before test

EXCITING CONDITION

Abrading with stainless steel brush at one atmosphere and 0.28×10^{-3} to 10^{-5} torr and at a temperature range from 195° to 500° K
Visible ultraviolet light (wavelength = 3000-4000 Å)

DETECTION EQUIPMENT

Ag-Mg electron multiplier

RESULT

For Al:

Abrasion at room temperature and below and emission at 0.28×10^{-3} and 10^{-5} torr: At 195° K and below, the emission rises rapidly after abrasion but quickly reaches a peak which is followed by a rapid decay; the maximum emission is always much smaller than that at room temperature and is inhibited by some thermal activation barrier; rate of emission at 195° K is very little dependent on pressure between 10^{-3} and 10^{-5} torr.
Abrasion between 343° and 473° K at 0.28×10^{-3} and 10^{-5} torr: The plateau reached after initial rise of emission is prolonged especially at low pressures. Decay is more prominent as the pressure is increased; at higher temperatures, the initial rise is much slower but is markedly pressure dependent.

For Zn:

The pattern of behavior is similar to that of Al, but the effects characteristic of elevated temperatures in Al are observed at room temperature for Zn.

A tentative mode suggests that oxygen vacancies of interstitial metal atoms in the developing metal oxide layer provide electron levels above the Fermi level of the metal, from which they are ejected by photon absorption.

ELEKTRONENNACHEMISSION UND PHOTOEMISSION VON ALUMINIUMBERFLÄCHEN

A. Scharmann and G. Seibert

Zeitschrift für Physik, Vol 183, 1965, pp 249-364

MATERIAL

Al

SPECIMEN PREPARATION

EXCITING CONDITION

Milling

5×10^{11} Sr-90 β particles

X-ray (10^{-5} R, 29 kv)

Electron bombardment (10^{15} electrons with 3.5 to 4 keV/ 5 mm^2)

Mercury vapor lamp

DETECTION EQUIPMENT

17-stage electron multiplier operating at 10^{-9} torr

RESULT

There is no emission from milled Al surface at 8×10^{-9} torr in darkness even if the surface is further bombarded by electrons; there is also no emission in darkness when the Al surface is irradiated with X-ray or intense ultraviolet light from a mercury vapor lamp.

A weak emission in darkness is observed from milled Al surface at 10^{-5} torr. Upon heating, emission peaks occur at 10^{-5} torr in definite temperature ranges whether the Al surface is milled, irradiated by β particles or X-ray, or bombarded by electrons; either visible light or ultraviolet light has no effect on thermoemission.

There is emission from milled Al surface at 10^{-9} torr when it is illuminated by light having 3540 Å wavelength; the emission increases with time, probably attributable to gradual adsorption of gas, which through the creation of a dipole layer, lowers the work function of Al.

Emission, however, decays with time at 10^{-5} torr; emission intensity of milled Al surface decreases with storage time in darkness at 10^{-5} torr; presence or absence of light has no effect on decay of emission.

EXOEMISSION OF ELECTRONS WITHOUT PHOTOSTIMULATION

C. Simoi, I. Hrianca, and P. Crăciun

Physica Status Solidi, Vol 29, 1968, pp 761-766

MATERIAL

Al

SPECIMEN PREPARATION

Specimen dimension: $3 \times 2 \text{ cm}^2$

EXCITING CONDITION

Scratching by brush for 30 seconds

Emission under daylight without photostimulation

DETECTION EQUIPMENT

Windowless Geiger-Müller counter filled with argon and butane

Distance between counter and specimen = 1.5 cm

Specimen potential = -250 v

RESULT

After repeated scratching and counting operations on the same specimen, the initial number of counts decreases from 1,370 to 23 electrons per second. The decay curve is composed of three distinct exponentials:

$$\frac{dN}{dt} = A_1 \exp(-\lambda_1 t) + A_2 \exp(-\lambda_2 t) + A_3 \exp(-\lambda_3 t)$$

where N is number of counts per second, t is second, A_1 , A_2 , and A_3 are the components of initial counts, and λ_1 , λ_2 , and λ_3 are decay constants of the components. λ_i may also be the probability for the emission of an electron per unit time at a local condition specific for component i . This probability is related to the energy E_i at the mentioned conditions by the equation $\lambda_i = C \exp(-E_i/kT)$ where k is Boltzmann constant, T is the absolute temperature, and C is a constant.

Impurities and defects in the lattice of metals produce relatively high local energy levels having a reduced work of function of electrons. There is a probability of emission due to internal excitation in the absence of photostimulation.

ELECTRON EMISSION FROM PLASTICALLY STRAINED ALUMINUM
W. D. von Voss and F. R. Brotzen
Journal of Applied Physics, Vol 30, 1959, pp 1639-1645

MATERIAL

99.993 percent Al and 1100-0 Al Alloy

SPECIMEN PREPARATION

16 x 2 x 0.063 inches

Annealing in air at 400° C for 2 hours

EXCITING CONDITION

Continuous tensile loading at 0.063, 0.10, and 0.159 in./min and irradiation with natural light

Tensile loading in steps (loading rate = 0.032 in./min), allowing about 10^3 sec between steps for the decay of emission and irradiation with mercury vapor lamp (with filter to eliminate wavelengths shorter than 3,000 Å)

DETECTION EQUIPMENT

Geiger-Müller flow counter containing 1 percent methane and 99 percent He and operating at about 900 v

RESULT

There is only little emission, difficult to detect above the background level, if the specimen is strained in complete darkness.

Emission starts at about 2 percent strain and increases with further straining; emission rate is higher at higher loading rate.

Emission behavior of pure Al (99.993 percent purity) is about the same as that of 1100-0 Al Alloy.

After plastic straining has stopped, the emission may continue to rise for a while before it begins to decay. This effect may be due to the draining of vacancies from the interior to the metal surface.

Emission rate at end of straining in each step (2 percent strain per step except the first step at 7 percent strain) is higher than that at end of the preceding step. This indicates that the state of deformation strongly affects the emission.

AN INVESTIGATION OF EXOELECTRON EMISSION FROM VARIOUS MATERIALS
USING ABRASION AND ULTRASONIC TECHNIQUES

R. A. Williams

RM 630.328-04, Naval Ordnance Systems, Navy Department, 1966

MATERIAL

6061 Al alloy, brass, Cu, stainless steel, cold rolled steel, Nb, Ni, and Pb

SPECIMEN PREPARATION

1-inch-diameter bar having plane cross-sectional surface or cross-hatched,
cross-sectional surface (ratio of plane area to cross hatched area = 4.2:1)

EXCITING CONDITION

Filing, grinding with steel brush, or sanding with No. 80 Al₂O₃ paper
Standard cleaning technique without further preparation to restrict or
eliminate surface film or oxide films

Ultrasonic irradiation using piezoelectric transducer with a resonant
frequency about 19 KHz

28-volt lamp

DETECTION EQUIPMENT

Proportional counter containing 90 percent argon and 10 percent methane
Anode voltage = 1,700 volts

RESULT

There is no emission above the background level from Cu, Nb, Ni, and cold
rolled steel; some counts above the background are noted from brass but
emission decays very rapidly; emission intensity of Pb is greater than
emission intensity of brass probably due to presence of radioactive
isotopes in Pb.

The best emission producer is 6061 Al alloy; the emission rate by sanding
with Al₂O₃ paper is greater than that by filing, which in turn is greater
than the emission rate by grinding with steel brush.

The greater the active surface area (the plane surface), the greater is the
emission.

Emission increases at elevated temperature.

Ultrasonic irradiation (intensity = 5 W/cm²) increases emission intensity.

UNTERSUCHUNGEN ÜBER EXOELEKTRONEN AN METALLISCHEN AUFDAMPFSCHICHTEN
UND EINIGEN NICHTMETALLISCHEN OBERFLÄCHEN

J. Wüstenhagen

Zeitschrift für Naturforschung, Vol 14a, 1959, pp 634-641

MATERIAL

Al

SPECIMEN PREPARATION

Evaporated film having 1.2 cm^2 surface area deposited on various substrates
(bright Pt, polished Al, and scratched Al)
Film thickness = 5 - 300 Å

EXCITING CONDITION

Admission of oxygen at 10^{-5} to 10^{-7} torr

DETECTION EQUIPMENT

17-stage electron multiplier
Potential at specimen = -250 v

RESULT

At 2×10^{-5} torr, the emission rate increases with surface roughness of the substrate and increases with decreasing rate of deposition, probably because the finer Al grains in the film which form at lower deposition rates contain more imperfections to react faster with oxygen. There is no emission at oxygen pressure of 4×10^{-7} torr, but emission rises to 500 counts/second when the pressure changes to 2×10^{-5} torr. Emission is also noted from Be, Li, and Mg but not from Cu and Fe. The metal layer-adsorbed oxygen system does not show any spontaneous emission; oxygen molecules must fall on the metal surface to maintain emission. No emission is observed from Al film at spectroscopically pure nitrogen pressure of 5×10^{-5} torr.

EFFECT OF TEMPERATURE ON PHOTO-EXOEMISSION
J. F. Young and D. J. Williams
Journal of Applied Physics, Vol 35, 1964, pp 2279-2282

MATERIAL

Commercial purity Al

SPECIMEN PREPARATION

EXCITING CONDITION

Abrading with 400 grade SiC paper

Ultraviolet lamp as a light source

Chemical etch using a mixture of chromic acid and sulphuric acid at 60° C

DETECTION EQUIPMENT

Geiger counter with a glass window to permit illumination

Counter gases: 98.7 percent He and 1.3 percent isobutane

No necessity to bias the specimen negative due to the use of an anode loop, resulting in a higher field strength at the specimen

RESULT

There is no emission above the background in the absence of illumination.

Upon heating, the emission intensity vs time curve for abraded surface is the same as that obtained for chemically etched surface.

The count rate at room temperature for an unabraded specimen is no greater than background; however, emission occurs as the temperature increases.

The peak emission rate is shifted to a higher temperature than the abraded specimen.

On lowering the temperature during emission, behavior becomes extremely anomalous. The emission rate as a function of temperature depends on past history in the counter, and decrease in temperature can result in an increase in emission rate.

The anomalous results cannot be explained by a vacancy mechanism or by electron traps.

Emission decay appears to depend on adsorption of counter gas. Photo-exoemission can be decreased by adsorption, and its intensity can be increased by desorption.

APPENDIX II
ELECTRON ENERGY SPECTROSCOPY

APPENDIX II

ELECTRON ENERGY SPECTROSCOPY

Estimation of the electron energy is essential for a better understanding of the mechanism of exoelectron emission. The type of spectrometer to be considered is based on the cylindrical, electrostatic mirror design principle because the accelerating potential does not involve the specimen itself.

The simplest electrostatic analyzer is the parallel-plate electrostatic mirror. However, in past years probably the most popular electrostatic analyzer has been the 127-degree, cylindrical deflection system (Pichanick, 1967). In more recent years, both of these analyzers have been surpassed in performance by the concentric spherical deflection system (Purcell, 1938). More recently, however, investigators have realized that even the concentric spherical system is surpassed in performance by the cylindrical electrostatic mirror (Zashkvara et al, 1966; Sar-el, 1967, Hafner et al, 1968).

The geometry of the cylindrical mirror system is shown in figure A-1. This geometry was used more than 10 years ago by Blauth (1957), but only recently, Zashkvara has shown that it gave the fortunate effect of second-order focusing when $\theta_0 = 42.3^\circ$ and when

$$\frac{E_0}{\text{eV}} = \frac{1.3}{\ln(r_2/r_1)}$$

where E_0 is the particle kinetic energy and V is the potential difference between the two cylinders. Refocusing occurs at $L_0 = 6.1 r_1$.

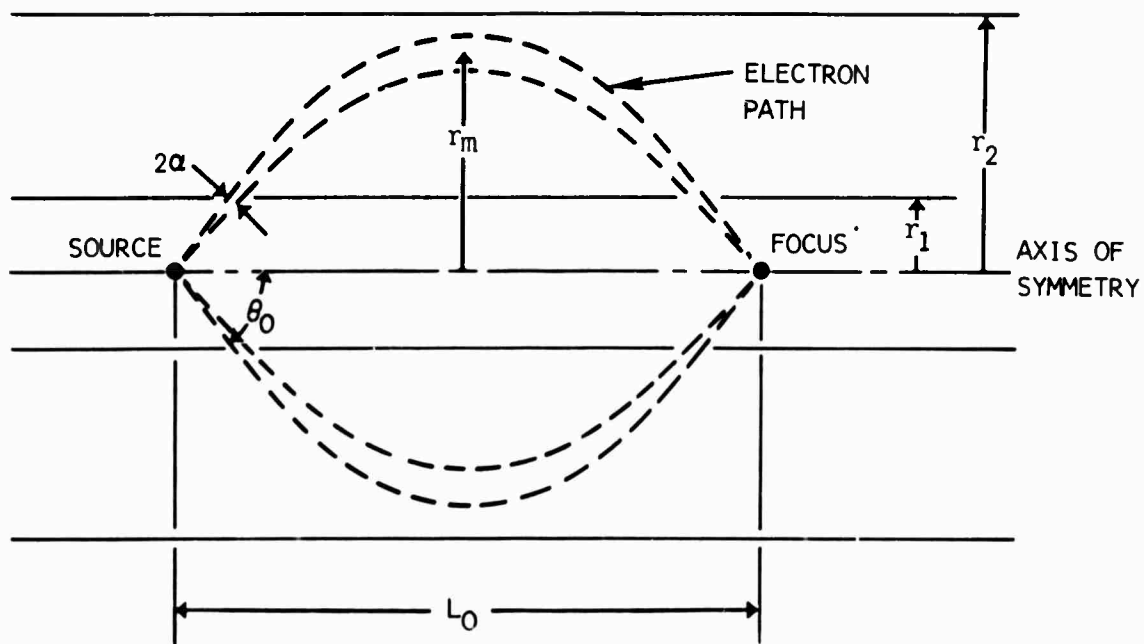
The resolution of this device, R_0 , for a point source is given simply by

$$R_0 = \frac{\Delta E}{E} = 21T^3$$

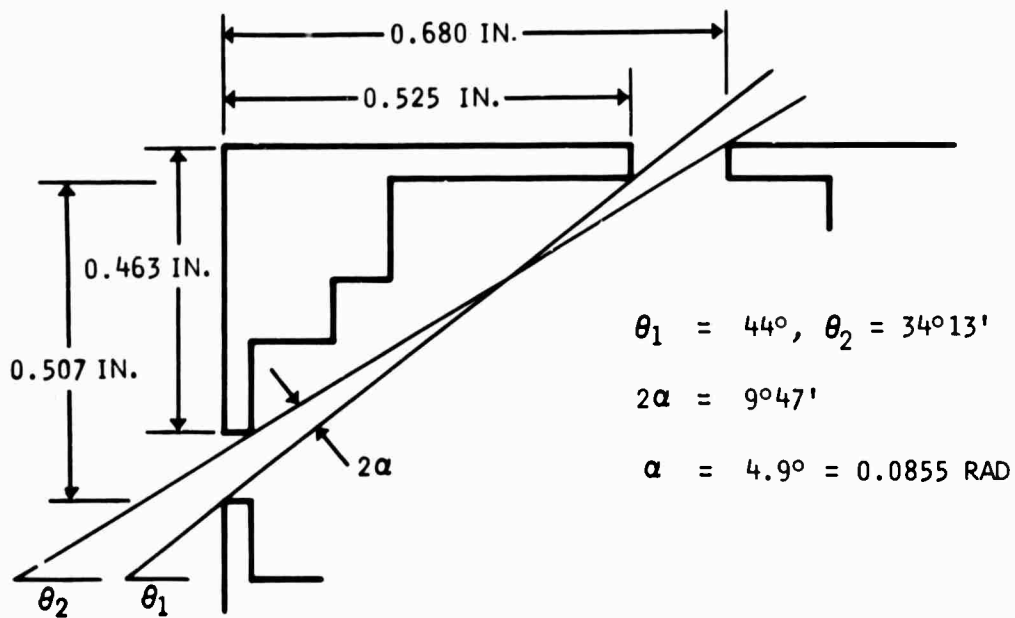
where T is the percent of solid angle transmission through the slit system. In this case we have

$$T = \sin \theta_0 \cdot \alpha$$

where α is the semiangular operative shown in figure A-1a. Due to the second-order focusing and the 2π entrance slit, this spectrometer has very good energy resolution with a relatively large-entrance solid angle.



A. SPECTROMETER GEOMETRY



B. SPECTROMETER DIMENSIONS

Figure A1. Electron Energy Spectrometer

The analysis giving the results of the previous section assumes a purely radial electrostatic field between two cylinders. This cannot be obtained in practice by using infinite cylinders or guard rings. Because of large samples to be used at the source and of large detectors near the focus, the spectrometer must terminate at these two points. Metal rings have been mounted on the end support insulators which separate the two cylinders. The proper potentials are placed on these rings to keep the field radial in the region of electron orbits. The potential between concentric, infinite cylinders is given by

$$\varphi - \varphi_1 = A \ln \left(\frac{r}{r_1} \right)$$

where φ is the potential of the inner cylinder which has a radius r_1 , and A is a proportionality constant. The device built has

$$r_1 = 0.50000 \text{ in.} \qquad r_2 = 1.4325 \text{ in.}$$

Thus, if we install four rings between the cylinders at radii such that potential jumps from the inner cylinder to the wires and to the outer cylinder can be in constant increments, we have for the radii:

$$\begin{aligned} r_{i_a} &= 0.6170 \text{ in.} & r_{i_c} &= 0.9395 \text{ in.} \\ r_{i_b} &= 0.7615 \text{ in.} & r_{i_d} &= 1.1595 \text{ in.} \end{aligned}$$

The design for constant potential jumps simplifies the construction of a potential divider for maintaining the proper potentials.

It is expected that the spectrometer will be exposed repeatedly to air at atmospheric pressure. Also, it is expected that the exoelectron flux will be sufficiently low that individual electrons must be counted. This presents a problem since the usual multistage electron multipliers have dynode surfaces which deteriorate in the presence of air. The more durable dynodes are of beryllium-copper, but even these are adversely affected. Thus the Bendix Channeltron electron multiplier is chosen for a detector (Evans, 1965). Although these are sensitive to diffusion pump oils, they are not affected seriously by air. The gain of the Channeltron is about 5×10^7 with the application of about 3,000 volts dc. At this voltage, the output current pulses are in the order of 20 nanoseconds wide.

The energy of the electrons passed by the spectrometer is given by

$$E_o = 1.3 \text{ eV} / \ln \left(\frac{r_2}{r_1} \right)$$

Thus, since $r_2 = 1.4325$ in. and $r_1 = 0.50000$ in. we have

$$E_0 = 1.23 \cdot eV$$

where V is the potential difference between the cylinders.

The resolution is given approximately by

$$P_0 = \frac{\Delta E}{E} = 21 \left(\sin \theta_0 \cdot \alpha \right)^3$$

The dimensions of the spectrometer as it is now constructed are shown in figure A-1b.

The spectrometer should be designed to work at $\theta_0 = 42^\circ 18.5'$ where we have $\sin \theta_0 = 0.673$. Thus, resolution is given by

$$\begin{aligned} R_0 &= \frac{\Delta E}{E} = 21 (0.673 \times .0855)^3 \\ &= 0.004 \end{aligned}$$

This resolution is achieved with a transmission of

$$T = 0.058$$

This figure neglects the obstruction of the three spacing sleeves.

The instrument constructed consists essentially of two concentric cylinders mounted coaxially and insulated from each other, as shown in figures A-2 and A-3. It will be mounted inside the vacuum glass chamber, facing the specimen under test, together with the amplifier, pulse spreader, and low-impedance-output emitter-follower. A pulse spreader is required to widen the approximately 20-nanosecond pulse width expected from the Channeltron multiplier to approximately 1 microsecond to allow standard pulse counters to be used. The emitter-follower permits the use of a long lead between it and the pulse counter. The bias voltage applied to the coaxial cylinders and end guard rings permits the selection of specific energy electrons to pass to the Channeltron electron multiplier.

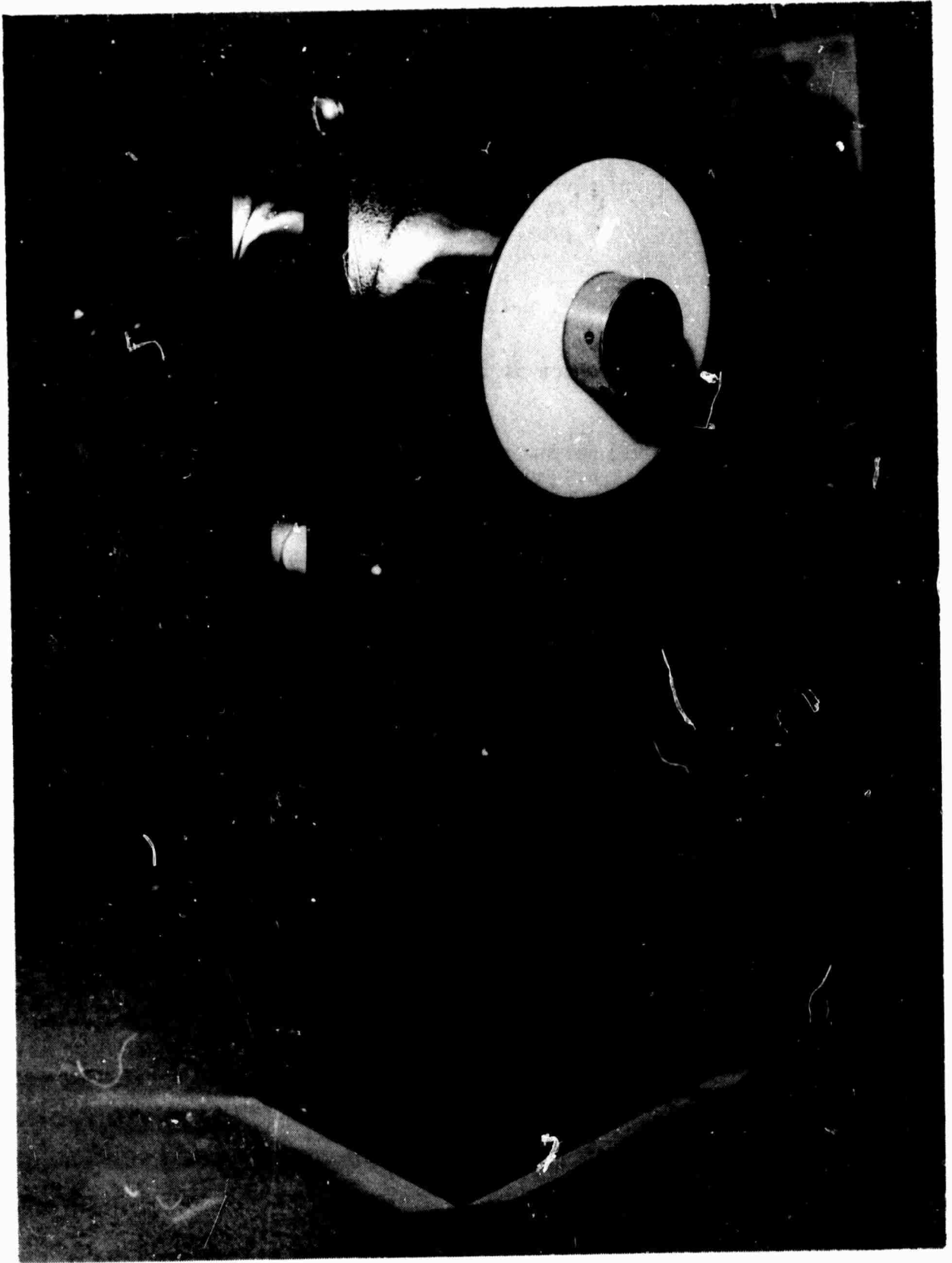


Figure A2. Spectrometer Photograph, Assembled View From Specimen Side

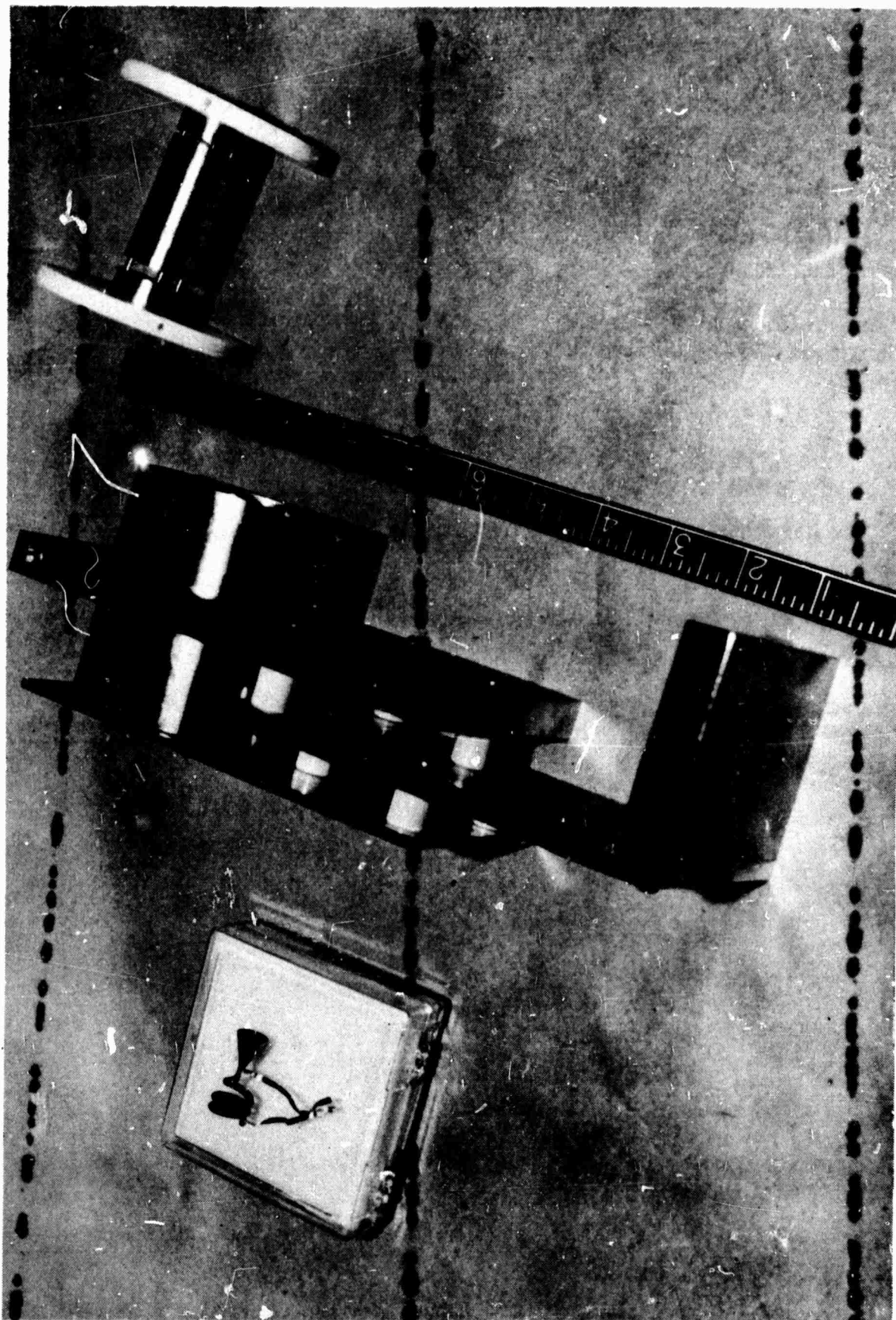


Figure A3. Spectrometer Photograph, Exploded View of Concentric Cylinders and Channeltron Electron Multiplier

BIBLIOGRAPHY

Blauth, E., "Zur Energieverteilung der von Protonen in Gases ausgelösten Sekundärelektronen," Z Physik, Vol 147, 1957, p 228

Evans, D. S., "Low-Energy Charged-Particle Detection Using the Continuous - Channel Electron Multiplier," Rev Sci Instr, Vol 36, 1965, p 375

Hafner, H., Simpson, J. A., and Kuyatt, C. E., "Comparison of the Spherical Detector and the Cylindrical Mirror Analyzers," Rev Sci Instr, Vol 39, 1968 p 33

Pichanick, F. M. J., "Ion Spectrometers," Methods of Experimental Physics, Vol 4, Part A, edited by V. W. Hughs and H. L. Schulz, Academic Press, New York, 1967, p 360

Purcell, G. M., "The Focusing of Charged Particles by Spherical Condenser," Phys Rev, Vol 54, 1938, p 818

Sar-el, H. Z., "Cylindrical Capacitor as an Analyzer - I. Nonrealistic Part," Rev Sci Instr, Vol 38, 1967, p 1210

Zashkvara, V. V., Korsunskii, M. I., and Kosmachev, O. S., "Focusing Properties of an Electrostatic Mirror With Cylindrical Field," Soviet Physics - Tech Phys Vol 11, 1966, p 96

REFERENCES

1. Air Force Contract F33615-68C-1706, ARPA Order 1244, Code 8D10 "Development of NDT Methods for the Early Detection of Fatigue Damage"
2. Air Force Contract F33615-68C-1707, ARPA Order 1244, Code 8D10, "New Technique in NDT by Acoustical and Exoelectron Emission," Dr. S. Hoenig, University of Arizona

BIBLIOGRAPHY

- Andreev, L. A., and Paligé, Ya., "Change of the Electron Work Function of Molybdenum and Tantalum Upon Cold Deformation Under Ultrahigh Vacuum Conditions," Soviet Physics - Doklady, Vol 8, 1964, p 1003
- Andreev, L. A., and Paligé, Ya., "The Effect of Deformation on the Work Function of Monocrystalline Molybdenum Filaments," Soviet Physics - Solid State, Vol 3, 1962, p 2238
- Barthow, G., "Über die Energie von Exoelektronen," Naturwiss., Vol 45, 1958, p 381
- Benson, R. W., and Associates, "Development of Nondestructive Methods for Determining Residual Stress and Fatigue Damage in Metals," Final Report, Contract No. NAS8-20208, Robert W. Benson and Associates, Inc, 1968
- Bogachev, I. N., Mints, R. I., and Kortov, V. S., "Application of the Method of Exoelectron Emission in Metal Science," Metal Science and Heat Treatment, Jul-Aug 1966, p 591
- Bohun, A., "Exoelektronenemission von Ionenkristallen," Phys Stat Sol, Vol 3, 1963, p 779
- Bohun, A., "L'émission Exoélectronique des Corps Solides," J Physique, Vol 26, 1965, p 149
- Brotzen, F. R., "Emission of Exoelectrons from Metallic Materials," Phys Stat Sol, Vol 22, 1967, p 9
- Clayton, R. N., Gragg, J. E., and Brotzen, F. R., "Electron Emission From Aluminum After Quenching," J Appl Phys, Vol 37, 1966, p 149
- Chuang, K. C., "Application of the Optical Correlation Measurement to Detection of Fatigue Damage," Materials Evaluation, Vol 26, No. 6, 1968, p 116
- Conrad, M. A., and Levy, S., "Photoemission From Metal Surfaces Measured With Geiger Counters," Nature, Vol 189, p 887
- Dover, W. D., and Jones, W. J. D., "The Initiation of Fatigue Cracks in Copper," Brit J Appl Phys, Vol 18, 1967, p 1257
- Dunegan, H. L., Harris, D. O., and Tatro, C. A., "Fracture Analysis by Use of Acoustic Emission," Engineering Fracture Mechanics, Vol 1, 1968, p 105
- Feltner, C. E., "Dislocation Arrangements in Aluminum Deformed by Repeated Tensile Stresses," Acta Met., Vol 11, 1963, p 817

Forsyth, P. J. E., "Fatigue Damage and Crack Growth in Aluminum Alloys," Acta Met., Vol 11, 1963, p 703

French, S. H., and Beams, J. W., "Contact Potential Changes Produced on Metal Surfaces by Tensile Stresses," Phys Rev B, Vol 1, 1970, p 3300

Gieroszynski, A., and Sujak, B., "Exoelectron Emission in Vacuum in the Absence of Light During Plastic Deformation of Aluminum Thickly Coated with Oxide," Acta Phys Polon, Vol 28, 1965, p 311

Gonser, U., and Martin, Geo., "Moessbauer Spectrometry for the Measurement of Residual Stress in Steel," NR Science Center Memo, 1963

Gonser, U., "Moessbauer Effect and Physical Metallurgy," NR Science Center Report SC-PP-68-77, August 1968

Gorshkov, G. A., and Postnikov, V. S., "Changes in Internal Friction of Aluminum, Cadmium, and Copper Produced by Cyclic Deformation" Russian Metallurgy (Metally), No. 1, 1965, p 67

Grosskreutz, J. C., and Benson, D. K. "The Emission of Exoelectrons From Aluminum During Fatigue," NASA CR-57918, 1963

Grosskreutz, J. C., Reimann, W. H., and Wood, W. A., "Correlation of Optical and electron-Optical Observations in Torsion Fatigue of Brass," Acta Met., Vol 14, 1966, p 1549

Grosskreutz, J. C., and Rollins, F. R., "Research on the Mechanism of Fatigue," WADC TR 59-192, 1959

Grunberg, L., "A Survey of Exoelectron Emission Phenomena," Brit J Appl Phys, Vol 9, 1958, p 85

Grunberg, L., and Wright, K. H. R., "A Study of the Structure of Abraded Metal Surfaces," Proc Roy Soc (London), Series A, Vol 232-233, 1955, p 423

Gushcha, O. I., "Investigation of the Process of Fatigue Destruction of Metals by the Method of Magnetic Hysteresis and Eddy Current Losses," FTD-MT-65-421, 1965

Haxel, O., Houtermans, F. G., and Seeger, K., "Die Elektronenemission von Metalloberflächen als Nachwirkung einer mechanischen Bearbeitung oder Glimmentladung," Z Physik, Vol 130, 1951, p 109

Hanstock, R. F., "Damping Capacity, Strain Hardening, and Fatigue," Proc Phys Soc, Vol 59, 1947, p 275

Hanstock, R. F., "Fatigue Phenomena in High-Strength Aluminum Alloys," J Inst Metals, Vol 83, 1954-55, p 11

Harris, D. O., Dunegan, H. L., and Tetelman, A. S., "Prediction of Fatigue Lifetime of Combined Fracture Mechanics and Acoustic Emission," Symposium of Air Force Conference on Fatigue and Fracture of Aircraft Structures and Materials, Miami Beach, Florida, 15-18 Dec 1969

Hempel, M., Kochendörfer, A., and Tietzke, A., "Untersuchungen über die Exoelektron-Emission mechanisch beanspruchter Metalle," Arch Eisenhüttenwes, Vol 35, 1964, p 465

Herlescue, T., Bernath, A., and Safta, V., "Contributions a l'Etude Phénomène de Fatigue par le Mesurage de la Variation des Constants Physico-Mecaniques," Rev Roum Sci Tech Serie Metall, Vol 12, 1967, p 269

Klesnil, M., and Lukáš, P., "Dislocation Arrangement in the Surface Layer of α -Iron Grains During Cyclic Loading," J Iron Steel Inst, Vol 203, 1965, p 1043

Kortov, V. S., and Mints, R. I., "Exoelectronic Emission as a Method of Studying the Deformed Surface of Metals," Physics of Metals and Metallography, Vol 19, 1965, P 72

Krogstad, R. S., and Moss, R. W., "Electron Emission During Metal Fatigue," Proceedings of the Symposium on Physics and Nondestructive Testing, 28-30 Sept 1965, Dayton, Ohio, p 9

Kryuk, V. I., Mints, R. I., and Kortov, V. S., "Exoemission From Ground Surfaces of Germanium and Silicon," Soviet Physics - Solid State, Vol 8, 1966, p 1295

Ku, T. C., and Pimbley, W. T., "Effect of Temperature on the Emission of Electrons From Abraded Surfaces of Beryllium, Calcium, Aluminum, and Magnesium," J Appl Phys, Vol 32, 1961, p 124

Kusenberger, F. N., Barton, J. R., and Donaldson, W. L., "Nondestructive Evaluation of Metal Fatigue," AFOSR-64-0668, 1964

Kusenberger, F. N., Leonard, B. E., Pasley, R. L., Barton, J. R., and Donaldson, W. L., "Nondestructive Evaluation of Metal Fatigue," AFOSR-66-0648, 1966

Laird, C., and Smith, G. C., "Crack Propagation in High-Stress Fatigue," Phil Mag, Vol 7, 1962, p 847

Lohff, J., "Die Elektronenemission bei der Oxydation mechanisch bearbeiteter Metalloberflächen," Z Physik, 1956, p 436

Lohff, J., "Die Energieverteilung der Elektronenemission mechanisch bearbeiteter Metalloberflächen," Z Naturforsch, Vol 12a, 1957, p 267

Meleka, A. H., and Farr, W., "A Possible Origin of Exoelectron Emission in Plastically Deformed Metals," Nature, Vol 187, 1960, p 232

Mints, R. I., and Kortov, V. S., "The Time Required to Reach Maximum Electron Emission From Deformed Metals," Russian Metallurgy and Fuels (Mining), No. 2, 1967, p 90

Mints, R. I., Kortov, V. S., Aleksandrov, V. L., and Kryuk, V. I., "Exoelectron Emission During Cyclic Loading of Austenitic Steels," Physics of Metals and Metallography, Vol 26, 1968, p 681

Mueller, H. J., "Exoelectron Emission and Related Electron Emissions," Research Report 1704-RR, U. S. Army Engineer Research and Development Lab, 1961

Mueller, R. K., and Pontinen, K., "Exoemission From Abraded and Etched Aluminum," J Appl Phys, Vol 35, 1964, p 1500

Nair, K. D., and May, I. Le, "Mechanisms of Fatigue Damage in Face-Centered Cubic Metals," Nature, Vol 217, 1968, p 634

Pimbley, W. T., and Francis, E. E., "Effect of Temperature on the Exoemission of Electrons From Abraded Aluminum Surfaces," J Appl Phys, Vol 32, 1961, p 1729

Ramsey, J. A., "Exoelectron Emission From Deformed Metal Surfaces," J. Australian Inst Metals, Vol 10, 1965, p 323

Ramsey, J. A., "The Emission of Electrons from Aluminum Abraded in Atmospheres of Air, Oxygen, and Water Vapour," Surface Sci, Vol 8, 1967, p 313

Ramsey, J. A., and Garlick, G. F. J., "Sensitized Photoelectric Emission During Oxidation of Aluminum," Brit J Appl Phys, Vol 15, 1964, p 1353

Seeger, K., "Die verzögerte Elektronenemission von Metallen," Z Physik, Vol 141, 1955, p 221

Seeger, K., "Verzögerte Elektronenemission und äusserer Photoeffekt von Germanium nach Elektronenbeschuss," Z Physik, Vol 149, 1957, p 453

Shlyapin, V. I., Vasserman, N. N., and Gladkovskii, V. A., "Study of the Fatigue Process by Means of Electric Impedance Measurements," Industrial Laboratory, Vol 33, 1967, p 1336

Sullivan, C. P., Averbach, B. L., and Cohen, M., "Repeated Tensile Loading of Iron and Steel," Trans ASM, Vol 54, 1961, p 299

Thompson, N., Wadsworth, N. J., and Louat, N., "Origin of Fatigue Fracture in Copper," Phil Mag, Vol 1, 1956, p 113

Truell, R., Chick, B., Anderson, G., Elbaum, C., and Findley, W., "Ultrasonic Methods for the Study of Stress Cycling Effects in Metals," WADC TR 60-920, 1961

Truell, R., Chick, B., Picker, A., and Anderson, G., "The Use of Ultrasonic Methods to Determine Fatigue Effects in Metals," WADC TR 59-389, 1959

Victorov, I. A., Rayleigh and Lamb Waves, Plenum Press, New York, 1967

Vogel, A., "Beiträge zur Exoelektronenemission von Kristallen und Metallen," Z Physik, Vol 158, 1960, p 77

von Voss, W. D., and Brotzen, F. R., "Electron Emission From Plastically Strained Aluminum," J Appl Phys, Vol 30, 1959, p 1639

Wei, R. P., and Baker, A. J., "A Metallographic Study of Iron Fatigued in Cyclic Strain at Room Temperature," Phil Mag, Vol 12, 1965, p 1005

Williams, R. A., "An Investigation of Exoelectron Emission From Various Materials Using Abrasion and Ultrasonic Techniques," TM 630.328-04, Naval Ordnance Systems, Navy Department, 1966

Wood, W. A., "Some Basic Studies of Fatigue in Metals," Fracture, edited by B. C., Averbach, D. K. Felbeck, G. T. Hahn, and D. A. Thomas, John Wiley and Sons, Inc, New York, 1959, p 412

Wood, W. A., and Bendler, H. M., "Effect of Superimposed Static Tension on the Fatigue Process in Copper Subject to Alternating Torsion," Trans AIME, Vol 224, 1962, p 18

Wood, W. A., Cousland, S. McK., and Sargant, K. R., "Systematic Microstructural Changes Peculiar to Fatigue Deformation," Acta Met., Vol 11, 1963, p 643

Wood, W. A., Reimann, W. H., and Sargant, K. R., "Comparison of Fatigue Mechanisms in BCC Iron and FCC Metals," Trans AIME, Vol 230, 1964, p 511